REMARKS

In the Office Action dated May 6, 2009, claims 1-60 were pending. Claims 4, 8-9, 13-16, 20-22, 25, 27-29, 33, 37-38, 42-45, 49-51, 54, 56-58 and 60 were withdrawn from further consideration as drawn to non-elected subject matter. Claims 1-3, 5-7, 10-12, 17-19, 23-24, 26, 30-32, 34-36, 39-41, 46-48, 52-53, 55 and 59 were under examination as they read on a method of modulating the inflammatory response/therapeutically and/or prophylactically treating a condition, wherein modulating is downregulation of activin functional activity, achieved by introducing a proteinaceous molecule which functions as an antagonist of the activin expression product, wherein the antagonist is follistatin, and wherein (i) airway inflammation is the elected specific condition; (ii) an acute inflammatory response is the elected inflammatory response; and (iii) activin A is being targeted.

The title of the application was objected to as not descriptive of the invention being claimed. A number of claims were objected to under 37 CFR § 1.75(c) as improper multiple dependent claims. Claims 31-32, 34-36, 39-41, 46-48, 52-53, 55 and 59 were rejected under 35 U.S.C. § 101. Claims 1-3, 5-7, 10-12, 17-19, 23-24, 26, 30-32, 34-36, 39-41, 46-48, 52-53, 55 and 59 were rejected under 35 U.S.C. §112, second paragraph, as allegedly indefinite. Claims 1-3, 5-7, 10-12, 17-19, 23-24, 26, 30-32, 34-36, 39-41, 46-48, 52-53, 55 and 59 were rejected under 35 U.S.C. §112, first paragraph, for allegedly failing to satisfy both the enablement requirement and the written description requirement. Claims 1-3, 5-7, 10-12, 17-19, 23-24, 26, 30-32, 34-36, 39-41, 46-48, 52-53, 55 and 59 were rejected under 35 U.S.C. §102(b) as allegedly anticipated by U.S. Patent Publication No. 20030162715. Claims 1-3, 5-7, 10-12, 17-19, 23-24, 26, 30-32, 34-36, 39-41, 46-48, 52-53, 55 and 59 were also rejected under 35 U.S.C. §102(b) as allegedly anticipated by WO 03/006057.

This Response addresses each of the Examiner's rejections and objections. Applicants therefore respectfully submit that the present application is in condition for allowance. Favorable consideration of all pending claims is therefore respectfully requested.

Claim Amendments

Independent claims 1 and 2 have been amended to further define the term "modulating" as "downregulating", consistent with the elected invention. Additionally, claims 1 and 2 have been amended to delineate that the downregulation is directed to "the functional activity of *activin A or activin B*", as supported by original claims 3-4, and is achieved by introducing an activin antagonist, as supported by claim 23.

Claims 5, 9, 10, 15, 18, 23 and 30 have been amended in their dependencies.

Claims 3-4, 17, 24-25 and 31-60 have been canceled without prejudice.

No new matter is introduced by the foregoing amendments.

Title

The Examiner has objected to the generality of the title. The title has been amended to more clearly delineate the claimed invention. Withdrawal of the objection to the title is requested.

Multiple dependent claims

A number of claims were objected to under 37 CFR § 1.75(c) as improper multiple dependent claims. Applicants have amended the claims such that the claims under examination do not include improper multiple dependent claims.

35 U.S.C. § 101

Claims 31-32, 34-36, 39-41, 46-48, 52-53, 55 and 59 were rejected under 35 U.S.C. § 101, because these claims were written as use claims without setting forth any steps involved in the process. The rejection is moot in light of the cancellation of these claims.

35 U.S.C. §112, Second Paragraph

Claims 1-3, 5-7, 10-12, 17-19, 23-24, 26, 30-32, 34-36, 39-41, 46-48, 52-53, 55 and 59 were rejected under 35 U.S.C. §112, second paragraph, as allegedly indefinite.

Specifically, regarding claims 31-32, 34-36, 39-41, 46-48, 52-53 and 59, the Examiner states that these claims (use claims) do not set forth any active steps involved in the process. The indefiniteness rejection of these claims is moot in light of the cancellation of these claims.

Regarding claims 1-3, 5-7, 10-12, 17-19, 30-32, 34-36, 39-41, 46-48, 53 and 59, the Examiner considers these claims to be incomplete for omitting essential elements, i.e., the modulatory agent. The claims, as amended, recite "introducing … an activin antagonist", which obviates the rejection.

In view of the foregoing, the rejection under 35 U.S.C. §112, second paragraph, is overcome, and withdrawal thereof is respectfully requested.

35 U.S.C. §112, First Paragraph (Enablement)

Claims 1-3, 5-7, 10-12, 17-19, 23-24, 26, 30-32, 34-36, 39-41, 46-48, 52-53, 55 and 59 were rejected under 35 U.S.C. §112, first paragraph, for allegedly failing to satisfy the enablement requirement. In raising this rejection, the Examiner has identified several issues, each of which is addressed hereinbelow.

In the first instance, the Examiner states that while the claims are directed to methods of modulating the inflammatory responses in a mammal, the claims do not recite any agent to be used to achieve modulation.

As submitted above, the claims have been amended to delineate downregulating the functional activity of activin A or activin B, wherein the down regulation is achieved by "introducing ... an activin antagonist". Clearly, the claims as amended employ an activin antagonist as the modulatory agent.

The Examiner has alleged that the specification fails to show a modulator or agent that would either upregulate or downregulate activin to a functional effective level. The Examiner refers to the specification on page 60, line 20 (Example 1), where it is disclosed that the peak release of activin A was not affected by the administration of rhfollistatin-288.

Applicants respectfully submit that given that follistatin functions as an antagonist to activin A, one would not expect it to affect the release of activin A, that is activin A levels. Rather, follistatin antagonizes the activin expression product such that activin becomes non-functional - that is, activin is effectively neutralized by follistatin. This is clearly demonstrated in Example 1 of the specification, showing that the concentration of TNFα was reduced by 50% as a result of the binding of follistatin to activin A, thereby blocking the functional activity of activin A. See page 29, bottom paragraph of the specification. The specification therefore clearly provides at least one actual example of an antagonist, specifically rhfollistatin-288.

In relation to the scope of modulatory agents as claimed, i.e., activin antagonists, it is respectfully submitted that activin, being the molecule which is the subject of modulation herein, is not a novel protein. Rather, activin is a well known protein, which is encoded by an extensively characterized gene. Accordingly, the present application is not directed to the

identification of a new molecule, but rather is based on the identification of a new functional outcome via modulation of the activity of a known molecule. More specifically, the invention as claimed is directed to the use of agents which antagonize the activity of a molecule that has been extensively characterized at both the structural and functional levels. In this regard, it is noted that agents which antagonize activin, and classes of agents in this regard, are well known and have been extensively described in the art. The specification provides non-limiting exemplification in this regard. For example, the specification disclose antibodies directed to activin (page 32, line 13), follistatin (page 34), Smad7 (page 34, line 16), activin α subunit βc subunit, activin mutants (page 34, line 24) and soluble activin receptor (page 34.

Further, identification of agents that antagonize the activity of activin has been and can be facilitated by virtue of the well characterized nature of activin. In this regard, Applicants draw the Examiner's attention to the fact that the specification also provides a general description of methodologies for screening and identifying relevant antagonists (page 35, line 9 – page 40, line 18). Moreover, the art has documented a number of activin assays, which were in use prior to the priority date of the present application and which detect the actions of activin bioactivity and immunoactivity; for example,

- *Anterior Pituitary cells in culture:* Activin A and B were first purified by their capacity to stimulate the secretion of Follicle Stimulating Hormone [FSH] by anterior pituitary cells in culture[Ling *et al.* 1986; Vale *et al.* 1986], the same culture system used earlier to isolate inhibin, a suppressor of FSH secretion [Robertson *et al.* 1984]. Later, the same assay system was used to isolate follistatin, also called FSH suppressing protein [Robertson *et al.* 1987; Ueno *et al.* 1987];
- *Human Leukaemia Cell Line THP*-1: In studying the nature of the factor that caused the above cell line to undertake erythroid differentiation, the purification process used the above assay to track and purify activin A [Eto *et al.* 1987*BiochemBiophys Res Commun* 142:1095-1103, 1987];

- *Rat Thymocyte culture*: Activin A was shown in this assay system to dose dependently inhibit thymidine uptake an action inhibited by inhibin [Hedger *et al.* 1989 *Mol Cell Endocrinol* 61:133-138, 1989];
- *3T3 cell cultures*: In the same study reported immediately above, activin A stimulated thymidine uptake in a dose dependent manner;
- *Plasmacytoma cell line MPC11*: Activin A dose-dependently inhibited the proliferation of these cells in vitro, an action that could be dose-dependently inhibited by follistatin [Phillips *et al.*1999, *J. Endocrinology* 162:111-116, 1999];
- *Radioimmunoassay for activin A*: This paper describes the quantitation of activin A in a range of biological fluids [McFarlane *et al.* 1996, *Eur J Endocrinol* 134:418-489];
- *Elisa for activin A*: This paper describes the development of an ELISA for activin A measurements in biological fluids and is still the assay system used to measure activin A levels [Knight *et al.* 1996 *J Endocrinol 148:267-279.*

Accordingly, assays for screening for or identifying activin antagonists were known before the priority date of the present application, and were routinely used both then and during the years since this application was filed.

Therefore, the specification both identifies specific antagonists and describes means of screening for antagonists. The art at the relevant time also documented assays for screening for activin antagonists. As such, those skilled in the art have knowledge of and access to a range of known agents or classes of agents which can antagonize the activity of activin, without the need to necessarily perform screening methodology. Additionally, those skilled in the art would also be able to readily determine whether a molecule or compound is an activin antagonist based on the assays routinely used in the art. It is therefore respectfully submitted that it would not require undue experimentation for the skilled person to practice the claimed invention by employing an activin antagonist.

Further, the Examiner has objected to the aspect of claim 2 relating to "prophylactically" treating a condition or a predisposition to the development of a condition.

Without prejudice and in order to advance prosecution, the claims have been amended to delete references to "prophylactically".

The Examiner has also rejected the recitation of "fragments, derivatives, mutants or variants" of activin. Without prejudice and in order to advance prosecution, the claims have been amended to delete these terms.

Moreover, the Examiner has raised a rejection that the specification only discloses the release of activin A in LPS challenged mice and does not provide sufficient support for any other activin.

Applicants would like to correct the Examiner's misinterpretation of the specification in this regard. Although the specification does provide exemplification in relation to the release of activin A in the context of the inflammatory response, it also provides, in Example 7, information in relation to the release of activin B in response to CCL_4 injection. Data are also provided in relation to the release of activin B in response to LPS treatment. The specification therefore provides detailed support for both activin A and activin B (see also Figure 6 and 7 of the specification) in the context of regulating inflammation.

In order to advance prosecution and without prejudice, the claims have been amended such that they are directed to the downregulation of activin A and activin B activity. The Examiner's rejection that the claims are directed to activin molecules which are not disclosed in the specification is therefore rendered moot.

The Examiner has also rejected claims 17-19 on the ground that they are directed to downregulating pro-inflammatory cytokines such as TNFα, IL-1 and/or IL-6. However, the Examiner points out that the results described at page 21 of the specification are arguably contradictory in that pre-treatment with recombinant follistatin-288 led to IL-6 peak

concentrations that were increased and not decreased in LPS challenged mice.

Applicants respectfully submit that these results are not contradictory. The introduction of follistatin to treat inflammation results in a shift in the cytokine cascade which subsequently occurs. Levels of TNFα are effectively halved subsequently to follistatin introduction and this does lead to what appears to be an increase in the level of IL-6 in the response. However, whereas IL-6 levels are increased at the 1 hr time point, the levels of IL-6 at later time points are significantly reduced. Overall, the IL-6 response is therefore shifted in response to follistatin such that although it peaks at 50,000 mg/ml at the 1 hr time point, this is effectively shifted forward and drops off very quickly; whereas in the absence of follistatin although peaking at only 20,000 mg/ml at the 2 hr time point, it is retained at significant levels for 12 hrs, in contrast to the situation in the presence of follistatin, by the 5 hr mark, the levels of IL-6 are negligible. Therefore, the data in the specification are not inconsistent with that which has been claimed. Nevertheless, claims 17-19 have been amended in an effort to clarify their language.

The Examiner has also taken the position that the specification is not enabled for a method for treating inflammatory responses which occur in the context of airway inflammation such as asthma.

In response, Applicants submit that the specification does provide prophetic examples in relation to airway inflammation (see Examples 3-6). Additionally, the specification also provides actual examples; e.g., the specification (Example 2 on pages 61-62) discloses examination of activin in a mouse of experimental allergic asthma. As additional support, Applicants provide herewith **Exhibit 1**, which include additional data in relation to airway inflammation. See the Results section, including particularly the paragraph on the last page

reporting the inhibitory effect of exogenous follistatin on establishment of an allergen-specific Th2 recall response in mice.

In view of the foregoing, Applicants have addressed each and every grounds of the enablement rejection. Applicants respectfully submit that the claims as presently recited are fully enabled. Reconsideration and withdrawal of the enablement rejection are therefore respectfully requested.

35 U.S.C. §112, First Paragraph (Written Description)

Claims 1-3, 5-7, 10-12, 17-19, 23-24, 26, 30-32, 34-36, 39-41, 46-48, 52-53, 55 and 59 are rejected under 35 U.S.C. §112, first paragraph, for allegedly failing to satisfy the written description requirement.

The Examiner has rejected the use of generic statements such as "modulating a functional activity of activin" or "modulating the level of activin or fragment..." on the ground that such general recitation does not define the invention or distinguish the claimed generic invention from others.

Applicants respectfully submit that the claims have been amended such that they are more specifically directed to the use of an activin antagonist to downregulate the inflammatory response. Applicants therefore believe that the issue raised by the Examiner in relation to the use of generic statements is rendered moot.

The Examiner also takes the position that the specification does not provide an adequate written description for any of the following genus of molecules recited in the claims: (i) activin or fragments, derivatives, mutants or variants thereof, (ii) proteinaceous or non-proteinaceous molecule (iii) follistatin functional fragments, derivative, homologue or mimetic

thereof, or (iv) an agent capable of modulating the functionally effective level of activin. The Examiner contends that the specification only describes rhfollistatin-288, and has essentially left those skilled in the art to determine how the genus of molecules looks like.

In terms of the Examiner's objection to "fragments, derivatives, mutants or variants" of activin or follistatin, these terms have been deleted from the claims.

The claims as amended are directed to the use of activin antagonists. The Examiner states that the specification has only disclosed recombinant follistatin-288 as an activin antagonist. However, at page 34 of the specification there is provided an extensive list of activin antagonists, other than follistatin, which can be used in the method of the invention. Further, the specification also describes assays which can be used to identify an activin antagonist or determine whether a given molecule is an activin antagonist. Therefore, Applicants respectfully submit that the specification provides adequate written description for the genus of "activin antagonist".

In view of the foregoing, Applicants respectfully submit that the claimed subject matter as presently recited is adequately described. Reconsideration and withdrawal of the written description rejection are therefore respectfully requested.

35 U.S.C. §102(b)

U.S. Patent Publication No. 20030162715

Claims 1-3, 5-7, 10-12, 17-19, 23-24, 26, 30-32, 34-36, 39-41, 46-48, 52-53, 55 and 59 were rejected under 35 U.S.C. §102(b) as allegedly anticipated by U.S. Patent Publication No. 20030162715 ("the '715 publication"). As noted by the Examiner, this publication relates to follistatin-3 protein.

Applicants respectfully submit that the follistatin-like-3 (FSTL3) protein disclosed in the '715 publication, also known as FST–related gene (FLRG) and FST-related protein (FSRP), is not the same protein as follistatin. Applicants take note of the title of the paper by Tortoriello *et al.*, "Human follistatin-related protein: A structural homologue of follistatin with nuclear localization (*Endocrinology* 142:3426-3434, 2001) (attached hereto as **Exhibit 2**). The reasons for the designation of FSTL3 as a follistatin homologue are provided below.

The proteins, FSTL3 and follistatin, are encoded by separate genes, and each is an unique protein which exhibits its own distinct roles, as demonstrated when the gene for each protein is knocked out (see Matzuk *et al.*, *Nature* 374:360-363, 1995 for follistatin knock-out & Mukherjee *et al., Proc Natl Acad Sci USA* 104:1348-1353, 2007; attached hereto as **Exhibits 3-4**). Although the two proteins have three follistatin domains with some homology, domain 1 in follistatin contains a heparin binding site that enables follistatin to bind to heparin sulphate proteoglycans on cell surfaces. In contrast, FSTL-3 has a different domain 1 that lacks a heparin binding site and is unable to bind to cell surfaces.

In a detailed study of the actions of follistatin and FSTL-3, Sidis *et al.* (*Endocrinology* 147:3586-3597, 2006) (**Exhibit 5**) made the following comments regarding the biological activity of the two proteins (see page 3587):

> *"FSTL-3 does not have an heparin binding site, cannot bind to cell surface proteoglycans and is a weak antagonist of endogenous [autocrine] activin despite being only slightly less potent in neutralizing exogenous [endocrine/paracrine] activin. These distinctions between FSTL-3 and follistatin support the concept that the presence of a functional heparin binding site is a critical biochemical determinant for endogenous activin inhibition."*

On page 3595, follistatin-3 state as a conclusion to their studies:

> *"In summary, our results clarify the activin-binding affinity among the follistatin isoforms and FSTL-3 and demonstrate that their differential activin regulating*

activity is dependent on their relative cell-surface-binding activity rather than on differential activin-binding affinity. Our results also define the relative specificity of binding and inhibitory activity for a number of related TGF-β-family ligands by the follistatin isoforms and FSTL-3, with FSTL-3 being almost completely inactive in regulating BMP ligands, thereby suggested that in vivo, FSTL-3 is unlikely to regulate BMP activity. Finally, our results suggest that the in vivo biological roles of the FST isoforms and FSTL-3 are likely to be distinct, dependent on their relative cell surface binding activity and consequent compartmentalization within the body as well as on colocalization of biosynthesis in different tissues."

These differences are highlighted by the different outcomes when their genes are subjected to targeted disruption. Matzuk *et al.* (**Exhibit 3**) report that knock-out of the follistatin gene results in death of all offspring within a few hours after birth due to an inability to breathe, and the pups have abnormal skin as well as whisker and skeletal abnormalities. In contrast, disruption of the FSTL3 gene is reported by Mukherjee *et al.* (**Exhibit 4**), which shows that the mice survive to adulthood, have enlarged islets of Langerhans in the pancreas, reduced visceral fat and enhanced glucose tolerance and increased insulin sensitivity, and also develop hypertension.

Therefore, the disclosure of the '715 publication, which relates to the follistatin-3 protein, is not relevant to the claimed invention involving follistatin. The '715 publication does not teach the claimed invention. Withdrawal of the §102(b) rejection based on the '715 publication is respectfully requested.

WO03/006057

Claims 1-3, 5-7, 10-12, 17-19, 23-24, 26, 30-32, 34-36, 39-41, 46-48, 52-53, 55 and 59 were rejected under 35 U.S.C. §102(b) as allegedly anticipated by WO 03/006057. As noted by the Examiner, WO'057 discloses the use of follistatin to treat fibrosis.

In response, Applicants submit that fibrosis is a different condition from inflammation. Although fibrosis can occur subsequently to inflammation, it is not itself an

inflammatory response. Fibrosis is a form of scarring which leads to loss of elasticity of the lung tissue, and is characterized by the deposition of a collagen avascular matrix in a wound. Although fibrosis is a condition which can occur subsequently to chronic inflammation, it can also occur in a situation such as fibrinolysis where a fibrin clot, which is the product of coagulation, is broken down.

The claimed invention is directed to the treatment of inflammation and not the treatment of fibrosis. These are two distinct conditions. Inflammation can occur without the onset of subsequent fibrosis, and fibrosis can be initiated without a preceding inflammatory response.

Accordingly, Applicants respectfully submit that the treatment of fibrosis does not equate to the treatment of an inflammatory response. The disclosure of WO'057, which relates to the treatment of fibrosis, does not anticipate the claimed invention. Withdrawal of the §102(b) rejection based on WO'057 is respectfully requested.

Conclusion

In view of the foregoing amendments and remarks, it is firmly believed that the subject application is in condition for allowance, which action is earnestly solicited.

Respectfully submitted,

Xiaochun Zhu
Registration No. 56,311

Scully, Scott, Murphy & Presser, P. C.
400 Garden City Plaza-STE 300
Garden City, New York 11530
Telephone: 516-742-4343 (XZ:ab)

Enc.: Exhibits 1-5.

EXHIBIT 1

Materials and methods

Mice

Female BALB/c mice aged 7–8 weeks were obtained from Laboratory Animal Services (Adelaide, SA, Australia) and housed in the Alfred Medical Research and Education Precinct animal facility. All experimental protocols were approved by the precinct Animal Ethics Committee.

Immunization protocol

Mice were sensitized and challenged to OVA as described previously [16]; mice sensitized and challenged according to this protocol develop airways hyper-reactivity 24 h after the last challenge (data not shown). Mice were sensitized intraperitoneally with saline or OVA (50 μg; Sigma-Aldrich, NSW, Australia) in alum (Rehels, NJ, USA) on days −24 and −12, and challenged via intratracheal instillation with saline or OVA (25 μg) on days 0, 2, 5 and 7. Mice were killed 24 h after each of the four challenges (days 1, 3, 6 and 8), and on days 9, 11, 14 and 17 (counted as days after the first intubation; Fig. 1a).

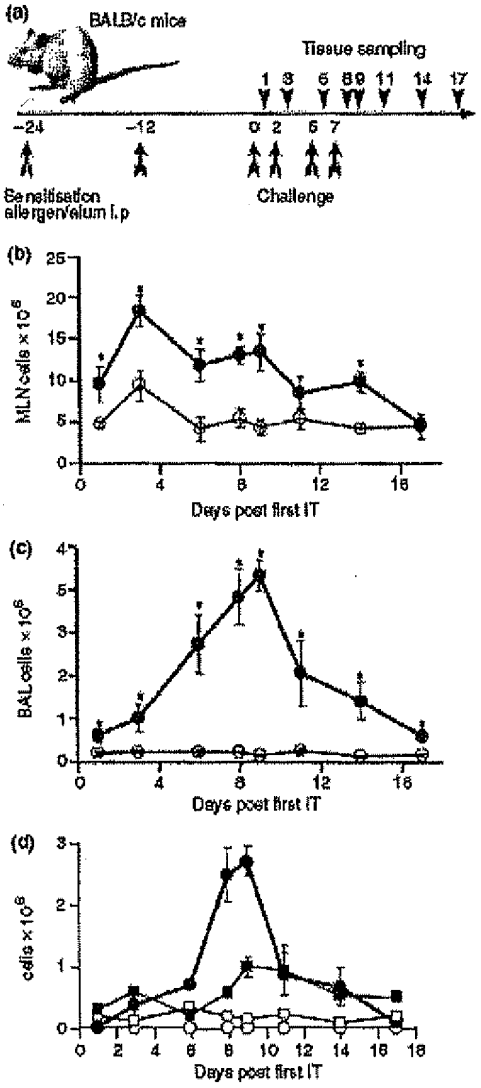

Fig. 1. Time course analysis of cell numbers and eosinophilia. Experimental protocol and sampling time-points (a), cell counts in mediastinal lymph node (MLN) (b) and bronchoalveolar lavage (BAL) (c). Total eosinophil (circles) and macrophage (squares) numbers in BAL (d). Open symbols, saline; closed symbols, OVA immunization. $n = 6$–10 mice per group per time-point, mean ± SEM. *Statistically significant difference between saline and OVA groups.

Follistatin administration

Mice were sensitized and challenged with saline or OVA (as above). Recombinant mouse follistatin (R&D Systems, Minneapolis, MN, USA; 769-FS, 0.05–1 μg in 0.1% BSA/saline) was administered intranasally (50 μL) 1 h before each challenge. Saline or OVA control groups did not receive follistatin. Mice were killed 24 h after the fourth challenge.

Bronchoalveolar lavage, differential counts and tissue sampling

Methods were as described previously [16]. Blood was collected from the inferior vena cava and serum collected by centrifugation. Bronchoalveolar lavage (BAL) was performed with 0.4 mL 1% fetal calf serum (FCS) in PBS followed by three further lavages of 0.3 mL. Viable mediastinal lymph node (MLN) lymphocytes and BAL leukocytes were counted in a hemocytometer. For differentials, BAL cytospots were Giemsa-stained (Merck, Kilsyth, Victoria, Australia) and ⩾200 cells identified by morphological criteria. For image analysis experiments mice were injected with heparin and killed via CO_2 asphyxiation before perfusion via the right ventricle with 10 mL freshly made 2% paraformaldehyde pH 7.3 in PBS. Lungs were paraffin-embedded and 3 μm sections stained with periodic acid–Schiff (PAS) for goblet cell quantitation.

Cytokine ELISPOT

ELISPOT plates (Millipore, North Ryde, NSW, Australia) were coated with IL-4 (BVD4-1D11), IL-5 (TRFK5; BD Pharmingen, San Jose, CA, USA) or IL-13 (MAB413; R&D Systems) antibody at 5 μg/mL in PBS overnight at 4 °C. Plates were blocked with 10% FCS in RPMI 1640 (Invitrogen, Mount Waverly, Victoria, Australia) for 1 h at 37 °C. Cells were resuspended in RPMI 1640 containing 2.5% FCS, 50 μM 2-mercaptoethanol (Sigma-Aldrich M-7522), penicillin–streptomycin–glutamine (Invitrogen 10378-016) and 10 mM HEPES. Blocking solution was discarded, and 0.5×10^6 cells in 100 μL added to the wells with 10 μL of appropriately diluted antigen. Following culture for 16 h at 37 °C, cells were discarded, plates soaked in distilled water for 10 min and washed. Biotinylated IL-4 (BVD6-24G2), IL-5 (TRFK4) (BD Pharmingen) or IL-13 (BAF413, R&D Systems) antibodies diluted in PBS were added for 1.5 h. Plates were washed and ExtrAvidin® – alkaline phosphatase (Sigma-Aldrich E-2616) added for 1.5 h. Washes were in 0.05% Tween 20/PBS followed by PBS. Reaction product was developed (Bio-Rad, Regents Park, NSW, Australia 170-6432), plates washed in water and air dried. Plates were read on an ELISPOT reader (Autoimmun Diagnostika, Strassberg, Germany).

Activin ELISA and follistatin radioimmunoassay

Activin A was measured using a specific ELISA [17] according to the manufacturer's instructions (Oxford Bio-Innovations, Upper Heyford, Oxfordshire, UK) with some modifications as described previously [18]. Follistatin concentrations were measured in serum and BAL fluid (BALF) using a discontinuous radioimmunoassay as described previously [18]. Note that 1 nM activin A ≈ 25 ng/mL, 1 nM follistatin ≈ 35–45 ng/mL (variably glycosylated and different isoforms). The activin A antibody (E4) used for both the ELISA and immunohistochemistry was obtained from Professor Nigel Groome, Oxford Brookes University, UK. The follistatin antibodies (#204 and 2E6) used for the immunoassay and immunohistochemistry were developed 'in house' and have been raised against purified native bovine follistatin or human recombinant follistatin. The assay buffer for the BALF samples was 0.05% BSA/PBS. Mouse serum and BALF sample dilutions were parallel to a standard curve (data not shown). The limit of activin A detection for both serum and BALF samples was 0.01 ng/mL. The limit of follistatin detection was < 0.5 and < 1.04 ng/mL for serum and BALF samples, respectively.

Activin and follistatin immunohistochemistry

Paraffin sections were dewaxed and rehydrated and antigens retrieved by immersing slides in 0.01 M citrate buffer, pH 6.0, heating in a 1000 W microwave oven (high for 2.5 min, low for 5 min), cooling at 4 °C for 20 min, and washing in water for 5 min. Endogenous peroxidase was blocked in 3% H_2O_2 for 10 min, and non-specific binding blocked for 1 h (CAS block with 10% normal rabbit serum, Zymed Laboratories, South San Francisco, CA, USA; 00-8120). Sections were incubated with antibodies specific for the activin β_A subunit (E4) or follistatin (2E6) at 10 μg/mL overnight at 4 °C. After washing, slides were incubated in rabbit anti-mouse-IgG_{2b}-peroxidase (Zymed 61-0320) or IgM-peroxidase (Zymed 61-6820) diluted 1 : 500 for 2 h, for activin A and follistatin primary antibodies, respectively. Slides were washed in Tris-buffered NaCl (TBS) 0.05% Tween-20 pH 7.5, then Milli$Q$ H_2O. Reaction product was developed with 3,3′-diaminobenzidine tetrahydrochloride substrate kit (Zymed 00-2014), and sections counterstained in Harris's hematoxylin. All wash steps were in TBS/0.05% Tween-20. Antibodies were diluted in 1% BSA/TBS. Non-immune mouse antibody of the appropriate immunoglobulin isotype was used for negative controls (Zymed 02-6800 and 02-6300 for IgM and IgG_{2b}, respectively).

Image analysis

Sections were analysed at × 200 or × 400 magnification using appropriately calibrated Image-Pro Plus 5.0 software (Media Cybernetics, Silver Spring, MD, USA). The

linear basement membrane length was measured (mm), and the number of activin A-, follistatin- or PAS-positive cells in the airway counted, yielding number of positive cells/mm basement membrane. Ten airways per mouse were assessed, except for the follistatin inhibition experiments where all airways in the lung sections from each mouse were assessed (50–100 airways per mouse). Semi-quantitative grading of mucus production by airways was performed blinded using a scale of 1–5, where 1 = negligible staining, and 5 is > 90% of airways showing high frequency and/or volume (cell size) of PAS-positive epithelial cells.

Statistical analysis

Statistics were determined using SPSS 12.0.1 software. The Mann–Whitney U test was used, with a P value ≤ 0.05 considered statistically significant. For analysis of IL-4, IL-5 and mucus cell frequency in the follistatin inhibition experiments, data were assessed for normality and log-transformed before analysis by ANOVA.

Results

Kinetics of the pulmonary allergic inflammatory response

Groups of mice were analysed after each challenge, and at various times after the final (fourth) challenge (Fig. 1a). MLN cell counts peaked after the second challenge in immunized mice, and gradually returned to pre-challenge levels by day 17 (Fig. 1b). In contrast, BAL cell numbers peaked at day 9, with numbers returning to pre-challenge levels by day 17 (Fig. 1c). Differential analysis of BAL cells showed that eosinophil frequency and total numbers peaked at days 8 and 9, declining rapidly thereafter (Fig. 1d). Macrophages numbers in BAL showed an approximate twofold increase at days 9–11 (Fig. 1d). There was an approximate twofold increase in BALF IL-5 concentration in OVA-immunized mice at day 8, although no difference was seen at other times; no significant differences in BALF IL-4 concentrations were seen at any time (data not shown). In contrast, ELISPOT analysis of IL-4 and IL-5 production by MLN showed an increased frequency of IL-4- and IL-5-producing cells immediately after the first challenge until day 14, 7 days after the final challenge. The kinetics of the IL-4 and IL-5 response were very similar, with peak frequency seen at day 6, and a broad shoulder of moderate frequency persisting until day 14 (Figs 2a and b). The frequency of IL-4 secreting cells was always greater than that for IL-5 at the corresponding time-point. IL-13 production peaked at day 8, but in contrast to the results for IL-4 and IL-5, the frequency of IL-13 producing cells was still significantly elevated at day 17 (Fig. 2c). Collectively these data indicate that the pulmonary immune response peaked after three to four challenges (days 6–8) and gradually subsided thereafter.

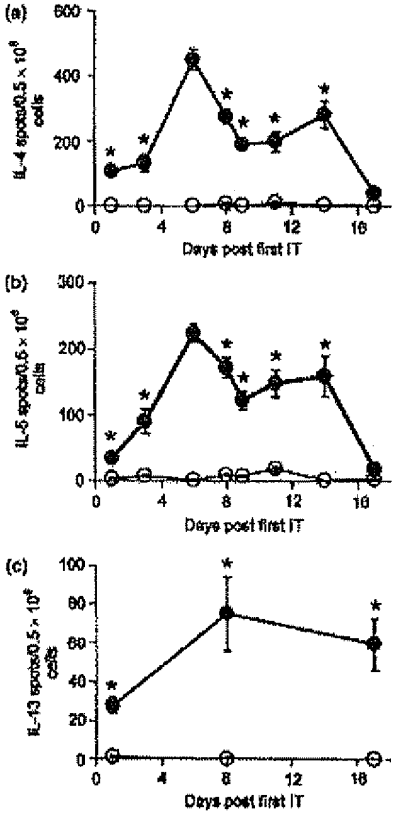

Fig. 2. Time-course analysis of IL-4, IL-5 and IL-13 production by draining lymph node (LN) cells. Frequency of IL-4- (a), IL-5- (b) and IL-13-producing (c) mediastinal LN (MLN) cells as measured by ELISPOT. Open circles, saline; closed circles, OVA immunization. $n = 5$–10 mice per group per time-point, mean ± SEM. *Statistically significant difference between saline and OVA groups.

Activin and follistatin concentrations in bronchoalveolar lavage fluid

BALF was collected at each time-point and activin A and follistatin concentrations determined. Activin A was barely detectable in BALF from control mice at all times. In contrast, in OVA-sensitized mice activin A concentrations were elevated after one OVA challenge, and peaked on days 6 and 8 (after three to four challenges). The activin A concentration dropped rapidly between days 9 and 11, and had returned to control levels by day 17

(10 days after final challenge) (Fig. 3a). There was also a clear increase in follistatin concentrations in BALF at days 6 and 8 (Fig. 3b), thus paralleling the activin A kinetics. Activin A and follistatin levels lagged behind the initial infiltration of inflammatory cells but coincided with peak inflammation. No obvious fluctuations in activin A or follistatin concentrations in serum were seen at any time-point (activin A, < 0.2 ng/mL for both saline and OVA groups; follistatin, 3–5 ng/mL for both saline and OVA groups).

Activin, follistatin and mucus localization/production in the inflamed lung

Bronchial epithelium from control mice showed strong and uniform activin A staining at all times. Pneumocytes expressed activin A at low density, and occasionally strong localization by macrophages was also seen (Fig. 4a). Mice which had received one OVA challenge (day 1) had airway morphology and localization of activin A essentially indistinguishable from controls, although mild inflammation was occasionally observed (Fig. 4c). In contrast, after three to four OVA challenges there was a dramatic loss of activin A staining in airway epithelium, accompanied by extensive peribronchial and perivascular inflammation and epithelial hypertrophy. Discrete macrophages in the inflammatory infiltrate strongly expressed

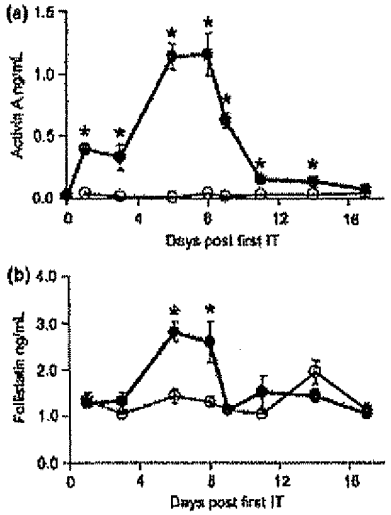

Fig. 3. Time-course analysis of bronchoalveolar lavage fluid (BALF) activin A (a) and follistatin (b) concentrations. Open circles, saline; closed circles, OVA immunization. $n = 5$–10 mice per group per time-point, mean ± SEM. *Statistically significant difference between saline and OVA groups.

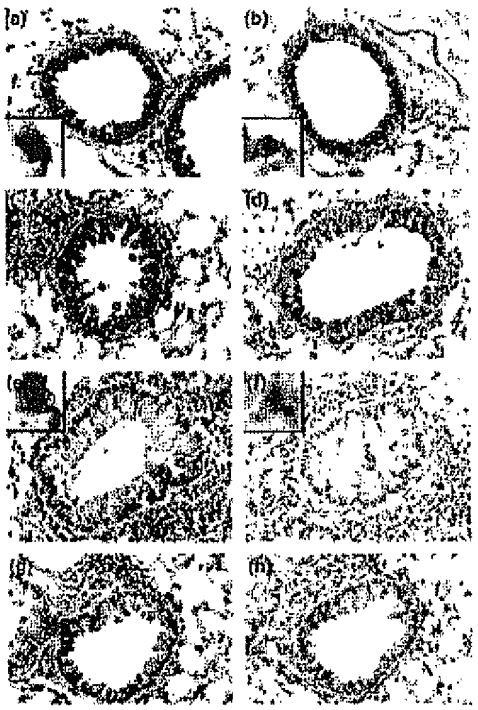

Fig. 4. Activin A and follistatin localization in airways. Activin A localization in saline-treated control mice remained stable at all time-points (a). Activin A localization at days 1 and 8 (c and e; after one and four OVA challenges, respectively), and day 17 (g; 10 days after the final OVA challenge). Follistatin localization in control lung (b) and at days 1, 8 and 17 (d, f and h, respectively). Inset shows a positive macrophage, the main non-epithelial source found in the study. Immunoperoxidase, hematoxylin counterstain, original magnification ×400. Representative micrographs from 11 to 16 mice per time-point.

activin A (Fig. 4e). There were no differences in the frequency of activin A-expressing macrophages between control and inflamed lung (data not shown). The structural changes and associated loss of activin A persisted through days 9–11 (data not shown). By day 17 inflammation, airway thickening and epithelial hypertrophy had subsided although most airways continued to show a marked loss of activin A staining (Fig. 4g).

The localization pattern for follistatin was also examined. Control mice had strong and uniform follistatin localization in bronchial epithelium at all time-points. Follistatin was expressed weakly by pneumocytes, although strong staining by macrophages was occasionally noted (Fig. 4b). After one OVA challenge the pattern resembled that of control mice (Fig. 4d). However, after three to four challenges the majority of airways showed a

near complete loss of follistatin staining. Pneumocytes expressed follistatin at increased density and discrete lymphoblasts/macrophages were positive (Fig. 4f). As with activin A, there were no differences in the frequency of follistatin-expressing macrophages between control and inflamed lung (data not shown). These changes persisted through days 9–11 (data not shown). Follistatin localisation remained markedly reduced in the majority of airways at day 17 (Fig. 4h).

Metaplasia of airway epithelium to goblet cells is a common feature of asthma in mouse models and the human. We investigated the possible relationship between loss of activin A/follistatin localization by airway epithelium and acquisition of a mucus-secreting phenotype. Control mice had a complete absence of mucus-producing cells in the airways at all time-points (Fig. 5a). After one OVA challenge mucus-producing goblet cells were very infrequently seen (Fig. 5b). However, after four challenges the number of airways containing goblet cells was dramatically increased, although the frequency of positive cells within individual airways was variable (Fig. 5c). The number of airways containing goblet cells had decreased by day 17 (10 days after the final challenge), although it was still clearly elevated compared to controls, and variation between individual airways was again noted (Fig. 5d).

Quantitative analysis of activin, follistatin and mucus localization/production by airway epithelium

Image analysis was performed at three key time-points to more precisely investigate the dynamics of activin A, follistatin and mucus localization in the airways. After one OVA challenge the frequency of activin A-positive epithelial cells was nearly identical to controls (130/mm basement membrane; Fig. 6a). However, after four challenges (day 8) the frequency of activin A-positive airway epithelial cells was significantly decreased (51/mm basement membrane). This change was still observed 10 days after the final challenge, although the frequency of activin A-positive cells had increased slightly (70/mm basement membrane). Similar changes were observed when follistatin-expressing airway epithelial cells were analysed. The frequency of follistatin-positive cells was approximately 100/mm basement membrane in both control and OVA-challenged mice at day 1. However, after four OVA challenges the frequency of follistatin-positive cells was significantly decreased (43/mm basement membrane).

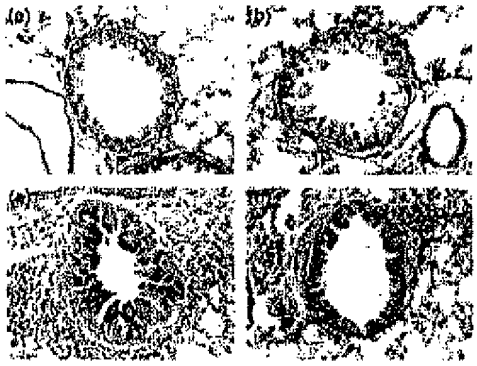

Fig. 5. Mucus production by bronchial epithelium. Airway epithelium from control mice did not contain mucus-producing goblet cells (a). Goblet cells in airways from OVA mice at days 1, 8 and 17 (b–d, respectively). Periodic acid-Schiff (PAS), original magnification ×400. Representative micrographs from 11 to 16 mice per time-point.

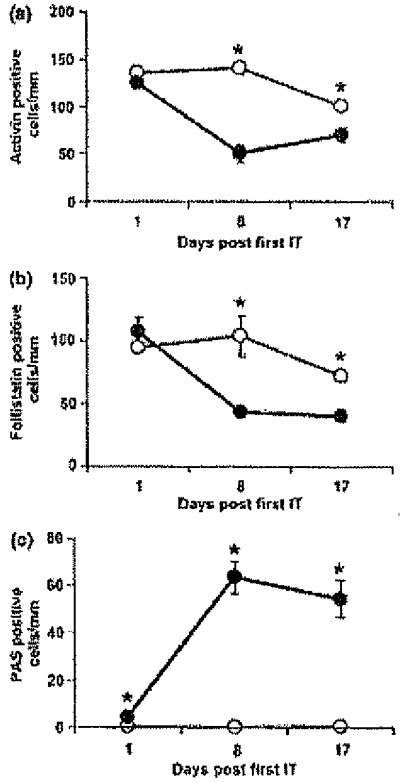

Fig. 6. Frequency of activin A-, follistatin- and mucus-expressing airway epithelial cells. Quantitative image analysis of activin A-, follistatin- and periodic acid-Schiff (PAS)-positive cells per mm basement membrane (a–c, respectively). Activin A- and follistatin-specific immunoperoxidase (a and b) and PAS (c). Open circles, saline; closed circles, OVA immunization. $n=6$ mice per group per time-point, mean±SEM. *Statistically significant difference between saline and OVA groups.

and an almost identical frequency was observed 10 days after the final challenge (Fig. 6b). There was a slight drop in the frequency of activin A- and follistatin-positive cells in control mice between days 8 and 17; this change was statistically significant for activin A only.

We performed a parallel quantitative analysis of mucus-secreting cell frequency. Goblet cells were almost undetectable in control mice at all time-points, while their frequency was very slightly elevated in OVA-challenged mice at day 1 (4/mm basement membrane) (Fig. 6c). However, by day 8 goblet cell frequency in OVA-challenged mice was dramatically elevated (64/mm basement membrane). This frequency had dropped marginally by day 17 but was still well above control values (Fig. 6c). The mucus-producing response was temporally linked to increased IL-13 production in draining LN (Fig. 2c), consistent with the key role for this cytokine in mucus production in allergic asthma [19, 20]. Collectively these findings reveal an inverse relationship between airway epithelial activin A/follistatin localization and metaplasia to goblet cells.

Effect of exogenous follistatin

To directly test whether follistatin can inhibit an allergen-specific Th2 response saline (control) or OVA sensitized mice received recombinant mouse follistatin before each of four saline or OVA challenges, respectively. Exogenous follistatin resulted in approximately 20% lower activin A concentrations in BALF (1.08 ± 0.08 vs. 0.88 ± 0.09 ng/ml. for OVA vs. OVA+follistatin groups, respectively, $P = 0.08$). Furthermore, exogenous follistatin caused decreased MLN cell numbers (Fig. 7a), and decreased frequency of cells producing IL-4 and IL-5 (Figs 7b and c) 24 h after the fourth challenge. Semi-quantitative blinded grading of the frequency and volume (cell size) of mucus-producing airway cells yielded mean scores of 3.36 ± 0.28 vs. 2.0 ± 0.16 ($P = 0.01$), and 3.0 ± 0.26 vs. 1.4 ± 0.29 ($P < 0.01$), for OVA vs. OVA+follistatin mice, respectively. Additionally, quantitative image analysis of all airways in the lung sections showed that follistatin decreased the frequency of mucus-producing airway epithelial cells (Fig. 7d). However, total BAL eosinophils were only slightly decreased in the OVA+follistatin groups (data not shown). Saline immunized groups had negligible IL-4, IL-5 or mucus production, and this was unaffected by exogenous follistatin. Overall these findings suggest that follistatin can inhibit the establishment of an allergen-specific Th2 recall response in mice.

EXHIBIT 2

0013-7227/01/$03.00/0
Printed in U.S.A.

Endocrinology 142(8):3426–3434

Human Follistatin-Related Protein: A Structural Homologue of Follistatin with Nuclear Localization

DREW V. TORTORIELLO, YISRAEL SIDIS, DOUGLAS A. HOLTZMAN, WILLIAM E. HOLMES, AND ALAN L. SCHNEYER

Reproductive Endocrine Unit and National Center for Infertility Research, Massachusetts General Hospital (D.V.T., Y.S., A.S.), Boston, Massachusetts 02144; Microbia, Inc. (D.A.H.), Cambridge, Massachusetts 02139; and Millennium Pharmaceuticals (W.E.H.), Cambridge, Massachusetts 02144

Follistatin-related protein is a recently discovered glycoprotein that is highly homologous in both primary sequence and exon/intron domain structure to the activin-binding protein, follistatin. We explored their potential for functional redundancy by investigating the relative affinities and kinetics of their interactions with activin, bone morphogenic protein-6, and bone morphogenic protein-7 and by exploring their expression and distribution in human tissues and cells. Follistatin and follistatin-related protein mRNA were ubiquitous by Northern analyses, although their sites of peak distribution differed, with follistatin-related protein and follistatin predominating in the placenta and ovary, respectively. Follistatin-related protein, like follistatin, preferentially bound activin with high affinity and in an essentially irreversible fashion. Although follistatin-related protein, like follistatin, possesses a signal sequence and no known nuclear localization signals, its secretion was undetectable in most cell lines by RIA. Intriguingly, follistatin-related protein was identified as a nuclear protein in human granulosa cells and all human cell lines tested. Furthermore, Western analyses of CHO cells transfected with human follistatin-related protein revealed this protein to reside within the insoluble nuclear protein fraction. We conclude that despite its remarkably high level of similarity to follistatin with regard to structure and activin binding kinetics, follistatin-related protein is a nuclear as well as a secretory protein that may perform distinct intracellular actions. (*Endocrinology* 142: 3426–3434, 2001)

FOLLISTATIN (FS) IS a secreted monomeric glycoprotein first isolated from ovarian follicular fluid on the basis of its ability to suppress FSH secretion by pituitary cells *in vitro* (1, 2). The mechanism underlying this effect involves the prevention of activin signaling. Indeed, the critical effects activin exerts on the ontogeny and physiology of several organ systems (3, 4) are at least partially regulated in a paracrine/autocrine manner by the coordinate expression of FS (5). FS selectively, nearly irreversibly, and with high affinity binds dimeric activin (6, 7), rendering it biologically inactive (8) and prone to endocytotic degradation (9). In addition, FS can bind proteoglycans (10) through a heparin binding motif, thereby forming a cell surface barrier that prevents activin from accessing its receptor (11).

A domain structure for FS has been proposed based upon the discovery that its exons encode distinct amino acid sequences that demonstrate a high degree of evolutionary conservation (2). The most salient feature of this structure is a series of 3 consecutive FS domains. Although encoded by separate exons, each FS domain is distinguished by an identical alignment of 10 cysteine residues. The 315-amino acid splice variant of FS contains an acidic C-terminal domain that may impede adherence to cell surfaces by neutralizing the basic heparin binding motif present in the first FS domain (10). FS also has a hydrophobic signal domain that facilitates entry of the nascent protein into the endoplasmic reticulum and is proteolytically cleaved before secretion of the mature peptide. The functional importance of FS, however, probably resides in its N-terminal domain, which has recently been implicated as the site responsible for the majority of FS's ability to bind activin, with 2 tryptophan residues at positions 4 and 36 being especially important in this capacity (12, 13).

A novel gene was recently cloned from a B cell leukemia line and was named FLRG (FS-related gene) based upon primary sequence homology to FS (14). Its five exons encode a signal domain, an N-terminal domain, two cysteine-rich FS domains, and a C-terminal domain, yielding an overall modular architecture remarkably similar to that of FS (Fig. 1).

FLRG has been detected in the conditioned media of HeLa, JAR, and LOVO cells by Western blotting (14). In addition, a mouse FLRG-glutathione-S-transferase fusion protein has been shown to bind activin in pull-down assays and to diminish activin-mediated gene transcription, albeit at relatively high concentrations, *in vitro* (15). Together these findings suggest that FLRG, like its structural homologue FS (16, 17), may serve as a secreted regulator of activin-mediated cellular processes functioning primarily in an autocrine/paracrine mode. FS has been demonstrated to play a key role in *Xenopus* embryonic neuralization (18), and functional redundancy with FLRG could theoretically explain the seemingly contradictory lack of neurological deficits in the FS knockout mouse (19).

As several extracellular matrix proteins, such as agrin, SPARC (secreted protein acidic and rich in cysteines), and testican (20–22), that are not known to bind TGFβ superfamily ligands, have previously been termed products of follistatin-related genes based solely upon their possession of

Abbreviations: BMP, Bone morphogenic protein; FLRG, FS-related gene; FSRP, follistatin-related protein; FS, follistatin; LGC, luteinized granulosa cells; SPARC, secreted protein acidic and rich in cysteines.

FIG. 1. Comparison of exon structure and amino acid sequence for human FSRP and human FS. The six exons of FS code for a signal peptide, N-terminal domain, three FS domains, and a C-terminal domain. FSRP has an identical structure, except for the absence of one FS domain that contains the heparin-binding site. The cleavage site of FSRP's signal peptide is presumed, based upon homology to FS. Thus, the overall structural and sequence homology suggest that these proteins may serve similar functions.

one or more FS domains, we refer to FLRG as FS-related protein (FSRP), to emphasize its uniquely high level of homology with regard to sequence, structure, and perhaps function.

We explored the hypothesis that FSRP serves a functionally redundant role with FS by first directly comparing their affinities and binding kinetics with activin and the closely related TGFβ superfamily members BMP-6 and BMP-7. As the extent and site of a protein's production as well as its subcellular destination can also be predictive of function, we investigated FSRP mRNA and protein biosynthesis in human tissues and cell lines. Our results indicate that FSRP, although clearly an activin-binding structural homolog of FS, has maximal expression in different tissues from FS, is located in the nucleus of all cells examined, and is only infrequently secreted. These findings suggest that FSRP may serve biological roles distinct from those of FS.

Materials and Methods

Materials

The FSRP cDNA was tagged at the C-terminus with either FLAG or hFc and was then expressed in 293 cells. Tagged FSRP was purified by immunoaffinity chromatography using anti-FLAG M2 affinity gel or protein A resin, respectively. Eluted fractions were neutralized, pooled, and dialyzed against PBS, pH 7.4. By Coomassie-stained SDS-PAGE gels, the purities of the proteins were estimated to be greater than 90%. The FSRP antibody was raised in rabbits to purified FSRP-Fc protein. High titer bleeds were pooled and purified by protein A affinity chromatography. Luteinized granulosa cells (LGC) were obtained from *in vitro* fertilization patients at the time of oocyte aspiration under approval of the Massachusetts General Hospital institutional review board. Pure recombinant human activin A, BMP-6, and BMP-7 were obtained from R&D Systems (Minneapolis, MN).

Ligand binding studies

Binding studies were conducted in 96-well microtiter plates that were coated with 25 ng FSRP-Fc or FS288 in 100 μl 0.1 M carbonate buffer (pH 9.6) and incubated overnight at 25 C on an orbital shaker as previously described (4). Unbound protein was removed by washing three times for 5 min each time with 200 μl wash buffer (0.01% Tween in 10 mM PBS solution). Blocking solution (200 μl; 3% BSA and 0.01% Tween in 10 mM PBS) was then added to each well, and the trays were incubated at 25 C for 2 h on an orbital shaker. The wells were rinsed three times with wash buffer, and 150 μl assay buffer (0.01 M PBS, 0.1% gelatin, and 0.05% Tween) containing approximately 100,000 cpm radiolabeled ligand were added to each well. Ligands were iodinated to a specific activity of approximately 35 μCi/μg using lactoperoxidase as previously described (23). Nonspecific binding was determined by the addition of 100- to 500-fold excess unlabeled ligand to some wells. This radioactivity was subtracted from the radioligand only wells to give specific ligand binding. To determine the association rate, the binding reactions were removed at the indicated times, the wells were washed, and bound radioligand was determined in a γ-counter. As steady state was reached by 2 h, the dissociation rate was determined by removing unbound radioligand at 3 h, washing the wells, and then adding a 300-fold excess of unlabeled ligand in 150 μl assay buffer. At the indicated times, the binding reaction was removed, and the wells were washed and then counted for bound radioactivity. The equilibrium association rate constant (Ka) was determined from these kinetic experiments using linearized binding data and least squares regression to determine association and dissociation rates as previously described (23), using the formula $K_a = k_1/k_{-1}$, where k_1 is the association rate, and k_{-1} is the dissociation rate.

To estimate their relative direct binding of FS and FSRP, equal amounts (counts per min) of radiolabeled activin, BMP 7, or BMP 6 were added to FS- or FSRP-coated wells. Nonspecific binding was determined in the presence of a 100- to 500-fold excess of unlabeled ligand and was

subtracted from the total to give specific binding, expressed as a percentage of the total counts added.

Northern analysis

For Northern analysis of FSRP expression in cell lines, approximately 20 μg total RNA/cell line were denatured at 70 C in a glyoxal/dimethylsulfoxide buffer (NorthernMax-Gly kit, Ambion, Inc., Austin, TX) and electrophoretically separated in a 1% agarose gel at a constant 120 V. RNA was transferred to a positively charged nylon membrane (BrightStar-Plus, Ambion, Inc., Austin, TX) using downward transfer for 2 h and microwave cross-linked. The membrane was hybridized overnight to a 472-bp radiolabeled double-stranded DNA human FSRP probe at approximately 5×10^6 cpm/ml in a roller bottle at 42 C. After washing twice at 42 C, the membrane was exposed to film for 12 h at −80 C, then stripped by boiling in diethylpyrocarbonate-water containing 0.1% SDS for 5 min and subsequently rehybridized to double stranded DNA probes specific for human FS (512 bp) or human β-actin (213 bp).

The Northern probes were generated as follows. DNA template (100 ng) and 5 μg random hexamers were boiled for 3 min, iced, and then added to a reaction mix containing 2.5 μl 0.5 mM deoxy (d)-NTPs (without dCTP), 2.5 μl 10 × Klenow fragment buffer, 5 μl 3000 Ci/mmol [α-^{32}P]dCTP, and 1 μl Klenow fragment (5 U). After incubating for 3 h at 25 C, the reaction was stopped by the addition of 1 μl 0.5 M EDTA, 3 μl 10 mg/ml tRNA, and 100 μl TRIS-EDTA buffer. The unbound radioactivity was removed by centrifuging the reaction mix through a Sephadex G-50 column. The DNA probes were then denatured by incubating with 1.5 ml 10 mM EDTA at 90 C for 10 min and mixed with 500 μl hybridization solution before adding them to the membrane for overnight hybridization.

The oligomer used as template for the FSRP probe was generated by PCR of the cloned human FSRP-coding sequence. The forward FSRP primer spanned the first intron, and its sequence was CGCCCCGGTGGTGTTTG. The reverse primer was located within exon 4, and its sequence was GCGCTGCCCGTCTGGTCC. FSRP cDNA was then amplified with 35 cycles at 94, 58, and 72 C and was purified using a PCR purification kit (Promega Corp., Madison, WI). The oligomers used for the FS and β-actin probes were generated by performing PCR on human granulosa cell cDNA using previously described primer sets (24).

To compare the expression of FSRP and FS in human tissues, the DNA FSRP and FS probes were hybridized sequentially to a Human Multiple Tissue Expression Array (CLONTECH Laboratories, Inc., Palo Alto, CA), which contains poly(A)$^+$ RNA from various human tissues spotted at equal densities, as calibrated by five different housekeeping genes. Autoradiograms were scanned using Adobe PhotoShop software (Abacus Concepts, Inc., Berkeley, CA), and the band densities were quantified using NIH Image software.

FSRP RIA

Iodinated pure recombinant human FSRP-FLAG was used as a radioligand with our polyclonal FSRP antibody. In 300 μl, 25 ng antibody in 1:400 normal rabbit serum, 50,000 cpm radioligand, and FSRP-FLAG standard or unknown sample were added and incubated overnight at 22 C. Goat antirabbit antiserum (1:16 in PBS) and 2.5% (final concentration) polyethylene glycol were added for 2 h, after which the tubes were centrifuged, aspirated, and counted in a γ-counter. The minimum detectable dose was approximately 5 ng/ml, and the intraassay coefficient of variation was 6.5%. All samples from a single experiment were analyzed in a single assay.

Immunocytochemistry

Cells grown on coverslips in six-well trays were treated sequentially with 4% paraformaldehyde, 0.1% Triton-X, and 0.2% gelatin solution, and then incubated in PBS with polyclonal anti-FSRP antibody (2.5 μg/ml) for 1 h at 22 C. Additional coverslips containing LGC were also incubated with a specific monoclonal anti-FS antibody (7FS30, 3 μg/ml) to compare the intracellular distributions of FS and FSRP in the same primary cell type. The coverslips were then placed into PBS containing 1:5000 FITC-conjugated donkey antirabbit or donkey antimouse IgG antibody (Santa Cruz Biotechnology, Inc., Santa Cruz, CA) for 1 h at 22 C.

In a separate experiment CHO cells permanently transfected with FSRP-FLAG cDNA using Effectene (QIAGEN, Valencia, CA) were analyzed by immunocytochemistry with the anti-FSRP antibody or 10 μg/ml monoclonal anti-FLAG M2 primary antibody (Sigma, St. Louis, MO) and 1:5000 rhodamine-conjugated donkey antimouse IgG (Santa Cruz Biotechnology, Inc.). Coverslips were mounted over a droplet of Vectashield (Vector Laboratories, Inc., Burlingame, CA), and inspected and photographed using a Nikon epifluorescent microscope (Melville, NY).

Western blot of fractionated cell extracts

Fractions selectively enriched for cytoplasmic proteins, soluble nuclear proteins, or insoluble nuclear proteins were extracted from CHO FSRP-FLAG cells according to previously published methods (25). Five micrograms of each fraction from the CHO FSRP-FLAG cells and 20 μg wild-type CHO whole cell extract underwent reducing (lithium dodecyl

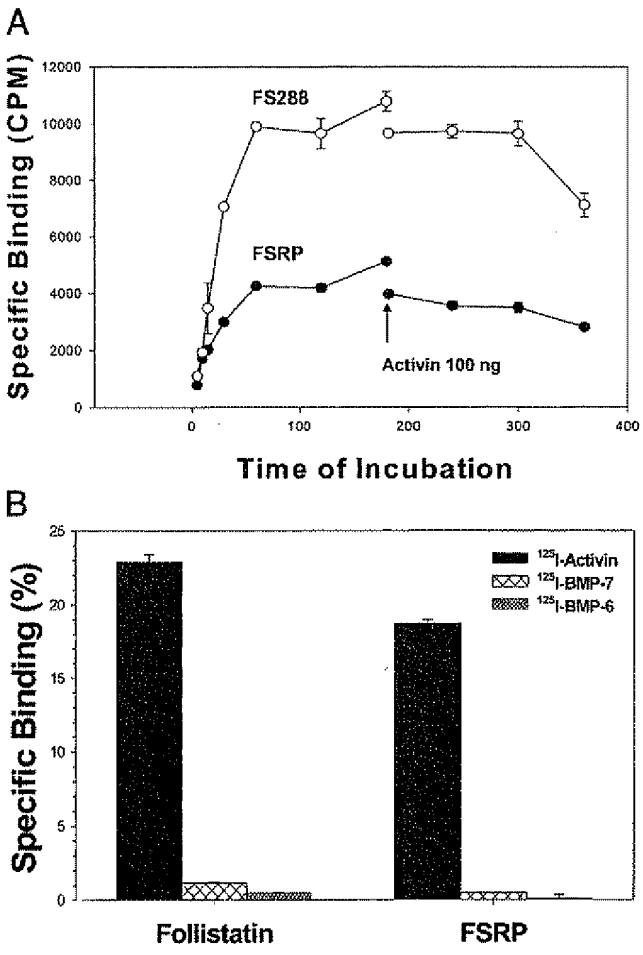

FIG. 2. Activin binding kinetics of FS and FSRP. A, Association/dissociation kinetics for FS and FSRP. Radiolabeled activin bound to both FS and FSRP with a relatively fast association rate. After steady state was reached (3 h), excess unlabeled activin was added for an additional 3 h, but almost no dissociation was observed for either protein. The K_d for FS was 4.63×10^{-10}, whereas for FSRP, a constant of 1.13×10^{-9} was observed, indicating that the affinity of FS for activin is about 2.4-fold greater than that for FSRP. B, Direct binding assay. Identical amounts of radiolabeled activin, BMP-6, and BMP-7 were added to wells coated with either FS288 or FSRP. A 100- to 500-fold excess of cold ligand was added to some wells to determine nonspecific binding. Both FS and FSRP bound 20-fold more activin than BMP-7 and 40-fold more activin than BMP-6, indicating that both FS and FSRP bind activin preferentially over even very closely related TGFβ superfamily proteins.

sulfate) PAGE in a 12% bis-Tris gel (NuPAGE System, Novex, San Diego, CA) and were then transferred to a polyvinylidene difluoride membrane. The primary antibody was either the polyclonal anti-FSRP antibody (2 μg/ml) or the monoclonal anti-FLAG M2 antibody (7.5 μg/ml). The secondary antibody was either donkey antimouse or donkey anti-rabbit conjugated to horseradish peroxidase (each 1:20,000).

Results

FSRP and FS domain structure

The previously described members of the FS domain-containing protein family are extracellular matrix proteins that are not known to bind TGFβ superfamily ligands. Unlike these proteins, FSRP's overall structure is remarkably similar to that of FS, including a signal peptide, an N-terminal domain with conserved cysteine and tryptophan residues, two FS domains, and an acidic C-terminal domain (Fig. 1). Alignment of the N-terminal domains of FSRP and FS reveals 32% sequence identity between FS and FSRP, including the six conserved cysteines. The tryptophans (W) at positions 4 and 36, which have been shown to be responsible for 95–99% of the activin-binding activity of FS (13), are also conserved in FSRP. Their high degree of structural similarity coupled with their shared abilities to bind activin suggest that FSRP and FS comprise their own separate follistatin subfamily.

Activin binding specificity and kinetics

As shown in Fig. 2A, specific [^{125}I]activin binding to both FSRP and FS reached 90% of the maximum after 20 min and achieved a steady state by 2 h. The addition of a 100-fold excess of unlabeled activin after 3 h revealed similarly slow dissociation rates of approximately 5% after 2 h and 10–20% by 3 h. As it is possible that some FSRP-activin complexes lifted off the plate during the 3-h incubation, the actual dissociation rate may be even less than depicted. As Scatchard analysis is not applicable to incompletely reversible binding reactions, equilibrium constants of dissociation were estimated by dividing the on rate by the off rate using linearized data from Fig. 2A. The K_d for FS was 4.63×10^{-10}, whereas for FSRP, a constant of 1.13×10^{-9} was observed. Thus, the affinity of FS for activin under these assay conditions was approximately 2.4-fold greater than that of FSRP.

Figure 2B depicts the relative direct binding of equal amounts (counts per min) of radiolabeled ligand to solid phase FS or FSRP. Activin binding to both FS and FSRP was more than 20-fold greater than BMP-7 and 40-fold greater than BMP-6. This suggests that both FS and FSRP specifically bind activin, as their relative affinities for even the structurally similar BMPs were quite low.

mRNA expression

FSRP and FS mRNA expression was quantified in a wide variety of human adult and fetal tissues using a commercial array containing normalized amounts of poly(A)$^+$ RNA. As shown in Fig. 3, both genes were expressed in nearly all tissues, but the sites of maximal expression were largely

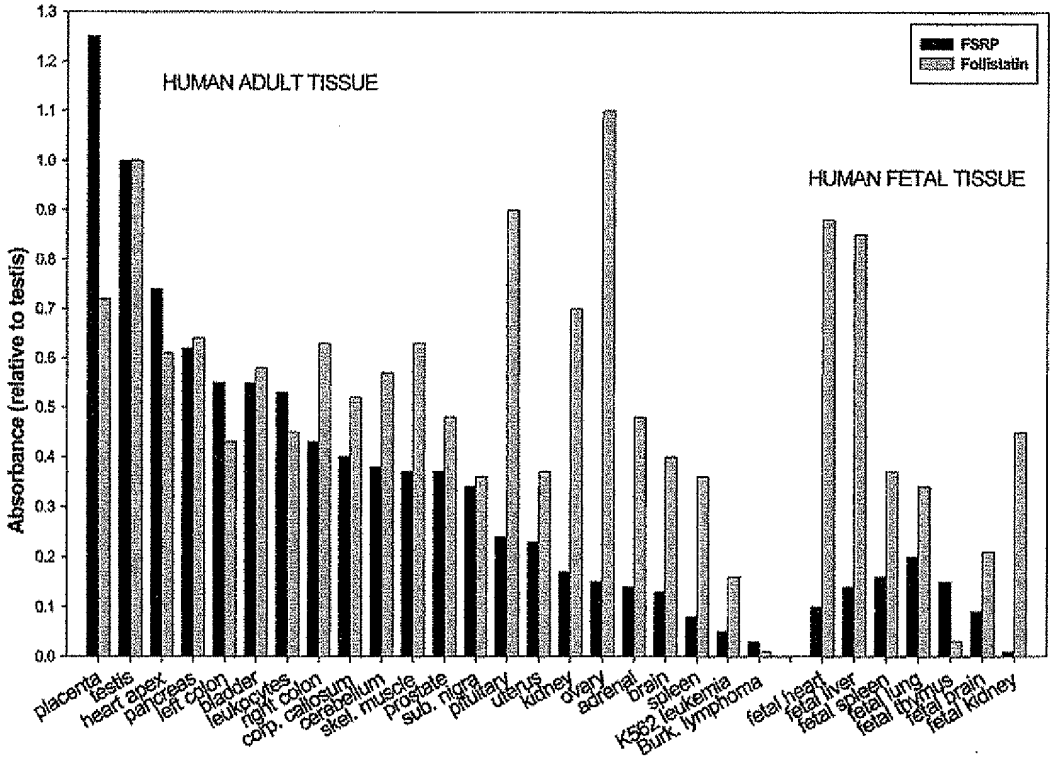

FIG. 3. Expression of FSRP and FS in human tissues. mRNA expression was analyzed using a multiple tissue array with normalized poly(A)$^+$ RNA spots for a wide variety of human adult and fetal tissues. Results are arranged from high to low FSRP expression, with placenta, testes, heart, and pancreas being maximal and lymphoma being minimal. In contrast, FS expression was maximal in ovary, pituitary, kidney, and testes, demonstrating partial overlap of expression, but largely unique sites of maximal expression for these two genes.

distinct. Testicular expression of both genes was quite high, so densitometric analyses were normalized to this tissue. Other than in the testis, however, FSRP expression was maximal in placenta, heart, and pancreas, whereas FS expression was maximal in ovary, pituitary, kidney, and fetal heart and liver. This largely nonoverlapping pattern of maximal expression suggests that in at least some tissues these two proteins do not serve redundant functions.

A separate Northern analysis revealed that mRNA levels varied over a wide range in the numerous cell lines tested, which included those of the breast (MCF-7, BT-20), endometrium (Ishikawa), kidney (HEK-293), and cervix (HeLa, End-1; Fig. 4). Both FSRP and FS mRNA were also detected in primary human LGCs.

RIA

We next examined FSRP secretion from these cells by RIA analysis of conditioned medium. Figure 5 depicts the RIA dilution curve for medium conditioned by HeLa cells, which is parallel to the standard curve, suggesting antibody specificity. Neither FS288 nor FS315 (100 ng) cross-reacted in this assay. In addition, preincubation of FSRP with excess human activin did not affect FSRP measurements, demonstrating that the RIA is capable of detecting both free and bound FSRP (data not shown).

Of all the cell lines we tested, FSRP could be detected by RIA in medium conditioned for 3 d by confluent HeLa, JEG, and CHO cells transfected with FSRP-FLAG cDNA, with a maximal level of approximately 70 ng/ml. On the other hand, human FSRP was undetectable in medium conditioned by the human cell lines MCF-7, BT-20, HEK-293, Ishikawa, and HepG2. Our antihuman FSRP antibody did not detect FSRP in medium conditioned by the nonhuman cell lines CHO and TT. Human follicular fluid aspirated from *in vitro* fertilization patients was also negative for FSRP, as was medium conditioned by their LGCs in primary monolayer culture.

Immunocytochemistry

As FSRP mRNA was detected in all cells examined to date, but secreted protein was detected only in the minority, we

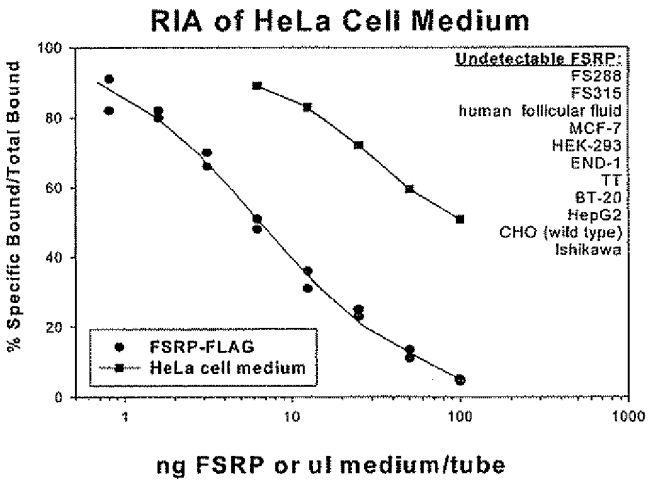

FIG. 5. Development of FSRP RIA. Pure human recombinant FSRP-FLAG and a polyclonal anti-FSRP antibody were used to develop an FSRP RIA. The dilution curve for HeLa medium is depicted and is parallel to the standard curve, indicating that HeLa-conditioned medium contains authentic FSRP protein. FS288 and FS315 were undetectable in this assay, which has a sensitivity limit of 5 ng/ml.

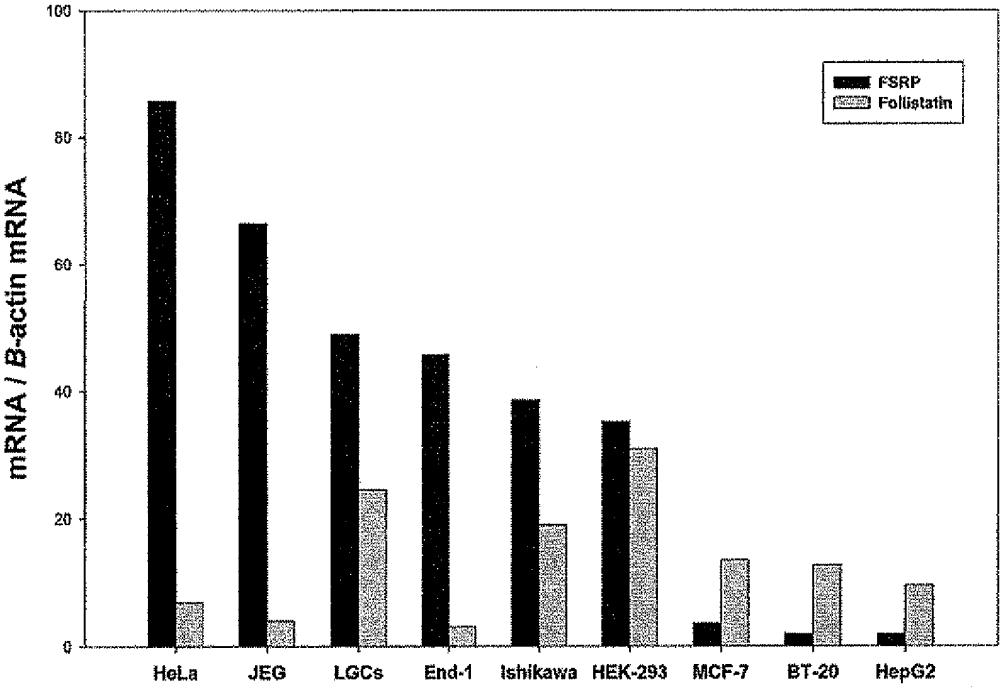

FIG. 4. Northern analysis of FSRP and FS expression in cells. FSRP was highly expressed in a number of cell lines, many of which expressed relatively low levels of FS, and was detectable in all cell lines examined to date. Human LGCs also express FSRP.

next assessed FSRP protein production using immunocytochemistry with the same FSRP-specific antibody as that used in the RIA. FSRP immunoreactivity was detected in all cells examined. However, rather than showing a cytoplasmic or endoplasmic reticular/Golgi pattern commonly observed for secreted proteins such as FS, in all cases FSRP immunoreactivity was predominantly confined to the nucleus (Fig. 6, A–C). Preincubation of the anti-FSRP antibody with a 10-fold excess of recombinant FSRP-FLAG completely abrogated antibody staining (Fig. 6D), indicating that this antibody is specific for an epitope on FSRP. In primary LGCs, which produce both FS and FSRP mRNA, FS immunoreactivity was detected exclusively in the cytoplasm (Fig. 7A). In contrast, FSRP immunoreactivity was again localized to the nucleus (Fig. 7B).

Western blotting

To determine whether the nuclear localization was due to an intrinsic property of the human FSRP-coding sequence as well as to further confirm the specificity of our human FSRP antibody, CHO cells were stably transfected with a human FSRP-FLAG cDNA construct under control of a cytomegalovirus promoter. Both the anti-FSRP antibody as well as the anti-FLAG monoclonal antibody (Fig. 8A) detected FSRP-FLAG within the nucleus, whereas in untransfected cells, no immunoreactivity was detected with either antibody (Fig. 8B).

To more precisely localize FSRP within the cell, compartmentalized proteins were differentially extracted from CHO FSRP-FLAG cells and Western blotted with both anti-FSRP and anti-FLAG antibodies. A prominent immunoreactive band of approximately 34 kDa was detected by both anti-FSRP and anti-FLAG antibodies in the lanes containing the insoluble nuclear protein fraction (Fig. 8C, lane 2). Untagged FSRP has previously been identified as a 32-kDa protein by Western analysis (1), which shifts to its expected M_r of 27.6 kDa after deglycosylation. Therefore, our 34-kDa immunoreactive band is appropriate for glycosylated FSRP possessing a 10-amino acid FLAG tag. Cytoplasmic and soluble nuclear protein from CHO FSRP-FLAG cells (Fig. 8C, lanes 1 and 3) and a 4-fold excess of whole cell protein extract from untransfected CHO cells (lane 4) showed little or no such immunoreactivity.

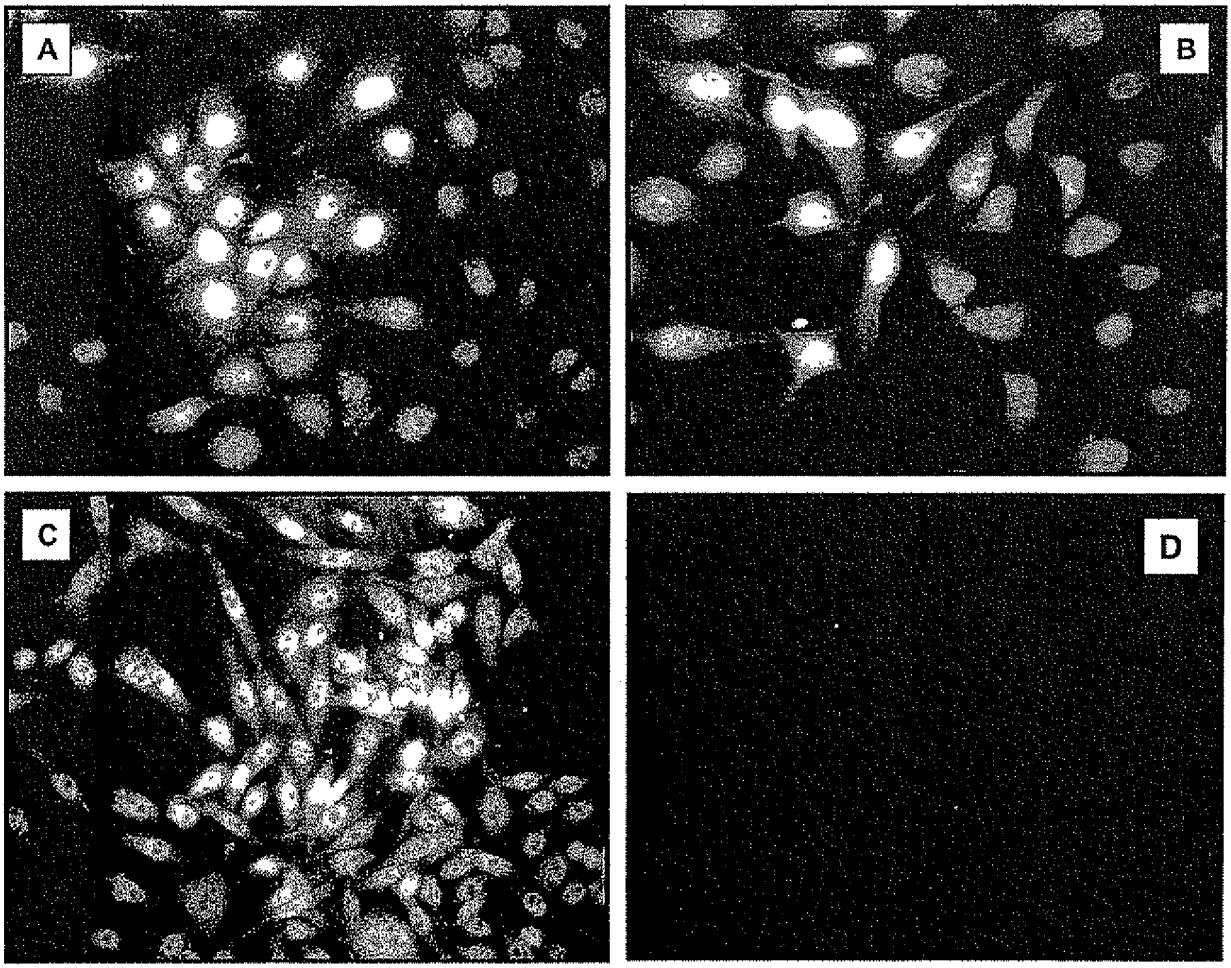

FIG. 6. Intracellular distribution of FSRP in cell lines. FSRP immunoreactivity is nuclear in Ishikawa (A), HeLa (B), and 293 cells (C) and preincubation of the FSRP antibody with a 10-fold excess of recombinant human FSRP-FLAG completely abrogates immunoreactivity in 293 cells (D).

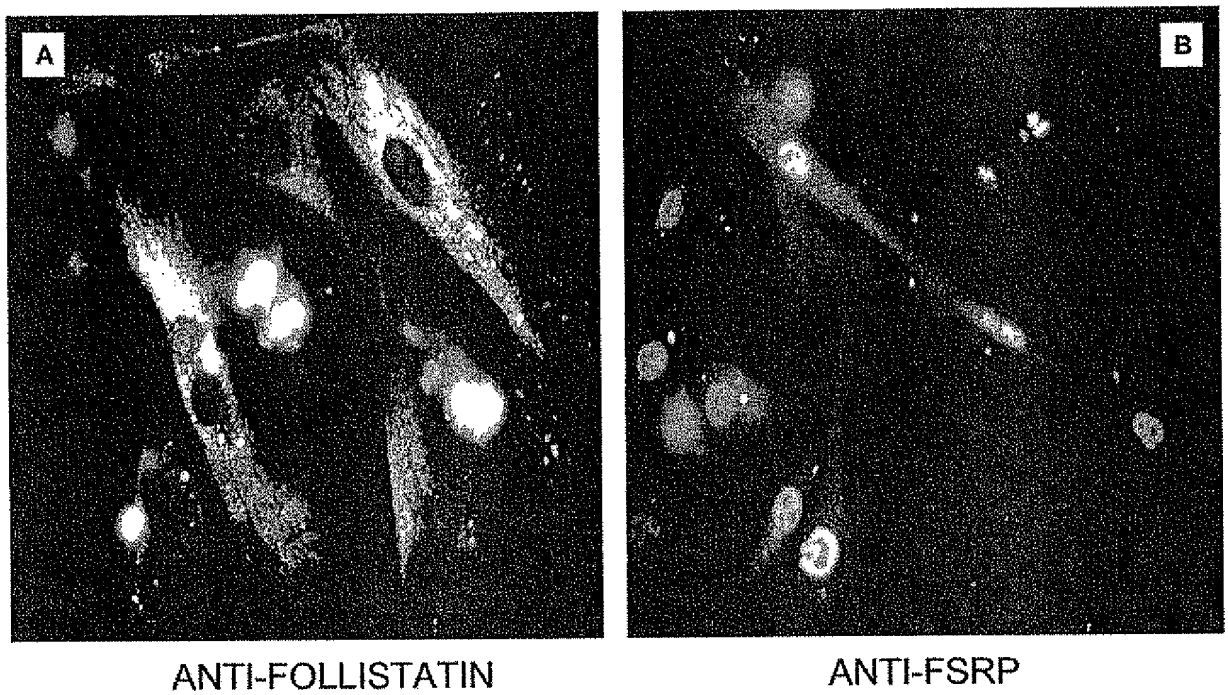

FIG. 7. FS and FSRP in LGC. FS immunoreactivity (A) is localized primarily to the cytoplasm, whereas FSRP (B) is localized almost entirely to the nucleus.

Discussion

FSRP's similarity to FS is more extensive than that of all other known FS domain-containing proteins. Thus, in addition to its two FS domains, FSRP also contains a signal sequence, an N-terminal domain, and a C-terminal domain, which, like FS, are each encoded by separate exons. Consistent with this structural similarity to FS, FSRP has also been shown to bind activin and, at least in very high concentrations, to diminish activin-mediated gene transcription (15).

As the relative affinities of FS and FSRP for activin as well FSRP's activin binding kinetics were unknown, we investigated these parameters in our evaluation of their potential for functional redundancy. We found that activin binding to both FS and FSRP was rapid and nearly irreversible, but the affinity for activin was approximately 2.4-fold greater for FS than for FSRP, suggesting that FSRP might be slightly less potent than FS in binding and neutralizing activin. In addition, the preferential ligand for both FS and FSRP appears to be activin, which, in a direct binding assay, was able to bind both FS and FSRP with at least 20-fold greater magnitude than its closely related TGFβ family counterparts, BMP-6 and BMP-7 (26).

Although both FSRP and FS mRNA are located in a wide and largely overlapping range of human adult and fetal tissues, their sites of peak expression are different, with FSRP expression being exceptionally high in the placenta, testis, and cardiovascular tissue, whereas FS was highest in the ovary and pituitary. Their relative gene expression was also different among fetal tissues and several human cell lines. These observations suggest that FSRP and FS are differentially regulated spatially and temporally.

Based upon identification of an N-terminal signal sequence and no known nuclear localization signals, FSRP was predicted to be a secretory glycoprotein, analogous to FS, by both PSORT II (27) and TargetP V1.0 (28). Indeed, FSRP has been detected by Western blotting in the conditioned medium of transfected COS-7 cells as well as certain tumoral cell lines (14). However, when we scrutinized several other cell lines that produced FSRP mRNA by Northern analysis, secreted FSRP was only detectable from confluent HeLa, JEG, and CHO cells permanently transfected with human FSRP-FLAG cDNA. In addition, follicular fluid aspirated from *in vitro* fertilization patients was negative for FSRP, a finding in stark contrast to FS, which is present at concentrations greater than 200 ng/ml in this fluid (29).

Several possible explanations exist for our failure to detect secreted FSRP in cells known to produce its mRNA. It is possible that certain cell lines secrete very low amounts of FSRP that are below our RIA's 5 ng/ml limit of detection. In addition, FSRP may be proteolytically processed after secretion and thereby escape detection by our polyclonal FSRP antibody. Alternatively, human FSRP may only be secreted under conditions of exceptionally high expression. This explanation seems plausible given that FSRP was detected in medium conditioned by JEG and HeLa cells, which we noted to produce among the highest levels of FSRP mRNA by Northern analysis.

To determine whether FSRP protein was being synthesized in cells that were negative for secretion by our RIA, we performed immunocytochemistry. Our analyses clearly indicate that at least a portion of the synthesized FSRP is located within the nucleus or associated with the nuclear membrane. This is supported by our finding that FSRP-FLAG, as detected with both an anti-FSRP and an anti-FLAG

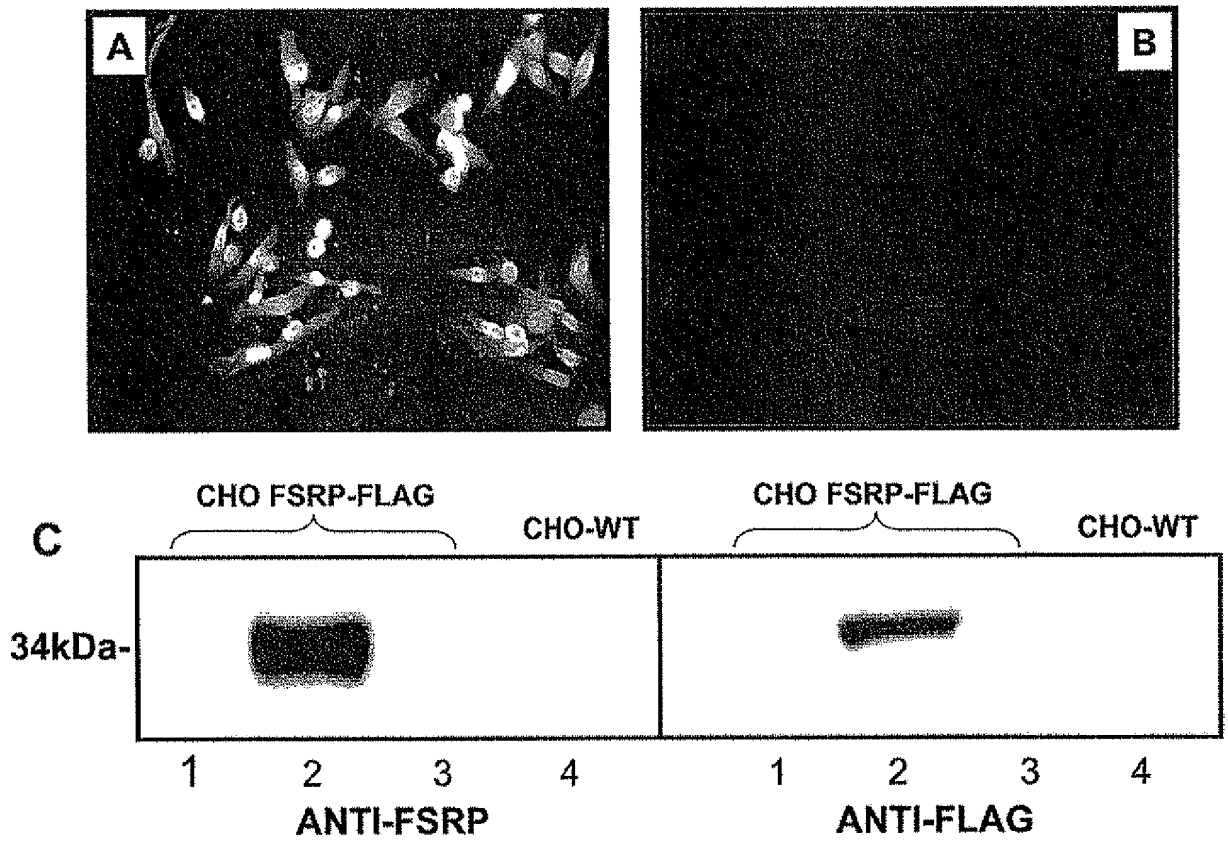

FIG. 8. The FSRP-coding sequence targets FSRP to the nucleus. A, Human FSRP-FLAG-transfected CHO cells stained with anti-FLAG show that exogenously introduced human FSRP cDNA encodes a protein that targets the nucleus. Identical immunoreactivity was seen with the anti-FSRP antibody (not shown). Untransfected CHO cells (B) contain no FLAG-immunoreactive proteins. These cells were also negative for antihuman FSRP immunoreactivity (not shown). C, Both polyclonal FSRP and monoclonal FLAG antibodies detect a protein at approximately 34 kDa, consistent with FLAG-tagged glycosylated human FSRP, in the insoluble nuclear protein fraction (lane 2) of CHO FSRP-FLAG cells. Equal amounts of soluble protein (5 μg/lane) from the cytoplasm and nucleus (lanes 1 and 3) of these cells are negative. Untransfected CHO whole cell extract (20 μg) shows no immunoreactivity to either antibody (lane 4).

antibody, is also localized to the nucleus. Western analyses of protein extracts from CHO FSRP-FLAG cells corroborate the immunocytochemical studies and further demonstrate that FSRP-FLAG is concentrated in the insoluble nuclear protein fraction, a fraction enriched for nuclear membrane-associated proteins. Importantly, the nuclear localization of FSRP-FLAG in transfected CHO cells demonstrates that the nuclear transport of human FSRP is a characteristic intrinsic to its amino acid sequence, which although very similar to FS in terms of overall domain structure, shares only approximately 40% identity with FS.

Unfortunately, our anti-FSRP antibody was unable to detect FSRP, nuclear or otherwise, on slides of fixed human tissues despite its ability to specifically recognize FSRP in immunocytochemistry, RIA, and Western blotting. We believe this is due to antigen masking, a not uncommon consequence of the fixing and processing of tissue for immunohistochemistry. It is worth emphasizing, however, that the nuclear localization of FSRP was seen prominently in monolayers of human granulosa cells, which are primary human cells in culture and not an immortalized cell line. The nuclear pattern of FSRP was also demonstrable in cultured nonluteinized granulosa cells (data not shown). As these cells were aspirated from early follicular phase antral follicles, they were never exposed to supraphysiological concentrations of gonadotropins *in vivo* and are therefore even further representative of normal human tissue.

Although it is possible that the nuclear localization of FSRP in cell lines is secondarily induced by *in vitro* culture conditions, we believe this to be improbable, as this was a universal finding in the cell lines screened, including both secretors and nonsecretors of FSRP. Moreover, we were able to detect nuclear FSRP in human granulosa cells that were in culture for only 48 h. Nonetheless, the finding that a protein so structurally similar to the secretory glycoprotein FS is targeted to the nucleus under any conditions is an intriguing discovery, suggesting a novel intracellular function and transport mechanism.

At this point, the precise pattern and regulation of FSRP's intracellular trafficking pattern are unknown. Although other proteins have been observed to translocate from the endoplasmic reticulum to the cytoplasm, this process usually involves removal of incorrectly folded proteins (30), or results from alternate splicing and processing of the signal peptide (31). However, one possible explanation for our observations is that transport of FSRP out of the endoplasmic

reticulum and into the nucleus requires binding of a chaperone whose concentration is limited. Thus, when FSRP is overexpressed, the chaperone becomes saturated, and excess FSRP gets secreted. Alternatively, as a functional nuclear localization signal has recently been identified in the activin β_A-subunit precursor (32), it is possible that FSRP may bind activin A en route to the nucleus. In fact, both β_A-subunit and an immunoreactive follistatin-like protein have been separately observed in the nuclei of rat spermatogenic cells using immunocytochemical approaches (32, 33).

In conclusion, despite their high degree of structural homology and mutual affinity for activin, additional evidence suggests that FSRP may not be functionally redundant to FS. Despite significant overlap, their sites of maximal mRNA expression are distinct in human tissues, and although FSRP clearly has a signal sequence and the capacity to be secreted, the majority of cell lines we tested secreted no detectable FSRP. FSRP was universally detectable, however, as a nuclear protein by immunocytochemistry and Western blotting. These intriguing findings suggest that FSRP may have unique intracellular functions distinct from those of FS.

Acknowledgments

Received February 9, 2001. Accepted April 16, 2001.

Address all correspondence and requests for reprints to: Dr. Drew V. Tortoriello, Columbia University College of Physicians and Surgeons, Division of Molecular Genetics, Ross Berrie Medical Sciences Pavilion, 1150 St. Nicholas Avenue, New York, New York 10032. E-mail: dvtortoriello@pol.net.

This work was supported in part by Grants DK-55838, HD-29164, and HD-39777 (to A.L.S.).

References

1. **Robertson DM, Klein R, de Vos FL, et al.** 1987 The isolation of polypeptides with FSH suppressing activity from bovine follicular fluid which are structurally different to inhibin. Biochem Biophys Res Commun 149:744–749
2. **Shimasaki S, Koga M, Esch F, et al.** 1988 Primary structure of the human follistatin precursor and its genomic organization. Proc Natl Acad Sci USA 85:4218–4222
3. **Kim SK, Hebrok M, Li E, et al.** 2000 Activin receptor patterning of foregut organogenesis. Genes Dev 14:1866–1871
4. **Asashima M, Aritzumi T, Malacinski GM** 2000 In vitro control of organogenesis and body patterning by activin during early amphibian development. Comp Biochem Physiol B Biochem Mol Biol 126:169–178
5. **DePaolo LV, Bicsak TA, Erickson GF, Shimasaki S, Ling N** 1991 Follistatin and activin: a potential intrinsic regulatory system within diverse tissues. Proc Soc Exp Biol Med 198:500–512
6. **Nakamura T, Takio K, Eto Y, Shibai H, Titani K, Sugino H** 1990 Activin-binding protein from rat ovary is follistatin. Science 247:836–838
7. **Schneyer AL, Rzucidlo DA, Sluss PM, Crowley Jr WF** 1994 Characterization of unique binding kinetics of follistatin and activin or inhibin in serum. Endocrinology 135:667–674
8. **de Winter JP, ten Dijke P, de Vries CJ, et al.** 1996 Follistatins neutralize activin bioactivity by inhibition of activin binding to its type II receptors. Mol Cell Endocrinol 116:105–114
9. **Hashimoto O, Nakamura T, Shoji H, Shimasaki S, Hayashi Y, Sugino H** 1997 A novel role of follistatin, an activin-binding protein, in the inhibition of activin action in rat pituitary cells. Endocytotic degradation of activin and its acceleration by follistatin associated with cell-surface heparan sulfate. J Biol Chem 272:13835–13842
10. **Nakamura T, Sugino K, Titani K, Sugino H** 1991 Follistatin, an activin-binding protein, associates with heparan sulfate chains of proteoglycans on follicular granulosa cells. J Biol Chem 266:19432–19437
11. **Delbaere A, Sidis Y, Schneyer AL** 1999 Differential response to exogenous and endogenous activin in a human ovarian teratocarcinoma-derived cell line (PA-1): regulation by cell surface follistatin. Endocrinology 140:2463–2470
12. **Wang Q, Keutmann HT, Schneyer AL, Sluss PM** 2000 Analysis of human follistatin structure: identification of two discontinuous N-terminal sequences coding for activin A binding and structural consequences of activin binding to native proteins. Endocrinology 141:3183–3183
13. **Sidis Y, Schneyer AL, Sluss PM, Johnson LN, Kentmann HT** 2001 Follistatin: essential role for the N-terminal domain in activin binding and neutralization. J Biol Chem 276:17718–17726
14. **Hayette S, Gadoux M, Martel S, et al.** 1998 FLRG (follistatin-related gene), a new target of chromosomal rearrangement in malignant blood disorders. Oncogene 16:2949–2954
15. **Tsuchida K, Arai KY, Kuramoto Y, Yamakawa N, Hasegawa Y, Sugino H** 2000 Identification and characterization of a novel follistatin-like protein as a binding protein for the TGF-β family. J Biol Chem 275:40788–40796
16. **Kogawa K, Nakamura T, Sugino K, Takio K, Titani K, Sugino H** 1991 Activin-binding protein is present in pituitary. Endocrinology 128:1434–1440
17. **Meriggiola MC, Dahl KD, Mather JP, Bremner WJ** 1994 Follistatin decreases activin-stimulated FSH secretion with no effect on GnRH-stimulated FSH secretion in prepubertal male monkeys. Endocrinology 134:1967–1970
18. **Hemmati-Brivanlou A, Kelly OG, Melton DA** 1994 Follistatin, an antagonist of activin, is expressed in the Spemann organizer and displays direct neuralizing activity. Cell 77:283–295
19. **Matzuk MM, Lu N, Vogel H, Sellheyer K, Roop DR, Bradley A** 1995 Multiple defects and perinatal death in mice deficient in follistatin. Nature 374:360–363
20. **Patthy L, Nikolics K** 1993 Functions of agrin and agrin-related proteins. Trends Neurosci 16:76–81
21. **Lane TF, Sage EH** 1994 The biology of SPARC, a protein that modulates cell-matrix interactions. FASEB J 8:163–173
22. **Alliel PM, Perin JP, Jolles P, Bonnet FJ** 1993 Testican, a multidomain testicular proteoglycan resembling modulators of cell social behaviour. Eur J Biochem 214:347–350
23. **Schneyer AL, Rzucidlo DA, Sluss PM, Crowley Jr WF** 1994 Characterization of unique binding kinetics of follistatin and activin or inhibin in serum. Endocrinology 135:667–674
24. **Fujiwara T, Lambert-Messerlian G, Sidis Y, et al.** 2000 Analysis of follicular fluid hormone concentrations and granulosa cell mRNA levels for the inhibin-activin-follistatin system: relation to oocyte and embryo characteristics. Fertil Steril 74:348–355
25. **Ausubel FM, Brent R, Kingston RE, et al.** 1995 Current protocols in molecular biology. New York: John Wiley & Sons
26. **Yamashita H, ten Dijke P, Huylebroeck D, et al.** 1995 Osteogenic protein-1 binds to activin type II receptors and induces certain activin-like effects. J Cell Biol 130:217–226
27. **Emanuelsson O, Nielsen H, Brunak S, von Heijne G** 2000 Predicting subcellular localization of proteins based on their N-terminal amino acid sequence. J Mol Biol 300:1005–1016
28. **Nakai K, Horton P** 1999 PSORT: a program for detecting sorting signals in proteins and predicting their subcellular localization. Trends Biochem Sci 24:34–36
29. **Lambert-Messerlian G, Taylor A, Leykin L, et al.** 1997 Characterization of intrafollicular steroid hormones, inhibin, and follistatin in women with and without polycystic ovarian syndrome following gonadotropin hyperstimulation. Biol Reprod 57:1211–1216
30. **Johnson AE, Haigh NG** 2000 The ER translocon and retrotranslocation: is the shift into reverse manual or automatic? Cell 102:709–712
31. **Kurys G, Tagaya Y, Bamford R, Hanover JA, Waldmann TA** 2000 The long signal peptide isoform and its alternative processing direct the intracellular trafficking of interleukin-15. J Biol Chem 275:30653–30659
32. **Blauer M, Husgafvel S, Syvala H, Tuohimaa P, Ylikomi T** 1999 Identification of a nuclear localization signal in activin/inhibin β_A subunit; intranuclear β_A in rat spermatogenic cells. Biol Reprod 60:588–593
33. **Ogawa K, Hashimoto O, Kurohmaru M, Mizutani T, Sugino H, Hayashi Y** 1997 Follistatin-like immunoreactivity in the cytoplasm and nucleus of spermatogenic cells in the rat. Eur J Endocrinol 137:523–525

EXHIBIT 3

8. Matzuk, M. M. *et al. Nature* **374,** 354–356 (1995).
9. Roberts, V. J. & Barth, S. *Endocrinology* **134,** 914–923 (1994).
10. Woodruff, T. K., Lyon, R. J., Hansen, S. E., Rice, G. C. & Mather, J. P. *Endocrinology* **127,** 3196–3205 (1990).
11. Mather, J. P. *et al. Endocrinology* **127,** 3206–3214 (1990).
12. Kalpla, A., Toppari, J., Huhtaniemi, I. & Pranko, J. *Endocrinology* **134,** 2165–2170 (1994).
13. Shikone, T. *et al. Molec. Endocr.* **8,** 983–995 (1994).
14. deWinter, J. P. *et al. Molec. Cell Endocr.* **83,** R1–R8 (1992).
15. Feng, Z.-M., Madigan, M. B. & Chen, C.-L. C. *Endocrinology* **132,** 2593–2600 (1993).
16. Cameron, V. A. *et al. Endocrinology* **134,** 799–808 (1994).
17. Ritzen, E. M., Hansson, V. & French, F. S. In *The Testis* 2nd edn (eds Burger, H. & de Kretser, D.) 269–302 (Raven, New York; 1989).
18. Vassali, A. *et al. Genes Dev.* **8,** 414–427 (1994).
19. Hemmati-Brivanlou, A. & Melton, D. A. *Nature* **359,** 609–614 (1992).
20. Hemmati-Brivanlou, A. & Melton, D. A. *Cell* **77,** 273–281 (1994).
21. Schulte-Merker, S., Smith, J. C. & Dale, L. *EMBO J.* **13,** 3533–3541 (1994).
22. Matzuk, M. M. & Bradley, A. *Biochem. biophys. Res. Commun.* **185,** 404–413 (1992).
23. Matzuk, M. M., Finegold, M. J., Su, J.-G. J., Hsueh, A. J. W. & Bradley, A. *Nature* **360,** 313–319 (1992).
24. Mathews, L. S. & Vale, W. W. *Cell* **65,** 973–982 (1991).
25. Bradley, A. in *Teratocarcinomas and Embryonic Stem Cells: A Practical Approach* (ed. Robinson, E. J.) 113–151 (IRL, Oxford, 1987).
26. Ramirez-Solis, R. *et al. Analyt. Biochem.* **201,** 331–335 (1992).
27. Ramirez-Solis, R. *et al. Cell* **83,** 279–294 (1993).
28. Kumar, T. R., Fairchild-Huntress, V. & Low, M. *Molec. Endocr.* **6,** 81–90 (1992).

ACKNOWLEDGEMENTS. We thank J. van den Eijnden-van Raaij for sharing activin-receptor expression data and other information before publication; N. Lu and R. Towns for technical assistance; C. McDonnell for help with cryostat sectioning; S. Topouzis for help with northern blot analysis; S. Baker and B. Powell for help with manuscript preparation; and R. Behringer and M. Meistrich for advice and review of the manuscript. FSH radioimmunoassay reagents were a gift from the National Hormone and Pituitary Distribution Program, National Institute of Diabetes and Digestive and Kidney Diseases. This research was supported in part by grants (to M.M.M.) from the NIH and the Lalor Foundation. A.B. is an investigator with the Howard Hughes Medical Institute.

Multiple defects and perinatal death in mice deficient in follistatin

Martin M. Matzuk*†‡, Naifang Lu†, Hannes Vogel†, Klaus Sellheyer‡, Dennis R. Roop‡ & Allan Bradley*§

Departments of * Molecular and Human Genetics, † Pathology, ‡ Cell Biology, § Howard Hughes Medical Institute, Baylor College of Medicine, Houston, Texas 77030, USA

FOLLISTATIN, **an activin-binding protein and activin antagonist *in vitro*[1,2], can bind to heparan sulphate proteoglycans[3] and may function *in vivo* to present activins to their receptors. In the mouse, follistatin messenger RNA is first detected in the deciduum (on embryonic day 5.5), and later in the developing hindbrain, somites, vibrissae, teeth, epidermis and muscle[4–11]. In *Xenopus laevis*, overexpression of follistatin leads to induction of neural tissue[12]. Here we use loss-of-function mutant mice to investigate the function of follistatin in mammals. We find that follistatin-deficient mice are retarded in their growth, have decreased mass of the diaphragm and intercostal muscles, shiny taut skin, skeletal defects of the hard palate and the thirteenth pair of ribs, their whisker and tooth development is abnormal, they fail to breathe, and die within hours of birth. These defects are more widespread than those seen in activin-deficient mutant mice, indicating that follistatin may modulate the actions of several members of the transforming growth factor-β family.**

To define the roles of follistatin in mammalian development, a targeted deletion (fs^{ml}) of the 6-exon follistatin gene was generated using embryonic stem (ES) cell technology (Fig. 1*a*), and mice heterozygous for this deletion ($fs^{ml}/+$) were intercrossed to generate mice homozygous for the deleted follistatin allele (fs^{ml}/fs^{ml}). Genotyping of mice at birth and at embryonic day 18.5 (E18.5) revealed that fs^{ml}/fs^{ml} mice (follistatin-deficient) could survive to birth but died within hours of delivery (Fig. 1*b*). Of 196 pups at E18.5, 44 were homozygotes (22.4%), 97 were heterozygote (49.5%) and 55 were wild-type (28.1%), consistent with the expected mendelian frequency of 1:2:1. Low-stringency hybridization with a follistatin complementary DNA could detect genomic fragments in wild-type mouse, chicken and *Xenopus laevis* but not in the fs^{ml}/fs^{ml} mice, confirming that we had deleted the only follistatin gene present in the mouse (Fig. 1*c*).

fs^{ml}/fs^{ml} newborns could be phenotypically scored because they were growth-retarded and had shiny, taut skin similar to that seen in the human condition of restrictive dermopathy[13] (Fig. 2*a*). The phenotypic effects of follistatin deficiency were independent of the genetic background (that is, the phenotype was similar on 129SvEv inbred, C57/129 hybrid and C57Bl/6 (3 backcrosses) genetic backgrounds). At birth, most fs^{ml}/fs^{ml} mice remained pale and cyanotic, the lungs of the fs^{ml}/fs^{ml} mice sank in liquid and, on histological examination, the alveolar spaces were poorly expanded, consistent with poor breathing, although primary pulmonary defects could not be detected (data not shown). Analysis of the central and peripheral nervous system by gross dissection and histological procedures did not detect any significant abnormalities. Immunohistochemistry of E10.5 whole-mount embryos using an antibody raised against the 155K neurofilament protein[14] indicated that cranial nerves V, VII, IX and X and the spinal ganglia were developing normally (data not shown).

Defects were detected in the musculoskeletal system. fs^{ml}/fs^{ml} mice lacked incisors (6 of 34, hybrid background; Fig. 2*b*) or had delayed incisor development (Table 1). Three of 19 (16%) hybrid background fs^{ml}/fs^{ml} mice had a cleft secondary palate. Six out of 11 129SvEv inbred mice (55%) and 6 out of 28 C57/

FIG. 1 Targeted deletion of the follistatin gene in ES cells and Southern blot analysis of DNA from offspring derived from heterozygous matings. *a*, The targeting vector contains 3.8 kb of isogenic DNA homologous to the 5′ non-translated sequence of the mouse follistatin gene, 3.4 kb of sequence homologous to the 3′ end of the mouse follistatin gene, a PGK–*hprt* (where PGK represents phosphoglycerate kinase I promoter) expression cassette, and an MC1-tk (thymidine kinase) expression cassette. Homologous recombination between this targeting vector and the endogenous follistatin gene in mouse ES cells should result in a 5.1-kb deletion of the 6 exons coding for follistatin, ensuring that no follistatin mRNA and therefore no follistatin protein was produced in animals homozygous for the targeted allele. Introduction of new diagnostic restriction endonuclease sites (*Bgl*II and *Xba*I) were used to differentiate wild-type versus recombinant alleles. Six ES cell clones out of 1,290 clones (1:215) screened by Southern blot analysis[21,22] were correctly targeted. One ES cell clone, FS3-C2, gave rise to multiple male chimaeras and germline transmission of the deleted allele was demonstrated for 3 of 4 chimaeric males. Male and female mice heterozygous for the deleted follistatin allele occurred at the expected ratio and were viable and fertile. *b*, Genomic (tail) DNA (~5 μg) from offspring from a single litter was restricted with *Xba*I and *Eco*RI and analysed by Southern blot analysis[21] using a 3′ probe as shown. The presence of a 5.9-kb fragment versus a 3.7-kb wild-type fragment is diagnostic of the deletion when using the 3′ probe. Homozygote offspring are dead within hours of birth. WT, wild type; +/−, heterozygote; −/−, homozygote mutant. *c*, Southern blots of wild-type (WT) and fs^{ml}/fs^{ml} (−/−) mice, chicken and *Xenopus laevis* genomic DNA (5 μg per lane) digested with *Bam*HI were analysed using a human follistatin cDNA. The absence of any hybridizable fragment bands in the lane genotyped as homozygote (−/−) confirmed that these mice lack the 6 exons coding for the follistatin gene, that this is a null allele (fs^{ml}), and that there were no follistatin-related genes in the mouse.

METHODS. More than 20 kb of DNA encompassing the 6-exon mouse follistatin gene sequences was isolated from a 129SvEv genomic library using a follistatin cDNA. Linearized vector (25 μg) was electroporated into the *hprt*-negative AB2.1 ES cell line, selected in HAT and FIAU (where HAT represents hypoxanthine, aminopterin, thymidine, and FIAU is (1-(2′-deoxy-2′-fluoro-β-D-arabinofuranosyl)-5-iodouracil), and clones were injected into blastocysts to generate chimaeras[21]. Enrichment in HAT and FIAU was 32-fold compared to HAT alone. Southern blot analysis of the ES cell clones was as described[21,22]. Low-stringency hybridization of the mouse, chicken and *Xenopus laevis* blot was by overnight hybridization at 60 °C followed by 4 washes for 30′ each at 50 °C with a 2 × SSC, 1% SDS solution.

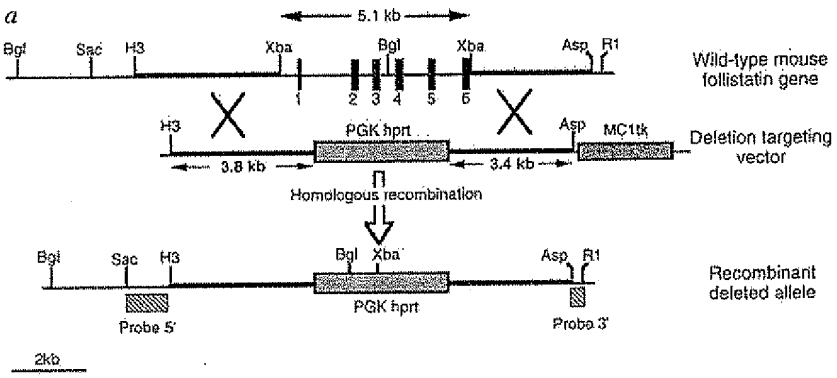

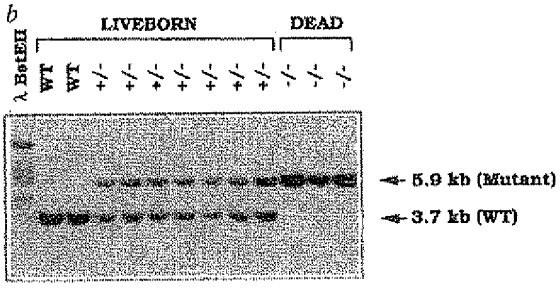

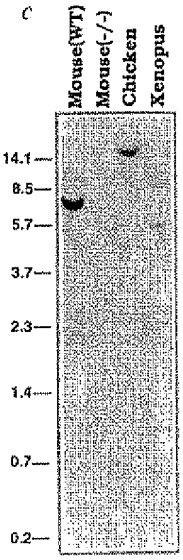

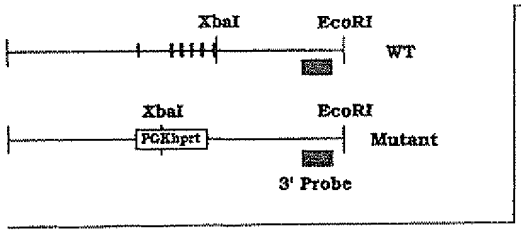

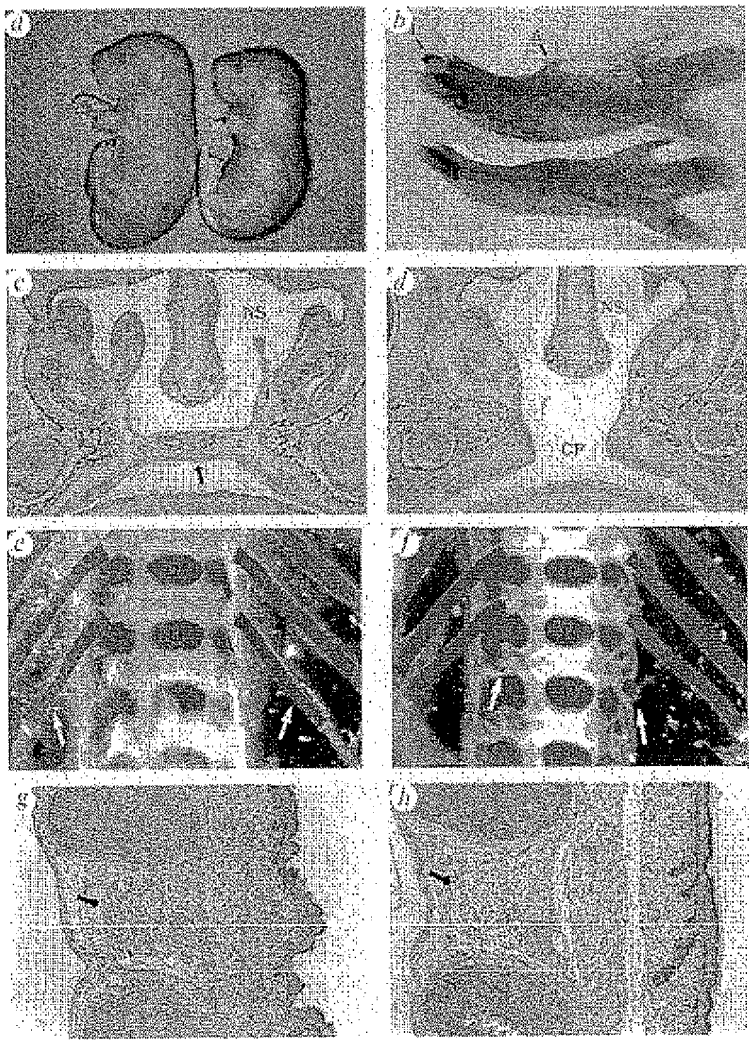

FIG. 2 Morphological and histological analysis of follistatin and control mice. *a*, Control (left) and fs^{ml}/fs^{ml} (right) newborn mice. The fs^{ml}/fs^{ml} mouse on the right was smaller, hypoxic (pale), and had shiny, taut skin compared to the control. Weighing of pups at E18.5 revealed that homozygotes (1.04 ± 0.10 g; $n = 30$) were ~12% lighter than their heterozygote (1.18 ± 0.10 g; $n = 52$) and wild-type (1.17 ± 0.13 g; $n = 18$) littermates. *b*, Medial view of wild-type (top) and fs^{ml}/fs^{ml} (bottom) dissected mandibles stained with alizarin red and alcian blue as described[23]. The alveolar ridge (A), the region of the mandible that surrounds the lower molars, is less prominent and the incisor (I) is missing in the mutant. *c* and *d*, Coronal sections of the head were made at the level of the eye of wild-type (c) and fs^{ml}/fs^{ml} (*d*) mice and the sections stained with alcian blue and neutral red. There is a cleft palate (CP) in the fs^{ml}/fs^{ml} mouse (*d*). The oral cavity is contiguous with the nasal sinus (NS) in *d*. The arrow points to the normal palate in *c*. *e* and *f*, Skeletal analysis (alizarin red stain) of the thirteenth pair of ribs from control (e) and fs^{ml}/fs^{ml} mutant (*f*) mice. The thirteenth pair of ribs is either absent or limited in its formation (arrows, *f*) compared to the same pair in the control (arrows, *e*). Thoracic vertebral bodies are numbered for orientation. *g* and *h*, Analysis of the intercostal (arrows) and pectoralis major musculature from wild-type (*g*) and fs^{ml}/fs^{ml} (*h*) mice taken at the same level (between ribs 3 and 4). Note that the muscle fibres from the mutant are more sparse and less full than the control. A comparable situation is seen in the diaphragm (data not shown).

129 hybrid genetic background mice (21%) lacked a hard palate similar to activin-βA-deficient mice[15] (see below; Fig. 2*c*, *d*). Both inbred and hybrid fs^{ml}/fs^{ml} mice had defects in the thirteenth pair of ribs and a decrease in the number of lumbar vertebrae (Fig. 2*e*, *f*; Table 1). The size of the ribs and penetrance of this phenotype was dependent on the genetic background (Table 1). The intercostal (Fig. 2*g*, *h*) and diaphragmatic (data not shown) muscles showed a decrease in muscle mass consistent with expression of follistatin in the muscle at birth[10]. Histological and electron microscope analysis of the musculature, including analysis of ATPase activity, glycogen content and mitochondria, failed to demonstrate any primary defect (data not shown). Thus, it is not clear whether the decrease in muscle mass in the fs^{ml}/fs^{ml} mice is primary or secondary to an overall growth deficiency.

Whisker development was abnormal: the whiskers were too thin and were inappropriately oriented, suggesting that follistatin may be an important modulator of activin-βA action (Fig. 3*a*–*d*; see accompanying Letter). The skin showed hyperkeratosis, as indicated by thickened granular and stratum corneum layers (Fig. 3*e*, *f*). Electron microscope examination revealed a 25% increase in the stratum corneum cells compared to controls. The shiny, taut skin of fs^{ml}/fs^{ml} mice (Fig. 2*a*) resembles the skin of transgenic mice with directed overexpression of transforming growth factor (TGF)-β1 to the epidermis using a human keratin-1 promoter (HK1.TGF-β1)[16]. Keratin-6 expression was abnormal in the interfollicular epidermis of the fs^{ml}/fs^{ml} mice, as it was in HK1.TGF-β1 mice (Fig. 3*h*). Normally keratin-6 is found only in the outer root sheath of hair follicles (Fig. 3*g*). Although abnormal keratin-6 expression is often associated with hyperproliferation[17], the fs^{ml}/fs^{ml} mice showed normal epidermal mitotic activity as judged by 5-bromodeoxyuridine labelling. These results, together with those obtained for the growth-arrested epidermis of HK1.TGF-β1 mice[16], suggest that keratin-6 expression can occur in response to a variety of stimuli that perturb normal epidermal development.

In conclusion, fs^{ml}/fs^{ml} mice have defects in the musculoskeletal system and in the epidermis, and this constriction effect probably contributes to their rapid demise. Follistatin is expressed in the rhombomeres in the mid-gestational mouse[5], and can cause differentiation of neural cell lines[18]; overexpression in *Xenopus laevis* suggests that follistatin may be essential for neural induction[12]. Our results show that the absence of follistatin in the mouse *in vivo* does not apparently affect the gross development of the nervous system. Interestingly, the fs^{ml}/fs^{ml} mice demonstrate abnormal whisker and tooth development and hard-palate defects similar to activin-βA-deficient mice[15]. In the vibrissae, teeth and palate, where follistatin is expressed adjacent to activin-βA[7], follistatin appears to play a role in activin signal transduction, possibly sequestering activins in heparan sulphate proteoglycans[3] and presenting activin to activin receptors similar to type III TGF-β receptors[19]. The follistatin-deficient mice also have other defects not seen in activin-deficient mice[15]. Some of these defects are similar to those of the BMP-5 (*short ear*) mutant mice, which have defects in the thirteenth pair of ribs[20], and the TGF-β overexpressors, which have shiny, taut skin[16]. These

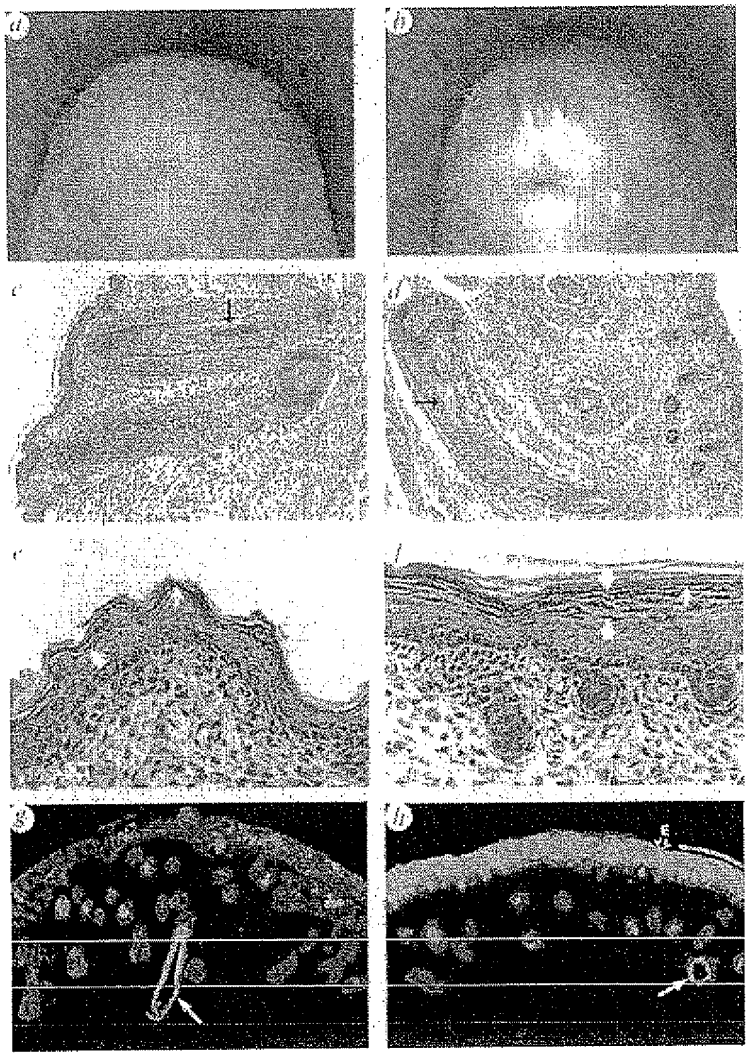

FIG. 3 *a* and *b*, Gross analysis of the whisker pads and face of control (*a*) and fs^{ml}/fs^{ml} (*b*) newborn mice demonstrating the disoriented whiskers and shiny skin of the mutant (*b*). *c* and *d*, Histological analysis (haematoxylin and eosin stain of transverse sections) of the whisker follicles of control (*c*) and fs^{ml}/fs^{ml} (*d*) newborn mice. The whisker shafts (arrow) are perpendicular to the surface in the control (*c*). In the mutant (*d*), the shaft (arrow) projects parallel before turning perpendicularly. *e* and *f*, Histology of the skin of control (*e*) and fs^{ml}/fs^{ml} (*f*) newborn mice photographed at the same magnification. Note the thickened granular (between large white arrows, left) and stratum corneum (between small white arrows, right) layes in the mutant (*f*) compared to the control (*e*). *g* and *h*, Double-label immunofluorescence of the skin from the back of E18.5 control (*g*) and fs^{ml}/fs^{ml} (*h*) mice. The antibody raised against keratin 14 (red) will stain both interfollicular epidermis and hair follicle, whereas the antibody against keratin 6 (yellow/green) will normally stain only the outer root sheath (arrow) of the hair follicle (*g*). In the mutant (*h*), abnormal keratin 6 expression seen in the interfollicular epidermis (E). Single-label immunofluorescence of the mutant skin did not reveal any abnormality in keratin 14 expression (data not shown).

METHODS. Histological analysis of the muscle and skeleton, and double-label immunofluorescence of the skin were performed as described[16,21,23].

TABLE 1 Skeletal, palate and tooth defects

	13th pair of ribs			Five lumbar	Palate defects		Lower incisors	
	Intact	Anlage	Zero ribs	vertebrae*	Cleft	Hard palate	Absent	Delayed
C57/129 hybrid								
Wild-type	15	0	0	2/15	0	0	0	0
Heterozygote	29	6	0	21/35	0	0	0	0
Homozygote†	3	17	8	28/28	3/19	6/28	6/34	23/34
129 inbred								
Wild-type	9	0	0	0/9		0	0	0
Heterozygote	11	4	0	13/15		0	0	0
Homozygote	0	9	2	11/11		6/11	0/11	11/11

* Six lumbar vertebrae are the normal complement in the mouse.
† In 4/28 homozygotes, one or both of the seventh ribs failed to fuse to the sternum.

similarities suggest that follistatin may be a modulator of other TGF-β-related proteins or may function independently. Thus, the results obtained by overexpression of follistatin in *Xenopus laevis*[12] may be a consequence of up or downregulation of the actions of several TGF-β-related proteins. It will be critical to compare mice deficient in other TGF-β superfamily members to our follistatin-deficient mice in order to establish the extent to which follistatin is involved in signal transduction of other TGF-β-related proteins. □

Received 9 November 1994; accepted 24 January 1995.

1. Michel, V., Farnworth, P. & Findlay, J. K. *Molec. cell. Endocr.* **91,** 1–11 (1993).
2. Nakamura, T. *et al. Science* **247,** 836–838 (1990).
3. Nakamura, T., Sugino, K., Titani, K. & Sugino, H. *J. biol. Chem.* **266,** 19432–19437 (1991).
4. van den Eijnden-van Raaij, A. J. M., Feijen, A., Lawson, K. A. & Mummery, C. L. *Devl Biol.* **154,** 356–365 (1992).
5. Albano, R. M., Arkell, R., Beddington, R. S. P. & Smith, J. C. *Development* **120,** 803–813 (1994).
6. Feijen, A., Goumans, M. J. & van den Eijnden-van Raaij, A. J. M. *Development* **120,** 3621–3637 (1994).
7. Roberts, V. J. & Barth, S. *Endocrinology* **134,** 914–923 (1994).
8. Shimasaki, S. *et al. Mol. Endocrinology* **3,** 652–659 (1989).
9. Michel, V., Albiston, A. & Findley, J. K. *Biochem. biophys. Res. Commun.* **173,** 401–407 (1990).
10. Michel, V., Rao, A. & Findley, J. K. *Biochem. biophys. Res. Commun.* **180,** 223–230 (1991).
11. Tashiro, K. *et al. Biochem. Biophys. Res. Commun.* **174,** 1022–1027 (1991).
12. Hemmati-Brivanlou, A., Kelly, O. G. & Melton, D. A. *Cell* **77,** 283–295 (1994).
13. Pierard-Franchimont, C. *et al. J. Path.* **167,** 2223–2228 (1992).
14. Chisaka, O., Musci, T. S. & Capecchi, M. R. *Nature* **335,** 516–520 (1992).
15. Matzuk, M. M. *et al. Nature* **374,** 354–356 (1995).
16. Sellheyer, K. *et al. Proc. natn. Acad. Sci. U.S.A.* **90,** 5237–5241 (1993).
17. Weiss, R. A., Eichner, R. & Sun, T.-T. *J. Cell Biol.* **98,** 1397–1406 (1984).
18. Hashimoto, M. *et al. J. biol. Chem.* **267,** 7203–7206 (1992).
19. Lopez-Casillas, F., Wrana, J. L. & Massague, J. *Cell* **73,** 1435–1444 (1993).
20. Kingsley, D. M. *et al. Cell* **71,** 399–410 (1992).
21. Matzuk, M. M., Finegold, M. J., Su, J-G. J., Hsueh, A. J. W. & Bradley, A. *Nature* **360,** 313–319 (1992).
22. Ramírez-Solis, R. *et al. Analyt. Biochem.* **201,** 331–335 (1992).
23. Ramírez-Solis, R. *et al. Cell* **83,** 279–294 (1993).

ACKNOWLEDGEMENTS. We thank S. Baker and B. Powell for assistance with manuscript preparation; W. Moyle and R. Myers for their help in isolating follistatin cDNA; R. Behringer, J. Bickenbach and T. Rajendra Kumar for critically reviewing the manuscript; and J. Bickenbach for advice on histology and electron microscopy. This research was supported in part by grants from the NIH (to M.M.M.). A.B. is an associate investigator with the Howard Hughes Medical Institute.

The product of *hedgehog* autoproteolytic cleavage active in local and long-range signalling

Jeffery A. Porter, Doris P. von Kessler, Stephen C. Ekker, Keith E. Young, John J. Lee, Kevin Moses* & Philip A. Beachy

Howard Hughes Medical Institute, Department of Molecular Biology and Genetics, The Johns Hopkins University School of Medicine, Baltimore, Maryland 21205, USA
* Department of Biological Sciences, University of Southern California, Los Angeles, California 90089, USA

THE secreted protein products of the *hedgehog* (*hh*) gene family are associated with local and long-range signalling activities that are responsible for developmental patterning in multiple systems, including *Drosophila* embryonic and larval tissues[1–8] and vertebrate neural tube, limbs and somites[9–15]. In a process that is critical for full biological activity, the *hedgehog* protein (Hh) undergoes autoproteolysis to generate two biochemically distinct products, an 18K amino-terminal fragment, N, and a 25K carboxy-terminal fragment, C (ref. 16); mutations that block autoproteolysis impair Hh function. We have identified the site of autoproteolytic cleavage and find that it is broadly conserved throughout the *hedgehog* family. Knowing the site of cleavage, we were able to test the function of the N and C cleavage products in *Drosophila* assays. We show here that the N product is the active species in both local and long-range signalling. Consistent with this, all twelve mapped *hedgehog* mutations either affected the structure of the N product directly or otherwise blocked the release of N from the Hh precursor as a result of deletion or alteration of sequences in the C domain.

To characterize the signalling molecules produced from the uncleaved Hh precursor U, we determined the site of autoproteolysis and the structures of the cleaved products using a purified Hh protein from a bacterial source. This purified protein, His_6C, contains primarily carboxy-terminal sequences and can generate a 25K cleavage product corresponding to the native C cleavage product produced in *Drosophila* cells (Fig. 1*a*). In reactions lasting 3 h and using a wide range of concentrations of starting material, this protein displayed kinetics that were independent of concentration, strongly suggesting that the cleavage was intramolecular (Fig. 1*b*).

Amino-terminal sequencing of the 25K cleavage product showed that Hh is cut between Gly 257 and Cys 258 (Fig. 1*c*). Sequence alignment with other insect and vertebrate *hh* proteins demonstrates the absolute conservation of the Gly-Cys-Phe sequence at the site of autoproteolysis (Fig. 1*d*). To test for the presence of a cysteine residue at the amino terminus of C fragments derived from *Drosophila* (*hh*), zebrafish (*twhh* and *shh*) (S.C.E., manuscript submitted) and mouse (*shh*) genes, ^{35}S-cysteine was incorporated during *in vitro* translation (Fig. 1*e*). Figure 1*f* shows that the first round of protein sequencing in each case released the proportion of total incorporated ^{35}S corresponding to a single cysteine residue, establishing that cysteine

EXHIBIT 4

FSTL3 deletion reveals roles for TGF-β family ligands in glucose and fat homeostasis in adults

Abir Mukherjee*, Yisrael Sidis*, Amy Mahan*, Michael J. Raher†, Yin Xia*, Evan D. Rosen‡, Kenneth D. Bloch†, Melissa K. Thomas§, and Alan L. Schneyer*¶

*Reproductive Endocrine Unit, †Division of Cardiology, and §Laboratory of Molecular Endocrinology and Diabetes Unit, Massachusetts General Hospital, Boston, MA 02114; and ‡Division of Endocrinology, Diabetes, and Metabolism, Beth Israel Deaconess Medical Center, Boston, MA 02215

Edited by Patricia K. Donahoe, Massachusetts General Hospital, Boston, MA, and approved November 27, 2006 (received for review September 11, 2006)

Activin and myostatin are related members of the TGF-β growth factor superfamily. FSTL3 (Follistatin-like 3) is an activin and myostatin antagonist whose physiological role in adults remains to be determined. We found that homozygous FSTL3 knockout adults developed a distinct group of metabolic phenotypes, including increased pancreatic islet number and size, β cell hyperplasia, decreased visceral fat mass, improved glucose tolerance, and enhanced insulin sensitivity, changes that might benefit obese, insulin-resistant patients. The mice also developed hepatic steatosis and mild hypertension but exhibited no alteration of muscle or body weight. This combination of phenotypes appears to arise from increased activin and myostatin bioactivity in specific tissues resulting from the absence of the FSTL3 antagonist. Thus, the enlarged islets and β cell number likely result from increased activin action. Reduced visceral fat is consistent with a role for increased myostatin action in regulating fat deposition, which, in turn, may be partly responsible for the enhanced glucose tolerance and insulin sensitivity. Our results demonstrate that FSTL3 regulation of activin and myostatin is critical for normal adult metabolic homeostasis, suggesting that pharmacological manipulation of FSTL3 activity might simultaneously reduce visceral adiposity, increase β cell mass, and improve insulin sensitivity.

activin | diabetes | metabolism | myostatin | β cell

Members of the TGF-β superfamily of growth factors play diverse roles in embryonic development as well as in organ homeostasis and injury/pathogen response in adults (1). Activin and myostatin form one structurally related branch of the TGF-β family that utilizes common cell-surface receptors and Smad second messengers (2–4). Activin is a critical regulator of embryonic cell fate determination and organ development as well as adult organ homeostasis (5). Activin deletion in mice results in developmental defects and early neonatal death (6), whereas activin overexpression results in cancer, cachexia, and liver necrosis (3, 7, 8). Loss of myostatin expression results in increased muscle mass and reduced adiposity (9–11), whereas overexpression of myostatin leads to a severe reduction of both muscle and adipose tissue mass, along with cachexia (12, 13). These findings demonstrate the requirement for tight regulation of activin and myostatin activity to maintain normal adult physiology.

Regulation of activin and myostatin activity occurs at multiple levels. Among the extracellular regulators, FSTL3 (follistatin like-3) and FST (follistatin) are structurally and functionally related glycoproteins that bind and antagonize actions of both activin and myostatin (14, 15). FSTL3 expression is highest in placenta, followed by testis, pancreas, and heart, whereas FST expression is high in ovary, testis, and kidney, suggesting that they may have nonoverlapping actions in different organs (16). Circulating FST was largely bound to activin (17), whereas FSTL3 was isolated from human and mouse serum as a complex with myostatin (18), indicating that FSTL3 and FST may be important physiological regulators of circulating myostatin and activin.

One experimental approach to examine the importance of regulating activin and myostatin action is to inactivate their physiological antagonists. Deletion of *Fst* resulted in a number of developmental defects and early neonatal death, confirming the importance of FST in mammalian development (19), although the early neonatal death precluded determination of the physiological roles of FST in juveniles and adults. Recently, *FST* was deleted specifically in adult ovaries which resulted in premature cessation of ovarian activity (20), confirming that FST indeed has important roles in postpubertal gonadal function in adults.

To determine the physiological actions of FSTL3, we generated *Fstl3*-null mice. In contrast to *Fst*-null mice, *Fstl3*-deficient animals survive to adulthood and develop a suite of metabolic phenotypes that collectively suggest that FSTL3 and the activin and myostatin ligands it regulates have important metabolic roles in the adult that were heretofore underappreciated.

Results

Generation of FSTL3 Knockout (KO) Mice. We generated mice heterozygous for an *Fstl3* allele missing exon 1 [see supporting information (SI) Fig. 6 *A* and *B*] that, when mated, produced homozygote $Fstl3^{tm1Alsc/tm1Alsc}$ (FSTL3 KO) mice in expected Mendelian ratios that survived to adulthood, allowing analysis of the effect of global FSTL3 deletion in adult mice. Although FSTL3 mRNA was detectable in WT heart, testis, white fat, and muscle, it was undetectable in KO mice (SI Fig. 6 *C* and *D*), verifying that FSTL3 was no longer expressed.

No Change in Body Weight or Muscle Composition in FSTL3 KO Mice. Because myostatin overexpression results in reduced muscle and fat mass (13) and FSTL3 deletion should increase myostatin bioactivity due to its identification as a circulating myostatin binding protein (18), we analyzed age-related changes in body weight in FSTL3 KO mice. The distribution of age-specific body weights in 1- to 4-month-old mice was not different between genotypes (Fig. 1*A*), nor were the mean body weights of 6- to 12-month-old mice (Fig. 1*B*). Moreover, there was no detectable difference between FSTL3 KO and WT mice in gastrocnemius and quadriceps muscle weight (Fig. 1*C*) or histological appearance (see SI Fig. 7 *A* and *B*), and analysis

Author contributions: A. Mukherjee, Y.S., Y.X., E.D.R., K.D.B., M.K.T., and A.L.S. designed research; A. Mukherjee, Y.S., A. Mahan, M.J.R., Y.X., and A.L.S. performed research; M.J.R., K.D.B., and M.K.T. contributed new reagents/analytic tools; A. Mukherjee, Y.S., A. Mahan, M.J.R., Y.X., E.D.R., K.D.B., M.K.T., and A.L.S. analyzed data; and A. Mukherjee, M.J.R., K.D.B., M.K.T., and A.L.S. wrote the paper.

The authors declare no conflict of interest.

This article is a PNAS direct submission.

Abbreviations: KO, knockout; PEPCK, phosphoenolpyruvate carboxykinase; G6Pase, glucose-6-phosphatase.

¶To whom correspondence should be addressed at: Reproductive Endocrine Unit, BHX-5, Massachusetts General Hospital, 55 Fruit Street, Boston, MA 02114. E-mail: schneyer.alan@mgh.harvard.edu.

This article contains supporting information online at www.pnas.org/cgi/content/full/0607966104/DC1.

www.pnas.org/cgi/doi/10.1073/pnas.0607966104

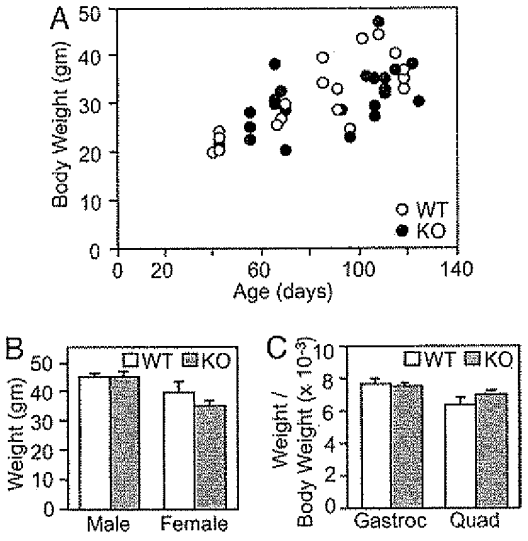

Fig. 1. Growth rate and body weights of FSTL3 KO and WT mice. (*A*) Distribution of age versus body weight of WT and FSTL3 KO male mice is shown for 1- to 4-month-old animals. (*B*) Mean body weights of male (average age, 9 months; $n = 20$ WT and 34 KO) and female (average age, 11 months; $n = 11$ WT and 27 KO) WT and KO mice. (*C*) Weights of dissected quadriceps (Quad) and gastrocnemius (Gastroc) muscles expressed as a ratio to body weight ($n = 25$ WT and 58 KO).

of muscle fiber area distribution of five WT and five KO animals revealed no significant differences (see SI Fig. 7*C*). These results indicate that loss of FSTL3 did not produce a detectable decrease in body weight, muscle mass, or fiber area, as might be expected if myostatin bioactivity were elevated with the loss of a circulating antagonist.

Increased Pancreatic Islet Size in FSTL3 KO Animals. Previous studies have suggested that activin regulates pancreatic β cell proliferation, islet size, and glucose-stimulated insulin secretion (21–23). Because FSTL3 is highly expressed in the pancreas (16), we examined the effect of FSTL3 deletion on pancreatic islets. Representative pancreas sections at low magnification from WT and FSTL3 KO mice immunocytochemically stained for insulin (Fig. 2*A* and *B*, respectively) demonstrate that FSTL3 KO islets are substantially larger than those from WT littermates. At higher magnification, the presence of more intra-islet capillaries can be discerned in FSTL3 KO islets (Fig. 2*D*) compared with WT islets (Fig. 2*C*). Immunofluorescence analysis demonstrated that these larger FSTL3 KO islets contained more insulin expressing β cells (Fig. 2*F*) compared with WT islets (Fig. 2*E*). In addition, although α cells were readily identified at the periphery of WT islets (Fig. 2*E*, white arrows), very few were found in the periphery of KO islets, whereas the majority of green staining resulted from nonspecific fluorescence from red blood cells within KO islets (Fig. 2*F*). Morphometric analysis of 36 WT and 99 KO islets revealed that mean islet size was nearly 50% larger in FSTL3 KO mice (Fig. 2*G*), but β cell size was not different (Fig. 2*H*), indicating that larger islets resulted from β cell hyperplasia. Moreover, FSTL3 KO mice had a broader distribution of islet sizes, with the islet size group containing the most islets being smaller than that for WT islets. In addition, FSTL3 KO islets contained a distinct population much larger than any observed in WT mice (Fig. 2*I*). This distribution increased the number of islets observed per section (Fig. 2*I Inset*). Taken together, these analyses suggest that existing islets grew larger because of β cell hyperplasia in FSTL3 KO mice although there was also a likely increase in islet neogenesis, all

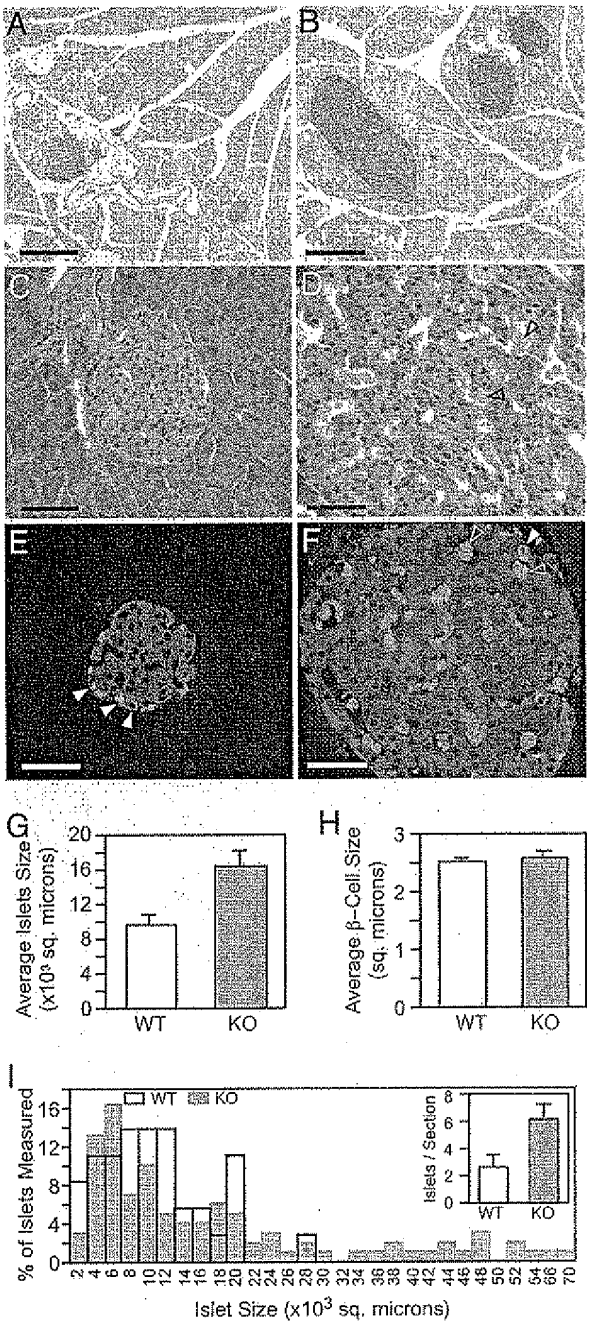

Fig. 2. Increased pancreatic islet size in FSTL3 KO mice. (*A* and *B*) Low-power photomicrographs of WT (*A*) and FSTL3 KO (*B*) pancreas immunocytochemically stained for insulin. (*C* and *D*) H&E staining of the same WT (*C*) and KO (*D*) tissues. Black arrowheads show numerous capillaries within the KO islet. (*E* and *F*) Immunofluorescence photographs showing insulin (red) and glucagon (green) localization in islets from WT (*E*) and KO (*F*) mice. In the KO islets, the majority of green staining is nonspecific staining of red blood cells within the islet, shown by open arrowheads. Glucagon producing α cells in both WT and KO islets are shown by solid arrowheads. (Magnifications: *A* and *B*, ×5; *C–F*, ×40.) (Scale bars, *A* and *B*, 200 μm; *C–F*, 50 μm.) (*G–I*) Histomorphometric analyses of pancreatic islets. Average islet size (*G*) ($n = 36$ WT and 99 KO) and β cell size (*H*) ($n = 119$ WT and 94 KO) in pancreas from WT and KO animals ($n = 6$ WT and 8 KO) (values shown in squared micrometers). (*I*) Size distribution of pancreatic islets in WT and KO animals; percent of total number of islets counted is plotted against islet size. (*Inset*) The mean number of islets seen per section of WT and KO animals. Both islets per section and average islet size is significantly increased ($P < 0.05$) in KO pancreas. All error bars are SEM.

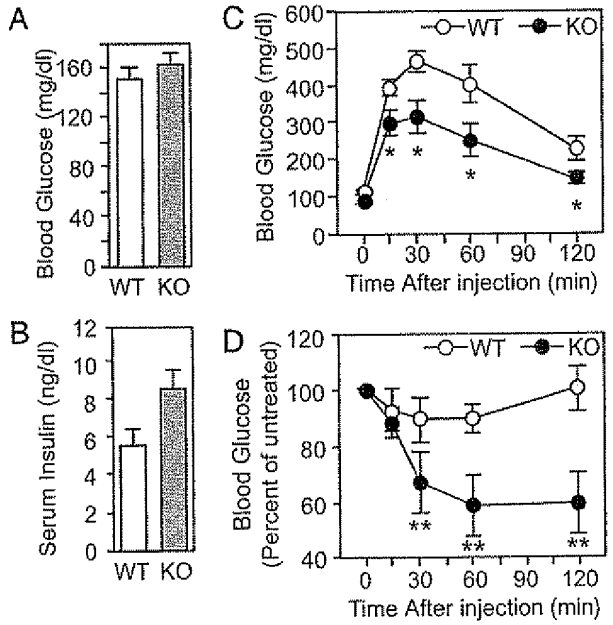

Fig. 3. Enhanced glucose metabolism in FSTL3 KO mice. (*A*) Glucose levels in tail blood of random-fed WT and KO mice are not different (n = 17 WT and 30 KO). (*B*) Serum insulin levels in these same mice are significantly greater ($P <$ 0.05) in KO animals compared with WT littermates. (*C*) Glucose tolerance test showing mean glucose levels of five animals per group after i.p. injection of 2 g/kg glucose at time 0. *, $P < 0.05$. (*D*) Insulin tolerance test showing glucose levels as a ratio to untreated glucose concentration (at time −15 min). Insulin (1 unit/kg) was injected i.p. at time 0. Glucose levels were significantly lower in FSTL3 KO mice from 30–120 min. **, $P < 0.01$. A total of 24 WT and KO mice were examined in these studies. All error bars are SEM.

of which may be due to increased activin bioactivity resulting from loss of FSTL3.

Altered Glucose Homeostasis in FSTL3 KO Animals. We next examined whether the larger and more numerous islets altered glucose homeostasis in FSTL3 KO mice. In 9-month-old, random-fed animals, there was no significant difference in serum glucose levels between FSTL3 KO mice and WT littermates (Fig. 3*A*). However, insulin concentrations were significantly ($P <$ 0.05) elevated in these same mice (Fig. 3*B*), suggesting that they might be insulin-resistant. To examine the dynamic response to glucose and insulin, we performed glucose and insulin tolerance tests. FSTL3 deletion significantly enhanced both glucose tolerance (Fig. 3*C*; $P < 0.05$) and insulin sensitivity (Fig. 3*D*; $P <$ 0.01) in FSTL3 KO mice relative to WT littermates, indicating that the islets in FSTL3 KO mice were not enlarged secondary to insulin resistance. These alterations in glucose and insulin homeostasis, along with the enlarged islets and increased β cell mass in FSTL3 KO mice, are consistent with FSTL3 regulation of activin bioactivity being critical for normal control of glucose metabolism in the adult.

Alterations in Liver Function in FSTL3 KO Mice. Because the liver is a major regulator of glucose metabolism (24) and activin may play a role in liver homeostasis (25, 26), we next determined whether FSTL3 deletion altered hepatic structure and function. Hepatic steatosis was detectable at 5 months of age in FSTL3 KO animals but not in WT littermates (data not shown) and increased in severity by 9 months (Fig. 4 *A–D*). Oil Red O staining confirmed extensive macrovesicular and microvesicular steatosis in FSTL3 KO mice (Fig. 4*F*) that was absent in WT littermates (Fig. 4*F*). However, there were no significant differences between FSTL3 KO and WT littermates in circulating free fatty acid or triglyceride concentrations (see SI Table 1). Moreover, there was no evidence of hepatic necrosis or fibrosis. In addition, serum concentrations of amino aspartate and amino alanine transferase enzymes, indicators of hepatocyte distress (27), were not different between the genotypes (see SI Table 1). These data indicate that overall liver function was not compromised in FSTL3 KO mice.

To further address the liver's role in the altered glucose dynamics in FSTL3 KO mice, we examined liver glycogen stores and found that glycogen content was substantially reduced in FSTL3 KO livers (Fig. 4*H*) compared with WT littermates (Fig. 4*G*). In addition, quantitative PCR analyses revealed that expression of key gluconeogenic enzymes phosphoenolpyruvate carboxykinase (PEPCK) and glucose-6-phosphatase (G6Pase) was elevated by 6- and 4.5-fold, respectively, in FSTL3 KO livers compared with WT littermates (Fig. 4*I*), indicating that gluconeogenesis was elevated in FSTL3 KO mice. We next evaluated whether activin or myostatin could directly regulate PEPCK or G6Pase mRNA expression by using HepG2 hepatoma cells. Activin treatment significantly increased G6Pase expression 1.3-fold ($P < 0.05$), whereas myostatin treatment suppressed G6Pase expression >50% ($P < 0.01$) (Fig. 4*J*), indicating that activin can directly enhance G6Pase mRNA expression. Thus, up-regulated gluconeogenesis in FSTL3 KO mice may be partially due to direct actions of activin on hepatocyte gene expression as well as a homeostatic response to prevent hypoglycemia due to mild, chronic hyperinsulinemia arising from the enlarged islets.

Alterations in Fat Deposition in FSTL3 KO Mice. Because myostatin overexpression also reduced fat mass (13), we examined adipose tissues in FSTL3 KO animals. Both male and female FSTL3 KO mice had significantly smaller abdominal visceral fat depots compared with WT littermates (Fig. 5 *A* and *B*, respectively). However, the fraction of body weight estimated to be composed of fat was not different between genotypes (Fig. 5*C*). Histological (see SI Fig. 8 *A* and *B*) and histomorphometric (see SI Fig. 8*C*) analyses demonstrated that the adipocyte size distribution in FSTL3 KO mice was not different from that in WT littermates, suggesting that the reduced fat pad weights were due to fewer adipocytes in FSTL3 KO mice. Despite the reduced abdominal fat pad mass in FSTL3 KO animals, serum concentrations of leptin and adiponectin, two adipokines that typically reflect fat mass, were not significantly altered (see SI Table 1). Taken together, these results suggest that fat storage is preferentially shifted from visceral to s.c. depots and/or other organs in FSTL3 KO mice. Because previous studies have demonstrated that myostatin administration at low, subpharmacological levels reduced only visceral fat mass (13) and not muscle mass, it is likely that increased myostatin bioactivity resulting from deletion of FSTL3 resulted in altered visceral fat deposition.

FSTL3 KO Animals Are Hypertensive. Because FSTL3 is highly expressed in heart tissue (16), we examined weight and function of hearts in 9-month-old female FSTL3 KO mice. We found that heart weight relative to body weight, left ventricular end systolic pressure, and systolic arterial pressure were all significantly increased compared with WT littermates (see SI Fig. 9 *A–C*). These observations demonstrate that mice lacking FSTL3 have altered cardiac structure and function that results in hypertension by 9 months of age.

Discussion

The activity of TGF-β superfamily growth factors is regulated at multiple levels. Regulators such as FSTL3 and FST constitute a subfamily of follistatin domain proteins that bind and neutralize TGF-β family ligands, including activin and myostatin (14). The

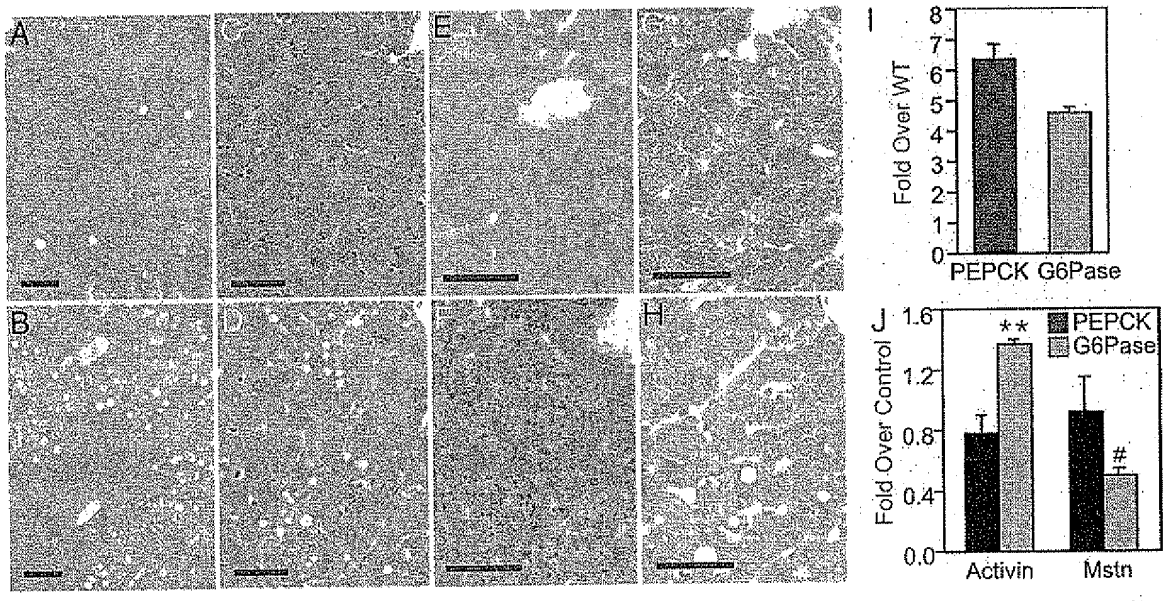

Fig. 4. Liver phenotypes of FSTL3 KO mice. (*A–D*) H&E staining of livers from WT (*A* and *C*) and KO (*B* and *D*) animals. (*E* and *F*) Frozen sections of liver stained with Oil Red O from WT (*E*) and KO (*F*) animals at 9.5 months. (*G* and *H*) Liver sections stained with Periodic acid-Schiff's stain showing vastly reduced glycogen content in FSTL3 KO mice (*H*) compared with WT littermates (*G*). (Magnifications: *A* and *B*, ×10; *C–H*, ×40.) (Scale bars, *A* and *B*, 100 μm; *C–H*, 50 μm.) (*I*) Gluconeogenic genes PEPCK and G6Pase are significantly ($P < 0.05$) elevated in FSTL3 KO mice relative to WT mice by 6- and 4.5-fold, respectively, as analyzed by quantitative PCR. (*J*) Activin (5 ng/ml) significantly ($P < 0.01$) stimulated G6Pase gene expression relative to untreated HepG2 liver hepatoma cells, whereas myostatin (25 ng/ml) suppressed G6Pase under the same conditions ($P < 0.05$).

critical importance of this regulation is emphasized by the previously described defects and early neonatal death resulting from *Fst* deletion (19). We now report that, in contrast to *Fst*-null mice, *Fstl3*-null mice survive to adulthood and are fertile, permitting investigation of the role of a natural activin and myostatin antagonist in adults. By 9 months of age, these mice developed a number of metabolic phenotypes, including increased pancreatic β cell mass and islet number, reduced visceral fat mass, elevated postprandial insulin concentrations, reduced hepatic glycogen, up-regulated gluconeogenesis, hepatic steatosis, and hypertension. These phenotypes were not secondary to peripheral insulin resistance because FSTL3 KO mice were more glucose-tolerant and insulin-sensitive than WT littermates. These findings demonstrate that FSTL3 has important roles in adult physiology, the abrogation of which results in altered glucose and lipid homeostasis. Because FSTL3 is an activin and myostatin antagonist (14), these phenotypes further imply that activin and/or myostatin have critical roles in regulating metabolism that were previously unappreciated.

FSTL3 KO mice have enlarged and more numerous pancreatic islets that primarily contain β cells, suggesting that FSTL3 influences islet size through altering β cell proliferation, survival, and/or differentiation. Activin mRNA, protein, and receptors have been detected previously in β cells (28, 29), and activin treatment increased β cell proliferation (23) and glucose-stimulated insulin secretion in rat and human islet cultures (21, 30). Moreover, transgenic mice expressing a dominant-negative activin receptor in islets had reduced β cell mass (31). In light of these findings, our observations suggest that FSTL3 deficiency resulted in augmented activin bioactivity within islets that induced increased β cell mass, islet size, and islet number *in vivo*. Moreover, enhanced glucose-stimulated insulin production resulting from this increased activin action in β cells could be at least partially responsible for the elevated postprandial insulin concentrations observed in FSTL3 KO mice.

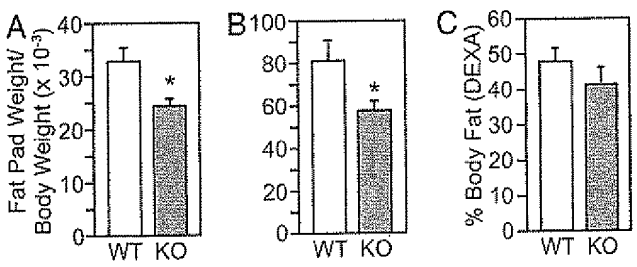

Fig. 5. Fat depot mass is reduced in FSTL3 KO mice. (*A* and *B*) Reduced visceral abdominal fat pad mass in FSTL3 KO males (*A*) ($n = 25$ WT and 56 KO; $P < 0.005$) and females (*B*) ($n = 19$ WT and 42 KO; $P < 0.05$). (*C*) Percent body fat of WT and FSTL3 KO mice, as measured by dual emission x-ray absorptiometry ($n = 6$ WT and 7 KO). All error bars are SEM.

The number and size of islets and the β cells they contain can vary in response to changing metabolic demands (32). Potential sources for these new islets and β cells include β cell proliferation (33) and/or recruitment from progenitor/stem cells (34). Activin has been reported to accelerate proliferation of β cells (23) but also to promote differentiation of ductal cells (35), suggesting that loss of FSTL3 and the consequent increase in activin activity leads to increased β cell proliferation and recruitment that together result in the larger β cell mass and the biphasic distribution of islet size we observed in FSTL3 KO mice.

Because pharmacological overexpression of myostatin in adults decreased muscle mass, visceral fat deposition, and development of cachexia (13) and because circulating myostatin was found complexed with FSTL3 (18), we hypothesized that FSTL3 KO mice would develop decreased total body weight and muscle mass with age. However, we were unable to detect any difference in growth patterns, muscle mass, or muscle fiber size between the genotypes. Importantly, it has been shown that administration of smaller (e.g., 1 μg) doses of myostatin resulted in nearly 50% reduction of visceral fat mass with no changes in body weight, muscle weight, or muscle diameter (13), suggesting that visceral adipose is more sensitive to myostatin action than muscle mass in adults. Because the total body fat of FSTL3 KO

mice was not significantly different from WT littermates but visceral fat was significantly reduced, increased myostatin bioactivity resulting from FSTL3 deletion may redirect lipid deposition from visceral fat pads to s.c. fat depots or to other tissues that are not myostatin-responsive. Thus, the reduced visceral fat mass observed in FSTL3 KO mice may be a primary action of excess myostatin bioactivity resulting from loss of its antagonist. Because accumulation of visceral fat is associated with glucose intolerance and insulin resistance (36), this myostatin-dependent reduction of visceral fat in FSTL3 KO mice may be responsible, at least in part, for the enhanced glucose tolerance and insulin sensitivity in FSTL3 KO mice. It is also possible that the improved glucose tolerance derives to some extent from direct actions of myostatin and/or activin on adipocytes (or muscle) to increase insulin-stimulated glucose uptake.

We propose that the phenotype of the FSTL3 KO mouse derives from loss of FSTL3 regulation of activin and myostatin in multiple tissues. One possibility is that mild, chronic hyperinsulinemia resulting from the increased β cell mass promotes glucose uptake by muscle, fat, and other tissues, which could be potentiated acutely by an activin-mediated increase in glucose-stimulated insulin secretion (21). To avoid hypoglycemia, FSTL3 KO mice would have a chronic need for generating glucose, thereby accounting for the vastly up-regulated gluconeogenic gene expression and decreased glycogen content observed in FSTL3 KO livers. However, because insulin normally suppresses gluconeogenesis through down-regulation of gluconeogenic enzyme expression (37), the enhanced gluconeogenesis might indicate that FSTL3 KO hepatocytes are mildly resistant to insulin. Alternatively, because we found that activin stimulated G6Pase mRNA expression in HepG2 hepatoma cells, the elevated gluconeogenic enzyme mRNA expression in FSTL3 livers could derive, at least in part, from the direct action of activin on hepatocytes, which exceeds the inhibition from insulin. Finally, the reduction in visceral fat mass in FSTL3 KO mice may lead to enhanced insulin sensitivity given that reductions in visceral fat mass are associated with improved insulin sensitivity (36).

Our results demonstrate that FSTL3 deletion, along with the presumed tissue-selective increase in activin and myostatin activity, has significant actions in regulating glucose homeostasis and lipid distribution. Pharmacologic interventions to promote human characteristics that resemble those in the FSTL3 KO mouse, including reduced visceral adiposity, enhanced insulin sensitivity, and augmentation of endogenous insulin production and β cell mass and function, could be potentially beneficial for the treatment of metabolic disorders, such as obesity, metabolic syndrome, and diabetes. Because the phenotypes were caused by deletion of a circulating binding protein, our results further suggest that development of FSTL3 antagonists or activin and/or myostatin agonists could present viable approaches for developing therapeutic agents to treat human metabolic disease.

Materials and Methods

Generation of *Fstl3*-Deletion Mouse. The *Fstl3* gene targeting vector was prepared by introducing a loxP sequence downstream of exon 1 at a BsphI site, and a floxed neomycin resistance gene (Neo) was inserted at an XbaI site 1.6 kb upstream of BsphI, thus flanking a 1.6-kb region of the *Fstl3* gene surrounding exon 1 by two loxP sequences. J1 ES cells were transfected, selected for correct *Fstl3* gene targeting, and microinjected into C57BL/6 mice blastocysts. Chimeric male mice were bred with C57BL/6 females, and their agouti pups were genotyped. Animals carrying the *Fstl3* targeted allele were then bred with transgenic *EIIa-Cre* mice. *Fstl3*-gene-targeted and Cre-positive animals were bred with WT animals to segregate the various recombinant alleles. Offspring were genotyped to identify Neo excision in animals that had undergone either partial recombination to produce a conditional *Fstl3* allele or a complete recombination to produce an *Fstl3* exon 1 deletion allele. These latter heterozygous animals were bred to obtain homozygous FSTL3-null mice ($Fstl3^{tm1Alsc/tm1Alsc}$). All animal studies complied with US Department of Agriculture guidelines under an animal-use protocol approved by the Massachusetts General Hospital Subcommittee on Research Animal Care.

DNA Analyses for Genotyping. DNA prepared from ES cells or tail biopsies were analyzed for genotyping either by Southern blot analysis, after appropriate restriction enzyme digestion, or by PCR as previously described in ref. 38 (see *SI Methods* for details).

RNA Analyses: Northern Blot and RT-PCR. Total RNA was extracted from tissues with TRIzol (Invitrogen, Carlsbad, CA). FSTL3 mRNA expression was assessed by Northern blot analysis with 10 μg of total RNA and a radiolabeled full-length mouse FSTL3 cDNA probe. Alternatively, 1 μg of total RNA was reverse-transcribed and used in quantitative PCR by using SYBR green incorporation with reagents from Stratagene (La Jolla, CA) on a Stratagene MX4000. A cDNA standard was run in each PCR for each target, and message concentrations were normalized to mouse ribosomal protein L19.

HepG2 Hepatoma Cell Culture and Analysis. HepG2 cells cultured in RPMI medium containing 10% FCS and antibiotics for 24–48 h were treated with fresh medium containing either 5 ng/ml activin or 25 ng/ml myostatin (R & D Systems, Minneapolis, MN) for an additional 16 h. Cells were then extracted with TRIzol (Invitrogen, Carlsbad, CA) and analyzed for mRNA expression level by quantitative PCR.

Serum Hormone Measurements. Serum hormone measurements were conducted by specific RIA, ELISA, or biochemical assay in the Reproductive Endocrine Unit Assay Core and the Boston Area Diabetes Endocrinology Research Center RIA Core Laboratory at Massachusetts General Hospital.

Histology and Histomorphometry. Tissues were isolated from mice at different ages and fixed in 4% paraformaldehyde overnight. The tissues were then processed for paraffin embedding. Multiple 6-μm-thick microtome sections from each tissue were stained with H&E and photographed. For measurement of islet size in pancreas, 20 consecutive 8-μm sections were H&E-stained and photographed. For each pancreas, all islets in two sections at least 80 μm apart were counted, and their area measured with SPOT image analyses software. For white adipocyte size measurement, all adipocytes in each field were counted, and the area was measured with ImageJ software. Muscle fiber size was similarly quantitated by using three $\times$40 fields.

Immunofluorescence and Immunohistochemistry. Immunofluorescence was performed as previously described in ref. 38 (see *SI Methods* for details). The primary antibodies used were either a guinea pig anti-insulin (Linco Research, St. Charles, MO) or a mouse anti-glucagon antibody (Sigma, St. Louis, MO). The secondary antibodies used were anti-mouse-FITC or an anti-guinea pig-TRITC (Jackson Immunoresearch Laboratories, West Grove, PA). For immunohistochemical detection, the sections were processed with a Vectastain Elite ABC kit (Vector Laboratories, Burlingame, CA) and 3,3′-diaminobenzidine (ICN Biomedicals, Solon, OH) and counterstained. For pancreatic β cell size estimation, 3,3′-diaminobenzidine-stained areas developed after immunochemical detection of insulin were measured with SPOT software and divided by the number of blue-stained nuclei counted.

Oil Red O Staining. Freshly dissected liver and muscle were fixed overnight in 4% paraformaldehyde, cryoprotected in 30% sucrose in PBS for another day, and then frozen in OCT blocks. Cryostat sections 10 μm thick were processed for Oil Red O staining as described in ref. 39 in a 0.3% solution of Oil Red O in 60% isopropanol for 1 h. After being washed, sections were counterstained with Gills hematoxylin.

Determination of Total Body Fat. Body fat content of FSTL3 KO and WT mice was measured by dual emission x-ray absorptiometry with a PIXImus2 Mouse Densitometer (GE Medical Systems, Madison, WI).

Glucose and Insulin Tolerance Tests. For glucose tolerance tests, animals fasted overnight and then were weighed, and their fasting blood glucose levels were measured by using a glucometer (OneTouch Ultra; Lifescan, Milpitas, CA). Mice were injected i.p. with glucose (2 g of D-glucose per kg of body weight), and blood glucose levels were assessed 15, 30, 60, and 120 min after injection. Insulin tolerance tests were performed similarly, except that animals fasted for 2–3 h and then were injected i.p. with human regular insulin at a concentration of 1 unit of insulin per kg of body weight (Eli Lilly, Indianapolis, IN).

Hemodynamic Analyses. Mice were anesthetized with 100 mg/kg ketamine, 250 μg/kg fentanyl, and 2 mg/kg pancuronium, intubated, and mechanically ventilated (10 μl per g of body weight, 120 bpm, FiO_2 = 1). A ventricular catheter (PE-10; Miller Instruments, Houston, TX) was placed for continuous monitoring of the heart rate and blood pressure.

We thank Dr. Ernestina Schipani and Jeffrey Lange for assistance with histology and dual emission x-ray absorptiometry analysis, Dr. Odile Peroni for facilitating dynamic metabolic testing, Dr. Milton Finegold for providing expert analysis of liver pathology, and Dr. Joseph Avruch for critical evaluation of the manuscript. This work was supported by National Institutes of Health Grant R01HD39777/DK076143 (to A.L.S.) with assistance from Boston Area Diabetes Endocrinology Research Center Grant P30DK57521 and by National Institutes of Health Grant R01HL070896 (to M.J.R. and K.D.B.).

1. Shi Y, Massague J (2003) *Cell* 113:685–700.
2. Rebbapragada A, Benchabane H, Wrana JL, Celeste AJ, Attisano L (2003) *Mol Cell Biol* 23:7230–7242.
3. Lee SJ, Reed LA, Davies MV, Girgenrath S, Goad MEP, Tomkinson KN, Wright JF, Barker C, Ehrmantraut G, Holmstrom J, *et al.* (2005) *Proc Natl Acad Sci USA* 102:18117–18122.
4. Welt C, Sidis Y, Keutmann H, Schneyer A (2002) *Exp Biol Med* 227:724–752.
5. Jones KL, de Kretser DM, Clarke IJ, Scheerlinck JP, Phillips DJ (2004) *J Endocrinol* 182:69–80.
6. Matzuk MM, Kumar TR, Vassilli A, Bickenbach RR, Roop DR, Jaenisch R, Bradley A (1995) *Nature* 374:354–356.
7. Matzuk MM, Finegold MJ, Mather JP, Krummen L, Lu L, Bradley A (1994) *Proc Natl Acad Sci USA* 91:8817–8821.
8. Matzuk MM, Finegold MJ, Su JJ, Hsueh AJW, Bradley A (1992) *Nature* 360:313–319.
9. Gonzalez-Cadavid NF, Bhasin S (2004) *Curr Opin Clin Nutr Metab Care* 7:451–457.
10. Lee SJ (2004) *Annu Rev Cell Dev Biol* 20:61–86.
11. Schuelke M, Wagner KR, Stolz LE, Hubner C, Riebel T, Komen W, Braun T, Tobin JF, Lee SJ (2004) *N Engl J Med* 350:2682–2688.
12. Reisz-Porszasz S, Bhasin S, Artaza JN, Shen R, Sinha-Hikim I, Hogue A, Fielder TJ, Gonzalez-Cadavid NF (2003) *Am J Physiol* 285:E876–E888.
13. Zimmers TA, Davies MV, Koniaris LG, Haynes P, Esquela AF, Tomkinson KN, McPherron AC, Wolfman NM, Lee SJ (2002) *Science* 296:1486–1488.
14. Sidis Y, Mukherjee A, Keutmann H, Delbaere A, Sadatsuki M, Schneyer A (2006) *Endocrinology* 147:3586–3597.
15. Schneyer A, Sidis Y, Xia Y, Saito S, Re EE, Lin HY, Keutmann H (2004) *Mol Cell Endocrinol* 225:25–28.
16. Tortoriello DV, Sidis Y, Holtzman DA, Holmes WE, Schneyer AL (2001) *Endocrinology* 142:3426–3434.
17. Schneyer AL, Wang Q, Sidis Y, Sluss PM (2004) *J Clin Endocrinol Metab* 89:5067–5075.
18. Hill JJ, Davies MV, Pearson AA, Wang JH, Hewick RM, Wolfman NM, Qin Y (2002) *J Biol Chem* 277:40735–40741.
19. Matzuk MM, Lu N, Vogel H, Sellheyer K, Roop DR, Bradley A (1995) *Nature* 374:360–363.
20. Jorgez CJ, Klysik M, Jamin SP, Behringer RR, Matzuk MM (2003) *Mol Endocrinol* 18:953–967.
21. Florio P, Luisi S, Marchetti P, Lupi R, Cobellis L, Falaschi C, Sugino H, Navalesi R, Genazzani AR, Petraglia F (2000) *J Endocrinol Invest* 23:231–234.
22. Yamaoka T, Idehara C, Yano M, Matsushita T, Yamada T, Ii S, Moritani M, Hata J, Sugino H, Noji S, *et al.* (1998) *J Clin Invest* 102:294–301.
23. Brun T, Franklin I, St-Onge L, Biason-Lauber A, Schoenle EJ, Wollheim CB, Gauthier BR (2004) *J Cell Biol* 167:1123–1135.
24. Michael MD, Kulkarni RN, Postic C, Previs SF, Shulman GI, Magnuson MA, Kahn CR (2000) *Mol Cell* 6:87–97.
25. Ho J, de Guise C, Kim C, Lemay S, Wang XF, Lebrun JJ (2004) *Cell Signal* 16:693–701.
26. Brown CW, Li L, Houston-Hawkins DE, Matzuk MM (2003) *Mol Endocrinol* 17:2404–2417.
27. Dufour DR, Lott JA, Nolte FS, Gretch DR, Koff RS, Seeff LB (2000) *Clin Chem* 46:2050–2068.
28. Ogawa K, Abe K, Kurosawa N, Kurohmaru M, Sugino H, Takahashi M, Hayashi Y (1993) *FEBS Lett* 319:217–220.
29. Wada M, Shintani Y, Kosaka M, Sano T, Hizawa K, Saito S (1996) *Endocr J* 43:375–385.
30. Verspohl EJ, Ammon HP, Wahl MA (1993) *Life Sci* 53:1069–1078.
31. Shiozaki S, Tajima T, Zhang YQ, Furukawa M, Nakazato Y, Kojima I (1999) *Biochim Biophys Acta* 1450:1–11.
32. Prentki M, Nolan CJ (2006) *J Clin Invest* 116:1802–1812.
33. Dor Y, Brown J, Martinez OI, Melton DA (2004) *Nature* 429:41–46.
34. Bonner-Weir S, Weir GC (2005) *Nat Biotechnol* 23:857–861.
35. Ogata T, Park KY, Seno M, Kojima I (2004) *Endocr J* 51:381–386.
36. Wajchenberg BL (2000) *Endocr Rev* 21:697–738.
37. Barthel A, Schmoll D (2003) *Am J Physiol* 285:E685–E692.
38. Xia Y, Sidis Y, Schneyer A (2004) *Mol Endocrinol* 18:979–994.
39. Boyanovsky BB, van der Westhuyzen DR, Webb NR (2005) *J Biol Chem* 280:32746–32752.

EXHIBIT 5

0013-7227/06/$15.00/0
Printed in U.S.A.

Endocrinology 147(7):3586–3597

doi: 10.1210/en.2006-0099

Biological Activity of Follistatin Isoforms and Follistatin-Like-3 Is Dependent on Differential Cell Surface Binding and Specificity for Activin, Myostatin, and Bone Morphogenetic Proteins

Yisrael Sidis, Abir Mukherjee, Henry Keutmann, Anne Delbaere, Miyuki Sadatsuki, and Alan Schneyer

Reproductive Endocrine Unit, Massachusetts General Hospital, Boston, Massachusetts 02114

Follistatin (FST) and FST-like-3 (FSTL3) are activin-binding and neutralization proteins that also bind myostatin. Three FST isoforms have been described that differ in tissue distribution and cell-surface binding activity, suggesting that the FST isoforms and FSTL3 may have some nonoverlapping biological actions. We produced recombinant FST isoforms and FSTL3 and compared their biochemical and biological properties. Activin-binding affinities and kinetics were comparable between the isoforms and FSTL3, whereas cell-surface binding differed markedly (FST288 > FST303 > FST315 > FSTL3). Inhibition of endogenous activin bioactivity, whether the FST isoforms were administered endogenously or exogenously, correlated closely with surface binding activity, whereas neutralization of exogenous activin when FST and FSTL3 were also exogenous was consistent with their equivalent activin-binding affinities. This difference in activin inhibition was also evident in an *in vitro* bioassay because FST288 suppressed, whereas FST315 enhanced, activin-dependent TT cell proliferation. Moreover, when FSTL3, which does not associate with cell membranes, was expressed as a membrane-anchored protein, its endogenous activin inhibitory activity was dramatically increased. In competitive binding assays, myostatin was more potent than bone morphogenetic proteins (BMPs) 6 and 7, and BMPs 2 and 4 were inactive in binding to FST isoforms, whereas none of the BMPs tested competed with activin for binding to FSTL3. Neutralization of exogenous BMP or myostatin bioactivity correlated with the relative abilities of the isoforms to bind cell-surface proteoglycans. These results indicate that the differential biological actions among the FST isoforms and FSTL3 are primarily dependent on their relative cell-surface binding ability and ligand specificity. (*Endocrinology* 147: 3586–3597, 2006)

FOLLISTATIN (FST) IS AN extracellular regulatory protein for activin and related TGFβ superfamily members that acts via high-affinity, nearly irreversible binding to prevent activin from accessing its receptor (reviewed in Refs. 1 and 2). Although originally isolated from gonadal fluids and thought to act as an endocrine regulator of pituitary FSH release, the subsequent identification of FST mRNA and protein in numerous adult and embryonic tissues as well as the colocalization of FST with activin A in many tissues supports the currently held view that FST acts largely in an autocrine/paracrine manner (reviewed in Ref. 3).

FST has a number of putative physiological roles, including regulating pituitary FSH production (4), ovarian follicle maturation (5), spermatogenesis (6), liver homeostasis (7), wound repair (8), and response to inflammatory stimuli (9). Moreover, disruption of the mouse *Fst* gene resulted in developmental abnormalities including loss of hair, weakened musculature, XX sex reversal, and early neonatal death, demonstrating that FST is required for normal mammalian development (10, 11). However, the identification of precise activities and mechanisms of action for FST in both embryos and adults has been hampered by the fact that multiple isoforms of FST are produced from the *FST* gene, each with potentially distinct activities. The primary FST transcript undergoes alternative splicing to produce mRNAs that code for two FST proteins, termed FST288 and FST315 (12). The FST315 isoform contains all six exons, whereas the FST288 splice variant is missing exon 6, which codes for the acidic C-terminal tail. A third isoform, FST303, appears to arise from proteolytic cleavage of the FST315 C-terminal tail between residues 300 and 303 (13). All three isoforms contain a region of basic residues known as the heparin-binding sequence (HBS), which is essential for binding to cell-surface heparin-sulfated proteoglycans (14–17). However, it has been proposed that the acidic tail in FST315 interacts with the basic residues within the HBS, thereby suppressing the cell-surface binding activity of FST315. FST303, with its shortened tail, has cell-surface binding activity intermediate between FST315 and FST288 (13). These biochemical distinctions suggest that each isoform may be responsible for different subsets of biological activities depending on their degree of cell-surface localization and subsequent compartmentalization within the body, a concept supported by the finding that FST315 is the predominant circulating FST isoform in human serum (18), whereas ovarian follicular fluid contains primarily FST303 (14). Nevertheless, differential biological activity as well as the underlying mechanisms among the FST isoforms remain to be fully elucidated.

FST-like-3 (FSTL3), also known as FST-related gene

First Published Online April 20, 2006

Abbreviations: BMP, Bone morphogenetic protein; FBS, fetal bovine serum; FST, follistatin; FSTL3, follistatin-like-3; HBS, heparin-binding sequence.

Endocrinology is published monthly by The Endocrine Society (http://www.endo-society.org), the foremost professional society serving the endocrine community.

(FLRG) (19) and FST-related protein (FSRP) (20), shares substantial structural and functional homology with FST (21), including inhibition of activin bioactivity *in vivo* (22). Importantly, FSTL3 does not have an HBS, cannot bind to cell-surface proteoglycans (23), and is a weak antagonist of endogenous (autocrine) activin despite being only slightly less potent in neutralizing exogenous (endocrine/paracrine) activin (23). These distinctions between FSTL3 and FST support the concept that the presence of a functional HBS and resultant cell-surface binding is a critical biochemical determinant for endogenous activin inhibition.

In addition to activin, FST and FSTL3 bind other members of the TGFβ superfamily, including myostatin (24, 25) and some bone morphogenetic proteins (BMPs) (26, 27). FSTL3 was recently identified as the circulating binding protein for myostatin in mice and humans (24), suggesting that FSTL3 may have an important role in regulating muscle development and/or adult muscle mass. These studies indicate that both FST and FSTL3 likely play important roles in regulating the physiological and homeostatic activities of activin and related TGFβ superfamily ligands and that the physiological significance of these regulatory interactions, as well as quantitative differences in specificity among the binding proteins, remains to be determined systematically.

Given the different biochemical properties and compartmentalization of the FST isoforms and FSTL3, we hypothesized that these proteins will also have distinct mechanisms of action and ligand selectivity that will ultimately determine their range of physiological actions *in vivo*. To explore molecular mechanisms responsible for this differential bioactivity, we produced recombinant FST isoforms and investigated their differential biochemical and biological activities compared with FSTL3. Our results indicate that the biological activities of the FST isoforms and FSTL3 are determined primarily by their differential cell-surface binding and ligand specificity and further support the concept that FST isoforms may have distinct physiological roles *in vivo*.

Materials and Methods

Reagents

Recombinant human activin A, BMP2, and BMP4 were purchased from R&D Systems (Minneapolis, MN). Myostatin was purchased from Cell Signaling (Canton, MA), whereas BMP6 and -7 (OP1) were a gift from Creative Biomolecules (Cambridge, MA).

Preparation of recombinant tagged FST and FSTL3 proteins

Human FST288, FST315, and FSTL3 (the latter a gift from Millennium Pharmaceuticals, Cambridge, MA) coding sequences were subcloned into pCDNA3.1Myc-His (Invitrogen, Carlsbad CA). The FST303 expression construct was prepared from the FST315 cDNA by deleting all sequence 3′ to codon 303 up to the start of the Myc-His tag using standard PCR methods. The resulting C-terminal Myc-His-tagged cDNA constructs were transfected into HEK-293-F cell suspension cultures in Freestyle serum-free medium (Invitrogen) as described (28). Recombinant proteins were purified by nickel-Sepharose affinity chromatography (QIAGEN, Valencia, CA) and concentrated by centrifugal dialysis into Dulbecco's PBS.

Quantitation of secreted proteins

FST concentrations in media and concentrated affinity-purified eluates were established by two independent immunological assays: 1) a two-site solid-phase immunochemiluminescent assay (29) and 2) a solution-phase assay directed toward the C-terminal Myc tag (28). The concentrations obtained by the two methods were usually in good agreement for all FST preparations. FSTL3 preparations were quantified by the Myc RIA. Concentration and purity of affinity-purified proteins were verified by SDS-PAGE and silver staining (Bio-Rad Laboratories, Hercules, CA) or Western blot as described below.

Western blot analysis

Proteins were separated on 12% Tris-HCl Ready-Gel system (Bio-Rad), transferred to polyvinylidene difluoride membrane (Bio-Rad), blocked in 10% nonfat dry milk, and probed with anti-Myc (1 μg/ml, clone 4A6; Upstate Biotechnology, Lake Placid, NY) and goat antimouse horseradish peroxidase-conjugated (1:7500 dilution; Santa Cruz Biotechnology, Santa Cruz, CA) antibodies. Immunoreactivity was visualized using Western Lightning chemiluminescence reagent (PerkinElmer, Boston, MA).

Iodination

Human activin A was iodinated by the lactoperoxidase method and purified by electrophoresis as described previously (30).

Binding to cell-surface heparan-sulfate proteoglycans

COS cells were cultured in DMEM supplemented with 10% FBS (Invitrogen) and plated into 24-well plates and cultured to confluence. FST isoforms or FSTL3 was added at 50 ng/ml for 1 h at 25 C in fresh medium containing 0.1% BSA, washed, and replaced with medium containing 75,000 cpm [^{125}I]activin A alone or together with 10 μg/ml heparan sulfate (Sigma Chemical Co., St. Louis, MO), which displaces FST-activin complexes. After 1 h incubation at 25 C, cells were rinsed, harvested, and counted to detect FST-bound activin.

Activin-binding kinetics

Binding kinetics of FST isoforms to radiolabeled activin was determined by solid binding assay as described (31) using 25 ng/well of each isoform passively adsorbed to microtiter plates. After blocking the wells with 3% BSA/0.01% Tween in 10 mM PBS, 75,000 cpm radiolabeled activin was added. To determine the association rate, the binding reactions were terminated at the indicated times, the wells were washed, and bound radioligand was counted in a γ-counter. For dissociation measurements, the binding reactions were allowed to continue to steady state (3 h), after which unbound radioligand was removed and 100-fold excess of unlabeled ligand was added. At the indicated times, the wells were washed and counted as before. Maximum binding in a typical experiment reached 10–15% of total counts. Observed association rate constants (K_{on}) and dissociation rate constants (K_{off}) were calculated by fitting an exponential association equation and exponential decay model, respectively, using Prism4 (GraphPad Software Inc., San Diego, CA). Binding kinetics was assayed in at least three independent experiments for each isoform.

FST and FSTL3 specificity assays

Nonequilibrium competitive binding assays were used to determine isoform specificity as described (31). Microtiter plates were prepared with FST isoforms or FSTL3 as described above. Unlabeled activin A or heterologous competitors at doses indicated in the figures were individually mixed with 75,000 cpm [^{125}I]activin A in 150 μl assay buffer for 1 h. This nonequilibrium assay format was used to compensate for the heavily favored and nearly irreversible activin-binding kinetics (31) that would have displaced competitors if the assay had been allowed to reach steady state (>2 h). At the end of the 1-h incubation, the wells were washed and counted. In a typical experiment, about 10–15% of the added total counts were bound in the absence of unlabeled competitor. Resulting inhibition curves were analyzed using the four-parameter logistic model. Each ligand was assayed in at least three independent experiments.

Cell culture and reporter assays

The capacity of FST isoforms and FSTL3 to inhibit bioactivity of activin and related TGFβ family ligands was determined by reporter assays in human HepG2 cells (for activin A and BMPs), and human embryonic kidney (HEK) 293 cells (for activin A and myostatin), because myostatin responses were relatively weak in HepG2 cells. HepG2 cells were maintained in MEM supplemented with Earle's salts, nonessential amino acids, sodium pyruvate, and 10% fetal bovine serum (FBS) (Life Technologies, Inc., Rockville, MD). Cells were cultured in 24-well trays and transiently transfected with the smad1/5-responsive reporter BRE-Luc (32) for BMP activity or the smad2/3-responsive reporter CAGA-luc (33) for activin A activity, along with pRL-TK (Promega Corp., Madison, WI) and the indicated doses of FST isoform cDNAs (for experiments examining bioactivity of endogenous FST or FSTL3) or empty vector, using Lipofectamine 2000 (Invitrogen). To examine the effect of isoforms on endogenous activin, 1 ng pINHβA cDNA construct (kindly provided by Genentech Inc., San Francisco, CA) was included in the transfection mix. After 20 h, 0.2 nM activin A (for experiments on exogenous activin) was added, or was premixed (60 min at 25 C) with increasing amounts of purified FST isoforms or FSTL3 (for exogenous FST/FSTL3 experiments). After 16 h of treatment, the cells were washed, lysed with Passive lysis buffer (Promega) and assayed for luciferase activity using the dual luciferase reporter assay kit (Promega). Interwell variations in transfection efficiency were corrected by normalizing to Renilla luciferase activity. For each ligand, experiments were repeated at least three times, and the mean and SE of representative experiments are reported.

HEK 293 cells were maintained in RPMI 1640 medium containing 10% FBS (Life Technologies). Transient transfections and reporter assays were performed as described above except for using Effectene as the transfection reagent (QIAGEN) and included the CAGA-luc reporter and pRL-TK control cDNA, as well as FST or FSTL3 expression constructs and pINHβA cDNA for endogenous FST/FSTL3 or activin experiments, respectively.

To examine the effect of cell-surface association on FSTL3 ability to block endogenous activin, FSTL3 coding sequence without the signal peptide was cloned in frame with the transmembrane domain of pDisplay (Promega) and tested in CAGA-luc reporter assays in HEK 293 as described above.

To verify that transfected FST isoforms and FSTL3 were expressed at similar levels, 10 μl cell extract and 20 μl conditioned medium from the highest-dose wells were subjected to reduced SDS-PAGE and Western analysis as described above.

TT cells transfection and proliferation assays

TT cells (provided by Dr. Aaron Hsueh, Stanford University, Stanford, CA) are a clonal, testicular tumor cell line derived from a p^{53}/α-inhibin subunit-deficient mouse line (34). Cells were cultured in DMEM-Ham's F-12 (1:1) supplemented with 10% heat-inactivated FBS (Invitrogen), 2 mM L-glutamine, and antibiotics.

TT cells were transfected with expression constructs containing full-length FST288 or FS315 cDNAs (kindly provided by Dr. S. Shimasaki, University of California, San Diego, La Jolla, CA) in pCDNA3 vector (Invitrogen). Stable colonies were isolated and screened for FST secretion using our two-site solid-phase immunochemiluminescent assay for free (unbound to activin) FST as previously described (29). Cellular proliferation was assessed using the CellTiter 96 AQueous One Solution Reagent (Promega) colorimetric assay according to the manufacturer's recommendations.

Generation of recombinant adenovirus and proliferation of infected TT cells

Adenoviruses encoding FST288 and FST315 were constructed using a previously described two-cosmid adenoviral system (35). Briefly, full-length FST288 and FST315 cDNAs were cloned into the pLEP plasmid and then ligated to a cosmid containing the adenoviral genome (pREP7). The ligation product was packaged in phage packaging extracts (MaxPlax; Epicenter Technologies) infected into host bacteria, and hybrid cosmids were selected, amplified, and transfected into HEK 293 cells. High-titer stock solutions of adenovirus were obtained by repeated amplifications in HEK 293 cells.

For cell proliferation studies with FST viruses, early-passage stocks of TT cells were plated into 60-mm culture dishes. After 24 h incubation, 500 μl of HEK 293-conditioned medium containing a high titer of FST288-AdV, FST315-AdV, or empty virus, which contained no cDNA, was added. The next day, the cells were washed and seeded into 96-well plates. Cell proliferation assays were then preformed as described above for transfected cells.

Immunocytochemistry

HepG2 cells were grown on coverslips, fixed in 4% paraformaldehyde in PBS for 20 min, and either left nonpermeabilized or permeabilized with 0.1% Triton X-100. Myc-tagged FST isoforms or FSTL3 (1 μg/ml) was then incubated with cells for 1 h at room temperature in the absence or presence of heparin sulfate (100 μg/ml). After washing, cells were treated with anti-Myc monoclonal 4A6 (Upstate, Charlottesville, VA) and antimouse-tetraethylrhodamine isothiocyanate second antibody (Jackson ImmunoResearch, West Grove, PA).

Statistics

Activin-binding kinetic data were analyzed by one-way ANOVA for differences between isoforms followed by Tukey test. Differences of $P < 0.05$ were considered significant.

Results

Production of recombinant FST isoforms

To compare the biochemical and biological properties of FST isoforms and FSTL3, we produced recombinant FST288, FST303, FST315, and FSTL3 and compared their biochemical and biological properties. All preparations were more than 90% pure when analyzed by silver stain and Western blot analysis (Fig. 1). Under reducing conditions, FST288, FST303, and FST315 migrated at apparent molecular weights (M_r)

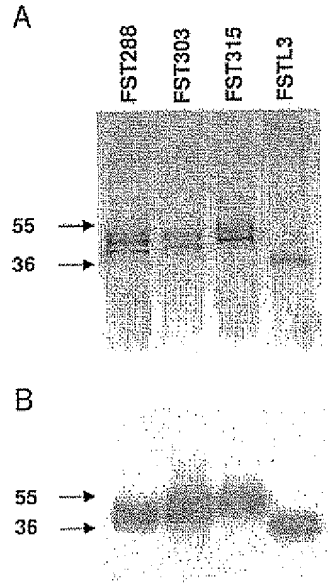

FIG. 1. Analysis of recombinant Myc-tagged FST isoform and FSTL3 proteins. A, Silver stain of FST isoforms and FSTL3 (200 ng/lane) after SDS-PAGE under reducing conditions showing proteins were more than 90% pure; B, Western analysis of similar gel containing 20 ng protein/lane using an anti-Myc antibody, verifying the identity of the nickel-affinity-purified proteins. The recombinant proteins ran as doublets or triplets indicating different degrees of glycosylation with M_r from 38,000–44000 (FST288), 42,000–47,000 (FS303), and 45,000–50,000 (FST315). FSTL3 migrated as a single 36,000 M_r species.

ranging from 38,000–50,000 and appeared as doublets or triplets, whereas purified FSTL3 migrated as a single molecular species at 36,000 M_r. These apparent molecular weights are consistent with previously reported estimates for these proteins, taking into account the size of the Myc-His tag and variable degrees of *n*-glycosylation. Moreover, relative concentrations of the purified proteins were verified by Western blot with anti-Myc antibody because all four proteins could be simultaneously analyzed with a single antibody. These Myc-tagged proteins had identical activin binding, cell-surface binding, and biological activity to untagged proteins (data not shown).

Activin-binding affinities of FST isoforms

It has been suggested that the FST isoforms have differential activin-binding affinity (14, 36). We therefore evaluated the activin-binding kinetics of the FST isoforms and FSTL3 using a solid-phase binding assay with radiolabeled activin A. All FST isoforms and FSTL3 demonstrated rapid activin binding (Fig. 2A) with nearly undetectable dissociation rates (Fig. 2B), similar to previous observations for untagged FST288 and FSTL3 (21). The different levels of total activin binding among the isoforms may represent differential isoform association with the solid-phase support. Nevertheless, dissociation constants determined as K_{off}/K_{on} demonstrated high-affinity activin binding that was not significantly different among the four proteins (Table 1). Thus, there does not appear to be a significant difference in direct binding to soluble activin between the FST isoforms.

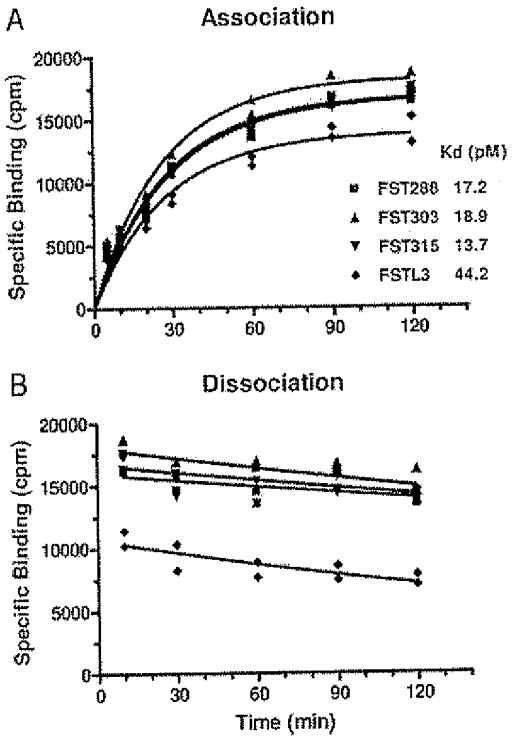

FIG. 2. Activin-binding kinetics of FST isoforms and FSTL3. Purified FST or FSTL3 isoforms were adsorbed to 96-well plates, blocked, and then incubated with 75,000 cpm [^{125}I]activin in the absence or presence of excess unlabeled activin. A, Reaction was terminated at indicated times, wells were washed, and then bound activin was determined. B, After binding reached steady state (3 h), excess unlabeled activin was added for indicated times, after which wells were washed and counted. Radiolabeled activin bound to FST isoforms and FSTL3 with a similar fast association rate but negligible dissociation rate. Affinities, calculated from the on and off rate constants, were not statistically different.

Differential association with cell-surface proteoglycans

Another mechanism whereby FST isoforms might differentially regulate activin action is through distinct association kinetics with cell-surface proteoglycans, an activity that has been shown to be modulated by the presence and length of the acidic C-terminal domain on FST315 (13). We first assessed the relative capacity of our isoform preparations to bind cell-surface proteoglycans using [^{125}I]activin as an indirect measure of FST cell-surface binding. FST288-treated COS cells bound 8-fold more radiolabeled activin compared with untreated cells, and this radioactivity could be removed by heparan sulfate treatment, indicating that the activin was bound to proteoglycan-associated FST288 (Fig. 3A). FSTL3 did not bind to cell-surface proteoglycans as previously reported (23). Only a small fraction of FST315, which contains a full-length C-terminal tail, bound to cell-surface proteoglycans (<50% above basal), whereas FST303, with about half the C-terminal tail removed, bound 5-fold more activin compared with basal but less than half of FST288, indicating an intermediate cell-surface binding ability.

To directly assess binding of FST isoforms to the cell surface, immunocytochemistry was used on nonpermeabilized cells treated with individual FST isoforms or FSTL3. FST288 bound quite well to plasma membranes, whereas substantially less FST303, and no FST315 or FSTL3, was detectable (Fig. 3B, *row* A). All FST was displaced in the presence of heparin (Fig. 3B, *row* B), indicating that this cell-surface-associated FST was reversibly bound to proteoglycans. Interestingly, when cells were first permeabilized, substantially more FST288 was detectable bound to membranes. This staining appeared to be intracellular as well as on the plasma membrane (Fig. 3B, *row* C), and the FST288 was again displaceable by heparin (Fig. 3B, *row* D), suggesting that FST288 may bind to membrane proteoglycans both outside and inside cells. Permeabilized cell staining was much reduced for FST303 and absent for FST315, consistent with binding to nonpermeabilized cells. However, slight staining was observed for FSTL3 in permeabilized cells that was not displaced by heparin (Fig. 3B, *rows* C and D), suggesting that Triton permeabilization treatment may have exposed a binding moiety for FSTL3 that is not used by FST isoforms. Taken together, these results demonstrate that the FST isoforms and FSTL3 have distinct capacities to interact with cell-surface proteoglycans and accumulate at the cell surface in correspondence with the presence of an HBS and the length of the C-terminal tail.

Differential inhibition of exogenous vs. endogenous activin by FST isoforms

To determine whether differences in cell-surface binding translated into differential bioactivity, the FST isoforms and FSTL3, added exogenously or expressed endogenously, were

TABLE 1. Activin binding on rates, off rates, and dissociation constants of FST isoforms

	FST288	FST303	FST315	FSTL3
K_{on} (M^{-1} min^{-1}) × 10^7	7.46 ± 1.5	6.21 ± 1.1	5.51 ± 0.99	5.87 ± 1.3
K_{off} (min^{-1}) × 10^{-3}	1.52 ± 0.12	1.81 ± 0.36	1.45 ± 0.21	2.48 ± 0.76
K_d (M × 10^{-11})	2.36 ± 0.58	3.02 ± 0.46	2.87 ± 0.52	3.93 ± 0.47

Shown are mean and SEM of four independent determinations. No significant differences were found among the isoforms by ANOVA.

examined for their ability to inhibit endogenous *vs.* exogenous activin in HepG2 hepatoma cells, which have a robust response to activin using the CAGA-luc reporter but do not express FST or detectable activin. When individual FST isoforms or FSTL3 was added with activin as exogenous treatments to the cells, the isoforms were equivalent in their ability to neutralize this activin (Fig. 4A), consistent with their comparable affinities for activin (see Table 1). In contrast, when the FST isoforms and FSTL3 were transfected, *i.e.* produced endogenously, but the activin treatment was exogenous, FST288 was clearly superior among the isoforms in inhibiting exogenous activin (Fig. 4B), and the order of their activity is consistent with the order of cell-surface association (see Fig. 3A). This pattern was also observed when FST

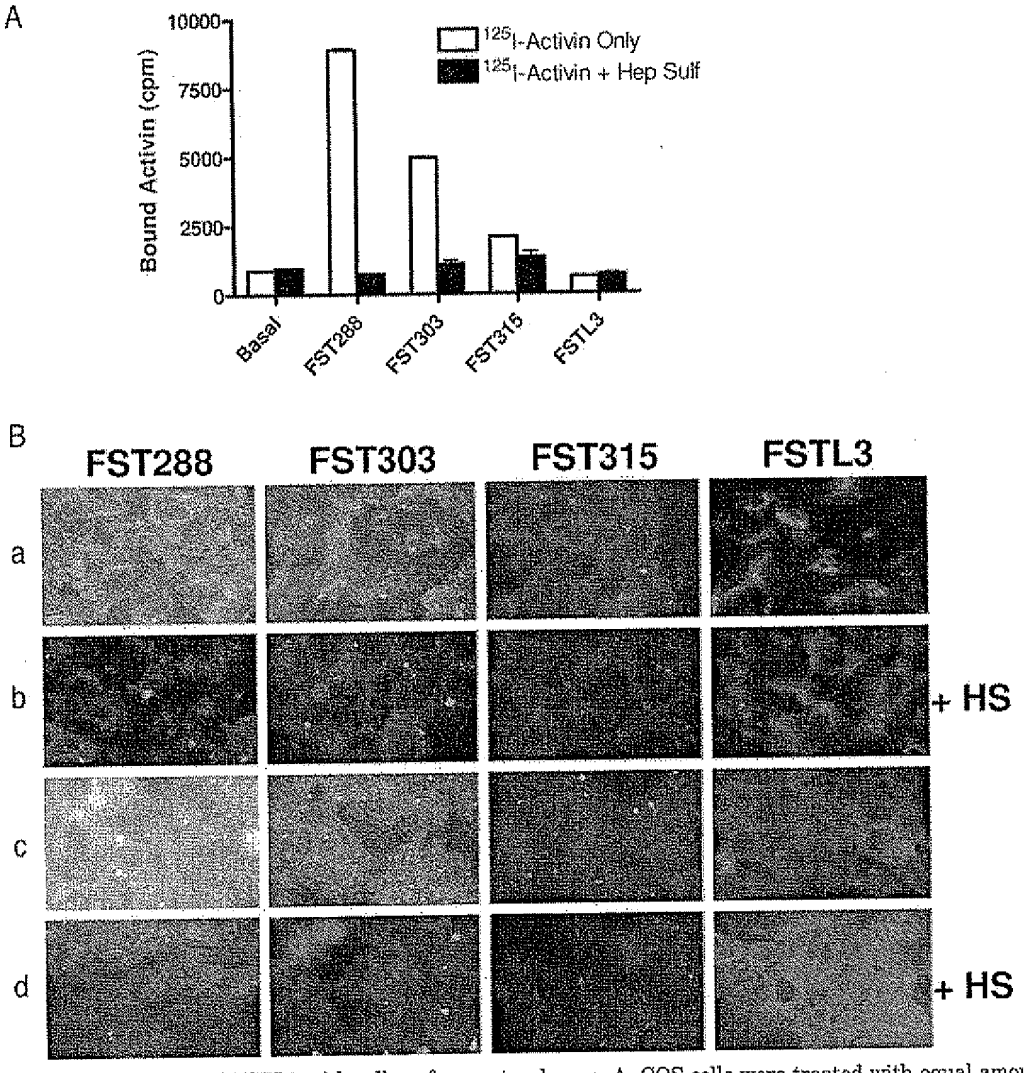

FIG. 3. Association of FST isoforms and FSTL3 with cell-surface proteoglycans. A, COS cells were treated with equal amounts (50 ng/ml) of FST isoforms or FSTL3 preps for 1 h, then washed and incubated for an additional hour with [^{125}I]activin A (75,000 cpm) alone or together with heparan sulfate (Hep Sulf) (10 μg/ml) to remove cell-surface-associated FST. FST288 efficiently bound to the cell surface, whereas FS315 and FSTL3 binding was negligible. FST303 exhibited an intermediate cell-surface binding capacity. A representative experiment is shown. B, HepG2 cells were incubated with FST isoforms or FSTL3 (1 μg/ml) in the absence (*rows* A and C) or presence (*rows* B and D) of heparin sulfate (HS). *Rows* A and B are without and *rows* C and D are with permeabilization before incubation with FST or FSTL3. Bound proteins were detected with anti-Myc primary and fluorescent second antibodies. As expected from Fig. 3A, FST288 bound to a greater degree than FST303, whereas FST315 and FSTL3 binding was undetectable. After permeabilization, FST288 binding was substantially increased, and this binding was eliminated by heparin sulfate, indicating that FST288, but not the other isoforms, bound to intracellular membrane-associated proteoglycans.

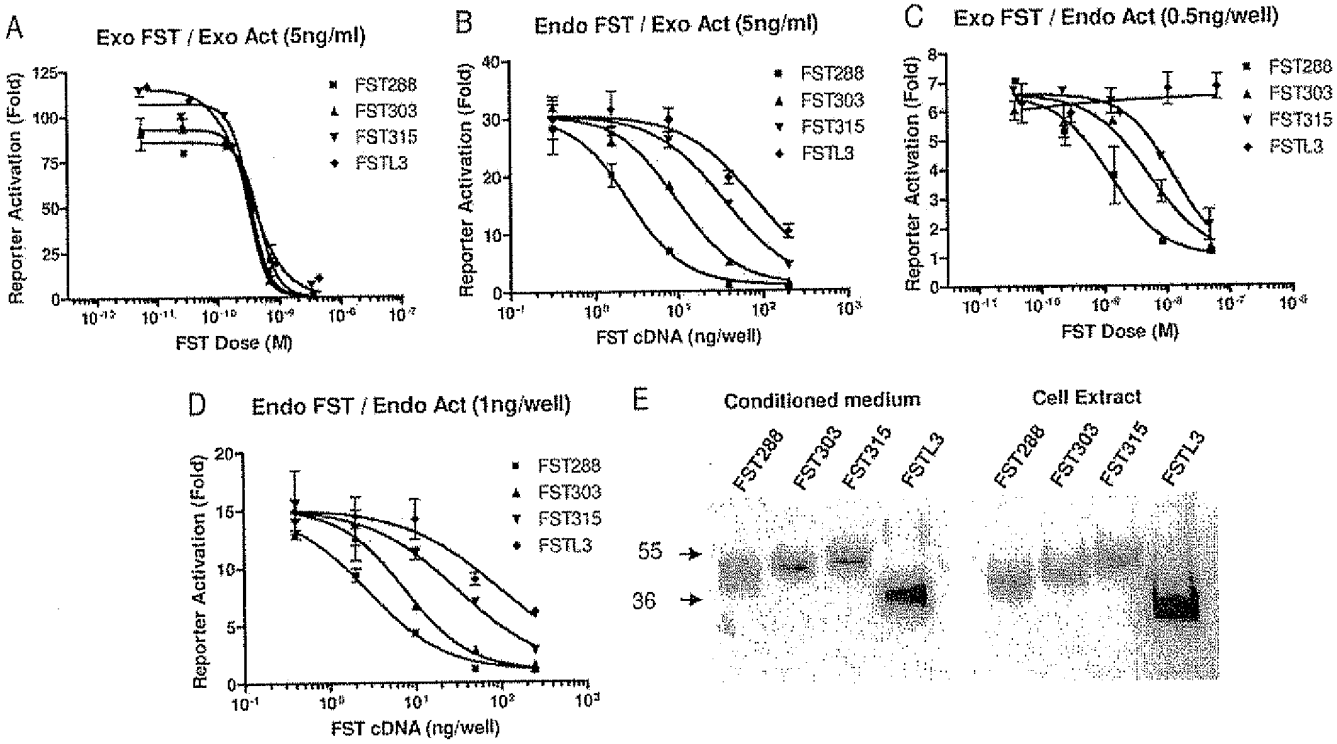

FIG. 4. Differential inhibition of exogenous *vs.* endogenous activin bioactivity by FST isoforms and FSTL3 in HepG2 cells. A, Increasing amounts of recombinant FST isoform or FSTL3 proteins were preincubated with 0.2 nM activin protein and then added to the cells. Binding proteins had equivalent inhibitory activity when both FST and activin were added exogenously (Exo). B, Cells were transfected with increasing amounts of FST/FSTL3 cDNA and then treated with 0.2 nM activin. When FST/FSTL3 proteins were made endogenously (Endo) but activin delivered exogenously (Exo), FST288 was most active, followed by FST303, FST315, and FSTL3, the order seen for proteoglycan binding in Fig. 3. C, Cells were transfected with 0.5 ng/well activin cDNA and then exogenously (Exo) treated with FST isoforms. When activin was endogenously (Endo) produced but FST/FSTL3 delivered exogenously, the same relative potency as in B was observed, but FSTL3 activity was undetectable. D, Both activin and FST/FSTL3 were transfected. When both activin and FST/FSTL3 were produced endogenously (Endo), all proteins were active in the same order as in B. Therefore, FST isoform capacity to inhibit endogenous activin correlates with cell-surface binding activity (FST288 > FST303 > FST315 > FSTL3). E, For experiments where FST isoforms or FSTL3 were transfected, cell extracts were analyzed by SDS-PAGE and Western blot to verify that equal amounts of protein were produced for each isoform. A representative experiment is shown.

isoforms and FSTL3 were added exogenously but the activin produced endogenously (Fig. 4C) as well as when both FST isoforms and FSTL3 along with activin were produced endogenously (Fig. 4D). To ensure that bioactivity differences were not a result of differential production of FST isoforms or FSTL3, we examined conditioned medium and extracts from transfected HepG2 cells (Fig. 5E). When analyzed by Western blot, all proteins were detected in both conditioned medium and cell extracts. Interestingly, FSTL3 was expressed to a greater degree than any of the other proteins, although it had the lowest bioactivity in Fig. 4, B–D. Conversely, FST288 was expressed at the lowest levels but was the most active. These results indicate that increased activity of FST288 was not because of superior protein biosynthesis. Thus, differential cell-surface binding among the FST isoforms and FSTL3 correlates with differential bioactivity when the FST/FSTL3, activin, or both are derived from endogenous sources, as would be expected when FST and/or activin are acting in an autocrine mode.

Differential modulation of activin-mediated proliferation by FST288 and FST315 in TT cells

The TT mouse testicular tumor cell line produces substantial levels of endogenous activin and depends on this activin for proliferation (34, 37), making these cells a more physiological *in vitro* model for comparing the ability of FST isoforms to differentially suppress activin-mediated proliferation. We evaluated the ability of FST288 and FST315, because they were the most distinct in suppressing activin signal transduction, to modulate TT cell proliferation by creating stably transfected cell lines. These stable cell lines express both FST and activin endogenously, which is critical because it was previously shown that exogenous FST288 treatments can only weakly inhibit activin-mediated cell growth in these cells (34, 37). The highest FST-secreting clones were selected using our free FST immunoassay, which ensured that in all cases, FST concentration in the medium was in excess of activin (data not shown). Compared with untransfected (wild-type) cells, proliferation in FST315-transfected TT cell lines was significantly enhanced (~25%; $P < 0.01$), whereas proliferation in FST288-transfected lines was suppressed by more than 50% ($P < 0.001$) (Fig. 5A).

To verify this differential activity in unselected cells, we generated adenoviruses expressing FST288 or FST315 under the control of the cytomegalovirus promoter and used them to infect different pools of wild-type TT cells derived from an identical stock. Free FST could easily be detected in conditioned medium of FST288 and FST315 virus-infected cells

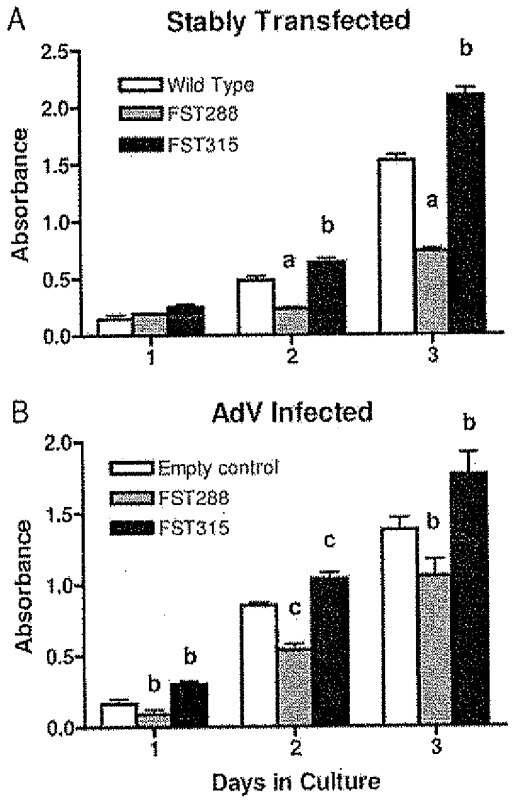

FIG. 5. Differential effect of FST288 *vs.* FST315 on TT cell proliferation. A, TT cells were transfected with FST288 or FST315 cDNA and stable colonies selected; B, Wild-type TT cells were infected with recombinant FST288, FST315, or empty adenoviruses. Cell proliferation was assessed using colorimetric proliferation assays. In both paradigms, FST288 significantly suppressed, whereas FST315 significantly stimulated, proliferation. a, $P < 0.001$; b, $P < 0.01$; c, $P < 0.05$.

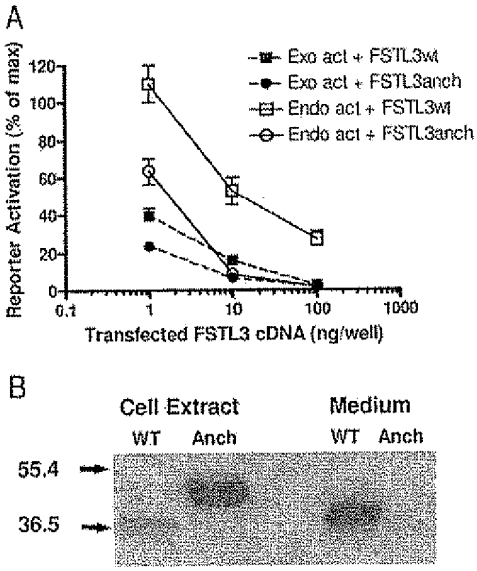

FIG. 6. Increased inhibition of endogenous activin of cell-surface-anchored FSTL3. A, FSTL3 was fused to the transmembrane domain of pDisplay and then transfected into HEK 293 cells together with the CAGA-luc reporter and βA cDNA [endogenous activin (Endo act)] or without activin βA cDNA. For exogenous activin (Exo act) wells, cells were treated with 0.2 nM activin. Cells transfected with wild-type (wt) FSTL3 cDNA were used as control. Results are graphed as percentage of maximum activin activity in the absence of FSTL3. Both wild-type and anchored (anch) FSTL3 (*squares* and *circles*, respectively) inhibited exogenous activin at all DNA doses (*dashed lines*) as expected from Fig. 4A. In contrast, anchored FSTL3 was nearly 10-fold more active (ED_{60} dose approximately 10-fold lower) than wild-type FSTL3 at inhibiting endogenous activin (*solid lines*), demonstrating that cell-surface localization by itself affords a substantial advantage for inhibiting endogenous activin. B, Cell extracts (10 μl) and conditioned medium (20 μl) from the 100 ng/well were analyzed by SDS-PAGE and Western blot. The vast majority of wild-type FSTL3 (WT) was found in the medium as expected, whereas anchored FSTL3 (Anch) was located only in the cellular fraction. In addition, the total FSTL3 protein for both fractions was quite similar, indicating that differences in activity were not because of differential expression. Results from a representative experiment are shown.

24 h after infection (54 and 76 ng/ml, respectively). As observed in the stable cell lines, expression of FST315 by viral infection significantly enhanced proliferation (~25%; $P < 0.05$), whereas FST288 significantly suppressed proliferation (25–40%; $P < 0.01$) (Fig. 5B). These observations demonstrate that FST288 and FST315 differentially regulate TT cell proliferation, likely reflecting their differential ability to suppress endogenous activin activity as described in Fig. 4.

Cell-surface binding of FSTL3 increases biological activity

To further test the hypothesis that cell-surface binding is responsible for the superior inhibition of endogenous activin by FST288, we expressed FSTL3 as a fusion protein with the transmembrane domain of the pDisplay vector, which anchors FSTL3 to the exterior surface of the plasma membrane (anchored FSTL3). When tested with exogenous activin, 1–10 ng of both wild-type and anchored FSTL3 suppressed more than 75% of activin's activity (Fig. 6A). However, 10 ng of wild-type FSTL3 suppressed less than 50% of endogenous activin activity, whereas the same amount of anchored FSTL3 suppressed 90%, reaching similar levels of activity as FST288. To verify that anchored FSTL3 was not secreted and thus must have been acting at the cell surface, we compared FSTL3 in cell extracts and conditioned medium by SDS-PAGE and Western blot. In cell extracts, both wild-type and anchored FSTL3 were detected whereas in conditioned medium, only wild-type FSTL3 was seen (Fig. 6B), and the protein concentration of wild-type FSTL3 in both compartments was similar to membrane-bound anchored FSTL3. Taken together, these results demonstrate that localization at the cell surface, as occurs for FST288 because of its HBS, and in anchored FSTL3, greatly enhances the ability of FST and FSTL3 to suppress endogenous activin activity.

FST isoforms and FSTL3 differentially bind related TGFβ-family ligands

FST isoforms and FSTL3 have been reported to bind myostatin (24, 25) and various BMPs (38), but isoform-specific differences in specificity have not been previously examined. Thus, we compared the ability of myostatin and BMPs to compete with radiolabeled activin for binding to the FST isoforms and FSTL3. Among the three FST isoforms, there was little difference in the binding potency of myostatin, BMP6, or BMP7 relative to activin, whereas BMP2 and BMP4

were inactive (Fig. 7, A–C, and Table 2). In contrast, whereas myostatin bound to FSTL3 at a relative potency comparable to the FST isoforms, BMP6 and BMP7 as well as BMP2 and BMP4 were inactive (Fig. 7D and Table 2). Thus, although there was little difference in TGFβ-family ligand specificity among the FST isoforms, BMP binding to FSTL3 was substantially reduced compared with FST isoforms.

To test the relevance of these relative binding activities on biological activity of TGFβ ligands, we examined the ability of exogenous FST isoforms and FSTL3 to inhibit the activity of exogenously added ligands in the HepG2 cell reporter assay. As observed earlier, and consistent with the binding results, the FST isoforms and FSTL3 had similar activin-inhibiting activity (Fig. 8A). In addition, neither the FST isoforms nor FSTL3 inhibited BMP2 or -4 activity (Fig. 8, B and C), and FSTL3 did not inhibit BMP6 and -7 bioactivity (Fig. 8, D and E). On the other hand, FST288 inhibited BMP6 and -7 bioactivity (Fig. 8, D and E) to a greater degree than the other FST isoforms despite little difference between the isoforms in the binding assay. Similarly, although the three FST isoforms were equally active in inhibiting myostatin bioactivity (Fig. 8F), FSTL3 had about 5-fold less inhibitory activity despite having similar binding activity. Taken together with the binding studies, these bioassay results demonstrate that differential binding specificity of the FST isoforms and FSTL3 for activin, BMPs, and myostatin cannot, by itself, account for differences in inhibition of TGFβ ligand biological activity.

Discussion

The three FST isoforms have different biochemical characteristics relating to the activity of their HBS through which they bind cell-surface proteoglycans, a property that also leads to isoform compartmentalization in different tissues (14–18). These distinctions suggest the possibility that the FST isoforms might be responsible for different subsets of the biological actions attributable to FST *in vivo*. To explore this possibility, we compared the activin-binding affinities and kinetics, cell-surface binding, ligand specificity, and biological activity of the isoforms to FSTL3, which unlike FST, does not contain an HBS and thus cannot bind to cell-surface proteoglycans (23). Our results demonstrate that the activin-binding affinity and kinetics of the FST isoforms and FSTL3 were not distinguishable. Moreover, the potencies of BMPs and myostatin for binding to the FST isoforms were not different, although BMP binding to FSTL3 was substantially reduced. However, the FST288 isoform, which was superior in cell-surface proteoglycan binding because of its uninhibited HBS, inhibited endogenous activin, myostatin, and BMP bioactivity to a greater degree compared with the other isoforms or FSTL3. Moreover, we found that FST288 suppressed, whereas FST315 enhanced, activin-mediated proliferation in TT cells. These observations indicate that the major biochemical parameter affecting biological activity among the isoforms and FSTL3 is the degree of cell-surface association. Additional support for this concept was obtained by expressing FSTL3 as a plasma membrane-anchored protein. In this context, the ability of anchored FSTL3 to inhibit endogenous activin was substantially increased rel-

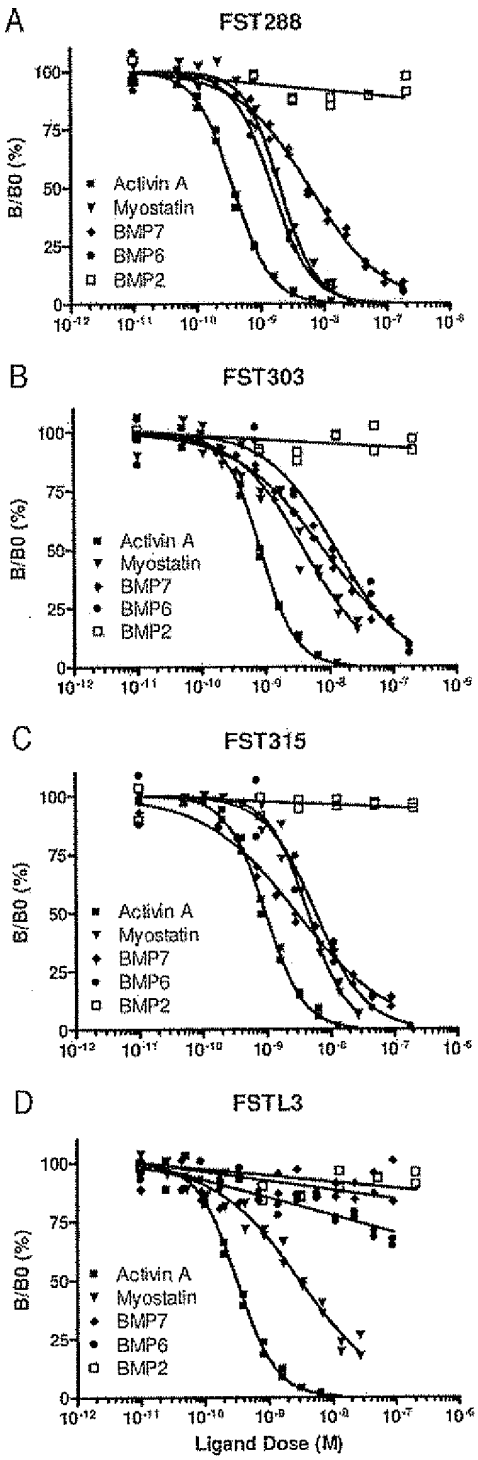

FIG. 7. Specificity of FST isoforms and FSTL3 for TGFβ family ligands. Purified FST proteins (25 ng/well) were attached to microtiter plates and then treated with radiolabeled activin A (75,000 cpm/well) together with increasing amounts of unlabeled activin A, myostatin, BMP7, BMP6, or BMP2. For the three FST isoforms (A–C), potency for competition with radiolabeled activin was as follows: activin A > BMP6 ≥ myostatin ≥ BMP7. BMP2 and BMP4 (not shown) were inactive. For FSTL3 (D), relative potency was activin A > myostatin, but there was no significant competition by BMP6, -7, -2, or -4 (not shown). A representative experiment of three to five determinations is shown.

TABLE 2. ED_{50} estimates for TGFβ superfamily members as competitors with radiolabeled activin

Ligand	FST288	FST303	FST315	FSTL3
Activin A	0.49 ± 0.09	1.37 ± 0.3	1.15 ± 0.3	0.34 ± 0.1
Myostatin	3.02 ± 0.08	2.46 ± 0.3	3.68 ± 0.9	1.53 ± 0.5
BMP7	5.45 ± 1.2	5.86 ± 0.8	14.3 ± 5.6[a]	NC
BMP6	1.24 ± 0.3	19.9 ± 12.5	3.88 ± 1.1	NC

FST isoforms and FSTL3 were passively adsorbed to solid-phase supports. Competition assays were performed by adding radiolabeled activin and increasing doses of unlabeled activin, myostatin, BMP7, or BMP6, and ED_{50} values were calculated. Results are mean ± SE (nM) for at least three independent experiments. NC, No curve.

[a] Estimate, slopes not parallel.

ative to soluble FSTL3, approximating the suppression afforded by FST288 itself. Our results therefore demonstrate that cell-surface association is the major biochemical determinant of biological potency in suppressing the bioactivity of endogenous activin and related ligands

Inhibition of activin and related TGFβ-family ligands by cell-surface-bound FST is analogous to inhibition of autocrine/paracrine actions of these ligands *in vivo*. Such situations might be encountered in tissue differentiation during embryonic development or in the neonate and adult in regulation of these ligands within tissues. In fact, the observations in TT cells are a model for autocrine/paracrine regulation of activin action because TT cells produce substantial amounts of activin. Thus, we found that endogenous FST288 was effective in inhibiting activin-dependent proliferation in TT cells, whereas FST315 was not. Although we did not test FSTL3 in this context, based on our results in the *in vitro* bioassays as well as previous studies (27), FSTL3 would be expected to be even weaker than FST315 in inhibiting autocrine activin. Nevertheless, when FSTL3 was anchored to the cell surface by a heterologous transmembrane sequence, its ability to inhibit endogenous activin was greatly enhanced. Our results are therefore consistent with the HBS and cell-surface binding being critical for maximal inhibition of endogenous activin and related ligands so that *in vivo*, FST288, and to a lesser degree, FST303, would be expected to serve these roles preferentially to FST315 and FSTL3. *In vivo* examination of this concept is underway.

The seemingly anomalous increase in TT cell proliferation when transfected or infected with FST315 vectors is more challenging to explain. However, it has been shown that increasing doses of activin resulted in receptor down-regulation in TT cells, suggesting that because these cells constitutively produce copious amounts of activin, their signaling system is chronically down-regulated (37). Although our results demonstrate that FST315 is a less effective inhibitor of

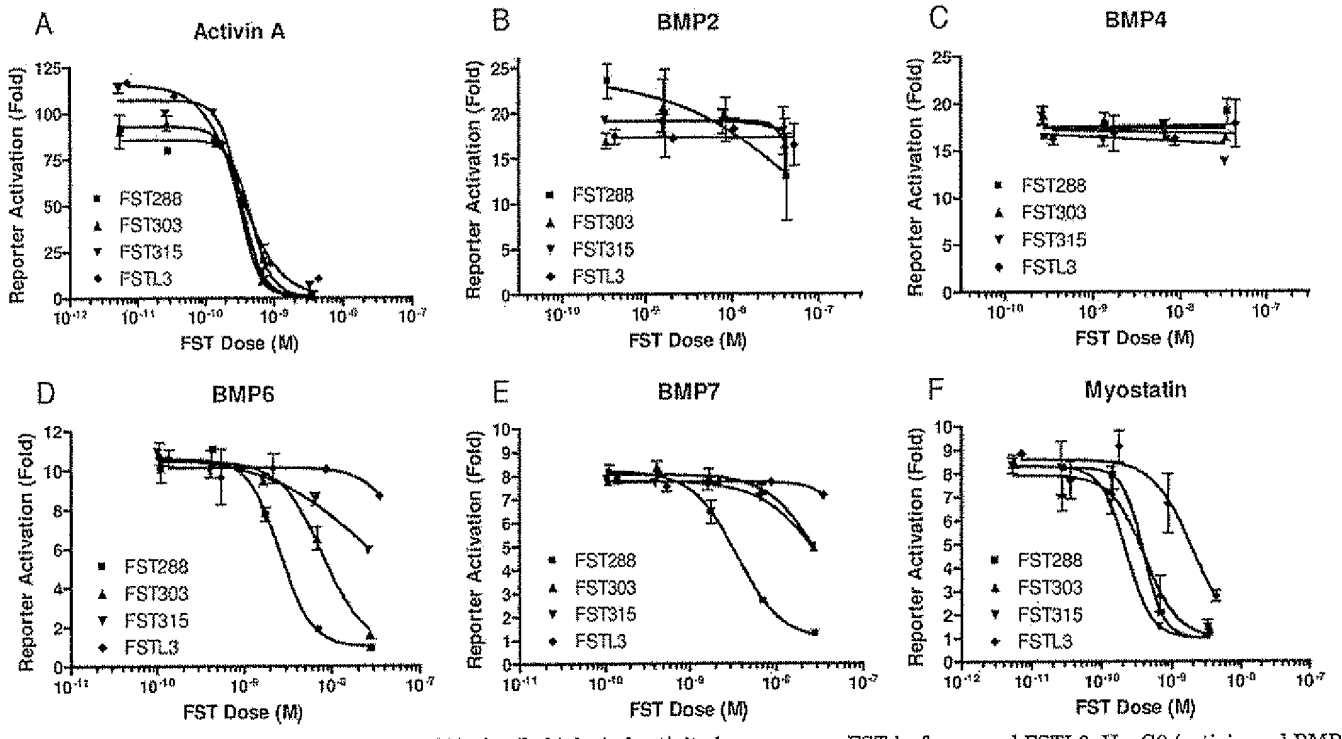

FIG. 8. Differential inhibition of exogenous TGFβ family biological activity by exogenous FST isoforms and FSTL3. HepG2 (activin and BMP assays) or HEK 293 (myostatin assays) cells were transfected with the CAGA-luc (activin and myostatin) or BRE-luc (BMPs) reporters and treated with TGFβ family ligands (activin and myostatin, 0.2 nM; BMP2 and -4, 0.4 nM; BMP6 and -7, 0.3 nM) together with increasing amounts of FST isoforms and FSTL3 as indicated in the figures. FST isoforms and FSTL3 inhibited activin (A) similarly, whereas they were all unable to inhibit BMP2 (B) and BMP4 (C). However, only FST288, and to a lesser degree FST303, significantly inhibited BMP6 (D), whereas only FST288 inhibited BMP7 (D). Inhibition of myostatin (F) was similar to activin except that FSTL3 was about 5-fold less active than FST isoforms.

endogenous activin compared with FST288, transfection with FST315 may still have inhibited activin activity sufficiently to reduce the level of receptor down-regulation, thereby resulting in a more sensitive activin signaling system. These more sensitive TT cells might then respond to the remaining endogenous activin with enhanced proliferation.

This situation in TT cells is somewhat analogous to the pituitary where activin is produced endogenously and constitutively and is regulated by FST (4, 39–41). It is not presently known which FST isoform is produced within the pituitary, although there is some suggestion that it might be FST315 (42, 43). Thus, one possible mode of FST315 regulation of activin-stimulated FSH biosynthesis in the pituitary may be through reducing down-regulation of gonadotroph activin receptors, thereby producing greater activin sensitivity and FSH release.

In contrast to inhibition of endogenous activin, exogenous FST isoforms and FSTL3 were equally effective at inhibiting exogenous activin. This is equivalent to the *in vivo* situation of inhibiting activin and related ligands in the circulation. Moreover, to maintain effective serum concentrations of FST and FSTL3, isoforms that do not bind cell-surface proteoglycans would be preferable. Consistent with differential distribution of FST isoforms within the body, we recently identified FST315 as the circulating FST isoform in humans (18), whereas FSTL3, but not FST, was identified as a circulating binding protein for myostatin (24). Thus, our results indicate that the distribution of FST isoforms correlates with their heparin-binding activity so that FST315 and FSTL3 act primarily as regulators of endocrine activin, myostatin, and perhaps BMPs. Moreover, our results are consistent with a compartmentalization of FST isoforms based on cell-surface binding that results in their being responsible for different biological actions *in vivo*.

In addition to the classical signaling pathway of activin binding to cell-surface receptors and transducing an intracellular signaling cascade, recent evidence has been presented for another pathway where activin or TGFβ, bound to type II receptor, is endocytosed to early endosomes. In this model, activin or TGFβ signals are transduced via contact with Smad anchor for receptor activation (SARA)-bound Smad proteins that reside in endosomes (44–46). Within this system, FST could act at the cell surface to antagonize activin binding or enter the cell via endocytosis along with the activin-receptor complex where it could then reduce signaling by sequestering activin as it dissociates from receptors. FST288 has also been reported to bind radiolabeled activin at the cell surface, where it is then internalized and presumably degraded (47). Thus, FST288, by virtue of its greater ability to bind cell-surface proteoglycans, may have greater activin-inhibitory activity by antagonizing activin both at the cell surface and within endosomes, whereas FST315 and FSTL3 can act only on activin that is extracellular. Intracellular localization and possibly activity of FST288 is supported by the immunocytochemical results in this study showing FST288 binding to intracellular membranes that is reversible by heparin treatment, as well as by our previous results demonstrating that some newly synthesized FST288 remains in the cytoplasm for up to 4 h (48). Regardless of where FST288 actually inhibits activin binding to its receptor, it clearly has increased ability to inhibit endogenous activin activity relative to the other isoforms and FSTL3. These results collectively indicate that the different FST isoforms may have different *in vivo* biological roles and that FST315 will have activities more closely related to FSTL3 because both have low cell-surface binding ability.

Although high-affinity binding of FST to activin and myostatin has been previously reported (21, 25, 31, 36, 49), the relative activity of the three FST isoforms, as directly compared here, has not been described. In addition, there is some disagreement over relative binding affinities for the different ligands owing to the wide range of different techniques used (36, 49, 50). For example, different dissociation constants were reported for FST288 and FST315 binding to activin immobilized on a Biacore chip (36), which contrasts with our determination of similar affinities among the FST isoforms. However, the recently reported crystal structure for the FST288-activin complex (51), which found two FST molecules bound to one activin dimer, appeared to require flexibility of the activin dimer because its configuration in complex with FST was distinct from its conformation in complex with its receptor (52). Thus, immobilization of activin during surface plasmon resonance analysis with the Biacore system may inhibit this flexibility, leaving activin in an unnatural conformation that favored one FST isoform over another. This may also be applicable to previously reported affinities for FST binding to BMP4 determined using the same technology (50). In our study, activin was presented in solution and may thus be more physiological because *in vivo*, TGFβ ligands are more likely to contact FST or FSTL3 in solution. Nevertheless, our results indicate that when compared directly in competition assays as in this study, activin appeared to be the preferred ligand for FST isoforms and FSTL3.

FSTL3 has been identified as a circulating binding protein for myostatin in humans and mice (24). However, these investigators were unable to identify any circulating myostatin bound to FST using SDS-PAGE followed by mass spectroscopy. This is unexpected because the FST isoforms appear to neutralize myostatin better than FSTL3. We have previously reported (21, 31), and confirmed here, that activin binding to FST is essentially irreversible, as appears to be the case for myostatin as well (49). Moreover, FST has been shown to inhibit myostatin activity when expressed transgenically in muscle (25). Taken together, these studies indicate that both FST and FSTL3 can bind and neutralize activin and myostatin. The preferred ligand may depend on which ligand gains access first to either FST or FSTL3, which is in turn a function of differential tissue or organ distribution of FST and FSTL3 (21).

In summary, our results clarify the activin-binding affinity among the FST isoforms and FSTL3 and demonstrate that their differential activin-regulating activity is dependent on their relative cell-surface binding activity rather than on differential activin-binding affinity. Our results also define the relative specificity of binding and inhibitory activity for a number of related TGFβ-family ligands by the FST isoforms and FSTL3, with FSTL3 being almost completely inactive in regulating BMP ligands, thereby suggesting that *in vivo*, FSTL3 is unlikely to regulate BMP activity. Finally, our results suggest that the *in vivo* biological roles of the FST iso-

forms and FSTL3 are likely to be distinct, dependent on their relative cell-surface binding activity and consequent compartmentalization within the body as well as on colocalization of biosynthesis in different tissues.

Acknowledgments

We are grateful to Dr. William Crowley for the engaging discussions on gonadotroph desensitization.

Received January 23, 2006. Accepted April 10, 2006.

Address all correspondence and requests for reprints to: Alan Schneyer, Ph.D., Reproductive Endocrine Unit BHX-5, Massachusetts General Hospital, Boston, Massachusetts 02114. E-mail Schneyer.alan@mgh.harvard.edu.

This work was supported by Public Health Service grants from the National Institutes of Health: R01DK55838 and R01HD39777 (to A.L.S.) and R01DK053828 (to H.T.K.) as well as a fellowship from the Belgian American Educational Foundation (to A.D.).

Current address for A.D.: Fertility Clinic, Erasme Hospital, Laboratory of Research on Human Reproduction, Universite Libre de Bruxelles, Belgium.

Disclosure: All authors have nothing to declare.

References

1. Welt C, Sidis Y, Keutmann H, Schneyer A 2002 Activins, inhibins, and follistatins: from endocrinology to signaling. A paradigm for the new millennium. Exp Biol Med (Maywood) 227:724–752
2. Phillips DJ 2000 Regulation of activin's access to the cell: why is mother nature such a control freak? Bioessays 22:689–696
3. DePaulo LV, Bicsak TA, Erickson GF, Shimasaki S, Ling N 1991 Follistatin and activin: a potential intrinsic regulatory system within diverse tissues. Soc Exp Med Biol 200:500–512
4. Besecke LM, Guendner MJ, Sluss PA, Polak AG, Woodruff TK, Jameson JL, Bauer-Dantoin AC, Weiss J 1997 Pituitary follistatin regulates activin-mediated production of follicle-stimulating hormone during the rat estrous cycle. Endocrinology 138:2841–2848
5. Jorgez CJ, Klysik M, Jamin SP, Behringer RR, Matzuk MM 2003 Granulosa cell-specific inactivation of follistatin causes female fertility defects. Mol Endocrinol 18:953–967
6. Guo Q, Kumar TR, Woodruff TW, Hadsell LA, DeMayo FJ, Matzuk MM 1998 Overexpression of mouse follistatin causes reproductive defects in transgenic mice. Mol Endocrinol 12:96–106
7. Takabe K, Wang L, Leal AM, MacConell LA, Wiater E, Tomiya T, Ohno A, Verma IM, Vale W 2003 Adenovirus-mediated overexpression of follistatin enlarges intact liver of adult rats. Hepatology 38:1107–1115
8. Wankell M, Munz B, Hubner G, Hans W, Wolf E, Goppelt A, Werner S 2001 Impaired wound healing in transgenic mice overexpressing the activin antagonist follistatin in the epidermis. EMBO J 20:5361–5372
9. Jones KL, Kretser DM, Patella S, Phillips DJ 2004 Activin A and follistatin in systemic inflammation. Mol Cell Endocrinol 225:119–125
10. Matzuk MM, Lu N, Vogel H, Sellheyer K, Roop DR, Bradley A 1995 Multiple defects and perinatal death in mice deficient in follistatin. Nature 374:360–363
11. Yao HH, Matzuk MM, Jorgez CJ, Menke DB, Page DC, Swain A, Capel B 2004 Follistatin operates downstream of Wnt4 in mammalian ovary organogenesis. Dev Dyn 230:210–215
12. Shimasaki S, Koga M, Esch F, Cooksey K, Mercado M, Koba A, Ueno N, Ying SY, Ling N, Guillemin R 1988 Primary structure of the human follistatin precursor and its genomic organization. Proc Natl Acad Sci USA 85:4218–4222
13. Sugino K, Kurosawa N, Nakamura T, Takio K, Shimasaki S, Ling N, Titani K, Sugino H 1993 Molecular heterogeneity of follistatin, an activin-binding protein. J Biol Chem 68:15579–15587
14. Sumitomo S, Inouye S, Liu XJ, Ling N, Shimasaki S 1995 The heparin binding site of follistatin is involved in its interaction with activin. Biochem Biophys Res Commun 208:1–9
15. Inouye S, Ling N, Shimasaki S 1992 Localization of the heparin binding site of follistatin. Mol Cell Endocrinol 90:1–6
16. Nakamura T, Sugino K, Titani K, Sugino H 1991 Follistatin, an activin-binding protein, associates with heparan sulfate chains of proteoglycans on follicular granulosa cells. J Biol Chem 266:19432–19437
17. Sidis Y, Schneyer AL, Keutmann HT 2005 Heparin and activin-binding determinants in follistatin and FSTL3. Endocrinology 146:130–136
18. Schneyer AL, Wang Q, Sidis Y, Sluss PM 2004 Differential distribution of follistatin isoforms: application of a new FS315-specific immunoassay. J Clin Endocrinol Metab 89:5067–5075
19. Hayette S, Gadoux M, Martel S, Bertrand S, Tigaud I, Magaud JP, Rimokh R 1998 FLRG (follistatin-related gene), a new target of chromosomal rearrangement in malignant blood disorders. Oncogene 16:2949–2954
20. Schneyer A, Tortoriello D, Sidis Y, Keutmann H, Matsuzaki T, Holmes W 2001 Follistatin-related protein (FSRP): a new member of the follistatin gene family. Mol Cell Endocrinol 180:33–38
21. Tortoriello DV, Sidis Y, Holtzman DA, Holmes WE, Schneyer AL 2001 Human follistatin-related protein: a structural homologue of follistatin with nuclear localization. Endocrinology 142:3426–3434
22. Xia Y, Sidis Y, Schneyer A 2004 Overexpression of follistatin-like 3 in gonads causes defects in gonadal development and function in transgenic mice. Mol Endocrinol 18:979–994
23. Sidis Y, Tortoriello DV, Holmes WE, Pan Y, Keutmann HT, Schneyer AL 2002 Follistatin-related protein and follistatin differentially neutralize endogenous *vs.* exogenous activin. Endocrinology 143:1613–1624
24. Hill JJ, Davies MV, Pearson AA, Wang JH, Hewick RM, Wolfman NM, Qiu Y 2002 The myostatin propeptide and the follistatin-related gene are inhibitory binding proteins of myostatin in normal serum. J Biol Chem 277:40735–40741
25. Lee SJ, McPherron AC 2001 Regulation of myostatin activity and muscle growth. Proc Natl Acad Sci USA 98:9306–9311
26. Tsuchida K, Arai KY, Kuramoto Y, Yamakawa N, Hasegawa Y, Sugino H 2000 Identification and characterization of a novel follistatin-like protein as a binding protein for the TGF-β family. J Biol Chem 275:40788–40796
27. Otsuka F, Moore RK, Iemura S, Ueno N, Shimasaki S 2001 Follistatin inhibits the function of the oocyte-derived factor BMP-15. Biochem Biophys Res Commun 289:961–966
28. Keutmann HT, Schneyer AL, Sidis Y 2004 The role of follistatin domains in follistatin biological action. Mol Endocrinol 18:228–240
29. McConnell DS, Wang QF, Sluss PM, Bolf N, Khoury RH, Schneyer AL, Midgley Jr. AR, Reame NE, Crowley Jr WF, Padmanabhan V 1998 A two-site chemiluminescent assay for activin-free follistatin reveals that most follistatin circulating in men and normal cycling women is in an activin-bound state. J Clin Endocrinol Metab 83:851–858
30. Bernstein JR, Crowley Jr WF, Schneyer AL 1990 An improved method of purifying inhibin radioligand for radioimmunoassay. Biol Reprod 43:492–496
31. Schneyer AL, Rzucidlo DA, Sluss PM, Crowley Jr WF 1994 Characterization of unique binding kinetics of follistatin and activin or inhibin in serum. Endocrinology 135:667–674
32. Korchynskyi O, Ten Dijke P 2002 Identification and functional characterization of distinct critically important bone morphogenetic protein-specific response elements in the Id1 promoter. J Biol Chem 277:4883–4891
33. Dennler S, Itoh S, Vivien D, Ten Dijke P, Huet S, Gauthier JM 1998 Direct binding of Smad3 and Smad4 to critical TGFβ-inducible elements in the promoter of human plasminogen activator inhibitor-type 1 gene. EMBO J 17:3091–3100
34. Shikone T, Matzuk MM, Perlas E, Finegold MJ, Lewis KA, Vale W, Bradley A, Hsueh AJW 1994 Characterization of gonadal sex cord-stromal tumor cell lines from inhibin α and p53-deficient mice: the role of activin as an autocrine growth factor. Mol Endocrinol 8:983–995
35. Wang X, Zeng W, Murakawa M, Freeman MW, Seed B 2000 Episomal segregation of the adenovirus enhancer sequence by conditional genome rearrangement abrogates late viral gene expression. J Virol 74:11296–11303
36. Hashimoto O, Kawasaki N, Tsuchida K, Shimasaki S, Hayakawa T, Sugino H 2000 Difference between follistatin isoforms in the inhibition of activin signalling: activin neutralizing activity of follistatin isoforms is dependent on their affinity for activin. Cell Signal 12:565–571
37. Di Simone N, Hall HA, Welt C, Schneyer AL 1998 Activin regulates βA-subunit and activin receptor messenger ribonucleic acid and cellular proliferation in activin-responsive testicular tumor cells. Endocrinology 139:1147–1155
38. Shimasaki S, Moore RK, Otsuka F, Erickson GF 2004 The bone morphogenetic protein system in mammalian reproduction. Endocr Rev 25:72–101
39. Bilezikjian LM, Corrigan AZ, Blount AL, Vale WW 1996 Pituitary follistatin and inhibin subunit messenger ribonucleic acid levels are differentially regulated by local and hormonal factors. Endocrinology 137:4277–4284
40. Corrigan AZ, Bilezikjian LM, Carroll RS, Bald LN, Schmelzer CH, Fendly BM, Mason AJ, Chin WW, Schwall RH, Vale W 1991 Evidence for an autocrine role of activin B within rat anterior pituitary cultures. Endocrinology 128:1682–1684
41. Bauer-Dantoin AC, Weiss J, Jameson JL 1996 Gonadotropin-releasing hormone regulation of pituitary follistatin gene expression during the primary follicle-stimulating hormone surge. Endocrinology 137:1634–1639
42. Besecke LM, Guendner MJ, Schneyer AL, Bauer-Dantoin AC, Jameson JL, Weiss J 1996 Gonadotropin-releasing hormone regulates follicle-stimulating hormone-β gene expression through an activin/follistatin autocrine or paracrine loop. Endocrinology 137:3667–3673
43. Schneyer AL, Wang QF, Weiss J, Boepple P, Hall J, Khoury R, Taylor A, Pralong F, Sluss P, Crowley WF 1997 Follistatin physiology and potential mechanisms of action in the human. In: Aono T, Sugino H, Vale WW, eds. Inhibin, activin and follistatin: regulatory functions in system and cell biology. New York: Springer-Verlag; 28–36
44. Lin HK, Bergmann S, Pandolfi PP 2004 Cytoplasmic PML function in TGF-β signalling. Nature 431:205–211

45. Panopoulou E, Gillooly DJ, Wrana JL, Zerial M, Stenmark H, Murphy C, Fotsis T 2002 Early endosomal regulation of Smad-dependent signaling in endothelial cells. J Biol Chem 277:18046–18052
46. Itoh F, Divecha N, Brocks L, Oomen L, Janssen H, Calafat J, Itoh S, Dijke PP 2002 The FYVE domain in Smad anchor for receptor activation (SARA) is sufficient for localization of SARA in early endosomes and regulates TGF-β/Smad signalling. Genes Cells 7:321–331
47. Hashimoto O, Nakamura T, Shoji H, Shimasaki S, Hayashi Y, Sugino S 1997 A novel role of follistatin, an activin-binding protein, in the inhibition of activin action in rat pituitary cells. J Biol Chem 272:13835–13842
48. Saito S, Sidis Y, Mukherjee A, Xia Y, Schneyer A 2005 Differential biosynthesis and intracellular transport of follistatin isoforms and follistatin-like-3 (fstl3). Endocrinology 146:5052–5062
49. Amthor H, Nicholas G, McKinnell I, Kemp CF, Sharma M, Kambadur R, Patel K 2004 Follistatin complexes myostatin and antagonises myostatin-mediated inhibition of myogenesis. Dev Biol 270:19–30
50. Iemura I, Yamamoto TS, Takagi C, Uchiyama H, Natsume T, Shimasaki S, Sugino H, Ueno N 1998 Direct binding of follistatin to a complex of bone-morphogenetic protein and its receptor inhibits ventral and epidermal cell fates in early *Xenopus* embryo. Proc Natl Acad Sci USA 95:9337–9342
51. Thompson TB, Lerch TF, Cook RW, Woodruff TK, Jardetzky TS 2005 The structure of the follistatin:activin complex reveals antagonism of both type I and type II receptor binding. Dev Cell 9:535–543
52. Thompson TB, Woodruff TK, Jardetzky TS 2003 Structures of an ActRIIB:activin A complex reveal a novel binding mode for TGF-β ligand:receptor interactions. EMBO J 22:1555–1566

Endocrinology is published monthly by The Endocrine Society (http://www.endo-society.org), the foremost professional society serving the endocrine community.